

# **Design and Analysis of Multi-Element Antenna Systems and Agile Radiofrequency Frontends for Automotive Applications**

Von der Fakultät für Elektrotechnik und Informatik der  
Gottfried Wilhelm Leibniz Universität Hannover zur Erlangung des  
akademischen Grades Doktor-Ingenieur genehmigte Dissertation

von  
Adrian Posselt

geboren am 06. Februar 1988 in Hannover

Hannover, 2019

1. Referent:

Prof. Dr.-Ing. Dirk Manteuffel

2. Referent:

Univ.-Prof. Dr. rer. nat. habil. Matthias Hein

Vorsitzender:

Prof. Dr.-Ing. Markus Fidler

Tag der Promotion:

24.04.2019

# Abstract

Vehicular connectivity serves as one of the major enabling technologies for current applications like driver assistance, safety and infotainment as well as upcoming features like highly automated vehicles - all of which having certain quality of service requirements, e. g. datarate or reliability. This work focuses on vehicular integration of multiple-input-multiple-output (MIMO) capable multi-element antenna systems and frequency-agile radio frequency (RF) front ends to cover current and upcoming connectivity needs. It is divided in four major parts. For each part, mostly physical layer effects are analyzed (any performance lost on physical layer, cannot be compensated in higher layers), sensitivities are identified and novel concepts are introduced based on the status-quo findings.

The first part studies requirements and architectures for current vehicular connectivity in the ecosystem of consumer-centric and machine-type communication technologies. Both the vehicle side as well as external influencing factors like standardization and regulation are considered and an area of conflict between the innovation cycles of the automotive industry and telecommunication industry is identified subsequently. Being pushed by the need of future-proof ubiquitous vehicular connectivity even for upcoming communication systems, a centralized and a distributed connectivity architecture are developed and distinguished from today's decentralized approach. The antenna system as well as the RF frontend are identified as potential bottlenecks when considering both performance and sustainability in a rapidly changing multi-standard environment.

The second part focuses on partitioning and evaluating approaches of vehicular multi-element antennas for use in MIMO communications systems. Special attention is paid to the characteristics of the vehicular domain, resulting integration effects and their influence on antenna performance. In order to properly assess and evaluate multi-element antennas in the automotive context, a new framework of system-level performance indicators for MIMO efficiency and channel capacity is developed for both high-datarate and zero-outage applications. A MIMO channel model is introduced and used for calibration of the framework. Subsequently, the methodology is completed by amending post-processing and visualization and is used to evaluate and compare a distributed versus a co-located multi-element antenna system based on test drives. The evaluation

allows for an elaboration and reconciliation of typical integration effects, that can only be captured on system level.

The third part deals with the design and implementation of multi-standard transceiver architectures for direct RF digitization based on a frequency-agile  $\Sigma\Delta$ -modulator with multiple sampling modes to extend its frequency coverage. After introducing the operating principles of analog-to-digital converters (ADC) in general and  $\Sigma\Delta$ -modulators in particular, a reconfigurable continuous-time bandpass  $\Sigma\Delta$ -modulator is synthesized and evaluated with regards to performance and sampling techniques both on power level and bitstream layer by investigating the quantization noise as well as the symbol error rate. The application of intentional aliasing by undersampling allows an extension of the operating range with an acceptable performance which enables the developed  $\Sigma\Delta$ -modulator-ADC to digitize services from 600 MHz up to 6 GHz.

The fourth part describes typical interference mechanisms within a vehicle and introduces an approach for a frequency-agile coexistence management based on signal canceling.

**Keywords:** Vehicular Connectivity, Multi-Element Antennas, Multi-Frequency Antennas, MIMO, Reconfigurable RF Frontend, Direct Sampling, Mobile Communication

# Kurzfassung

Fahrzeugvernetzung dient als eine der wesentlichsten Befähigungstechnologien für moderne Fahrerassistenzsysteme und zukünftig auch hochautomatisiertes Fahren. Sowohl die heutigen als auch zukünftige Anwendungen haben besondere Dienstgüteanforderungen, z.B. in Bezug auf die Datenrate oder Verlässlichkeit. Im Rahmen dieser Arbeit wird die Integration von Mehrantennensystemen für MIMO-Funkanwendungen (MIMO: engl. Multiple Input Multiple Output) sowie von frequenzagilen Hochfrequenzfrontends im Fahrzeugumfeld untersucht, um so eine technische Grundlage für zukünftige Anforderungen an die automobilen Vernetzung anbieten zu können. Die dabei gewonnenen Erkenntnisse lassen sich in vier Teile gliedern. Grundsätzlich konzentrieren sich die Untersuchungen vorrangig auf die physikalische Ebene. Auf Basis des aktuellen Status Quo werden Sensitivitäten herausgearbeitet, neue Konzepte hergeleitet und entwickelt.

Der erste Teil analysiert Anforderungen und Architekturen der Fahrzeugvernetzung im Umfeld des klassischen durch Endkunden genutzten Mobilfunks sowie dem Internet der Dinge. Hierbei werden sowohl fahrzeugseitige Faktoren als auch externe Einflüsse durch Standardisierung und Regulierung berücksichtigt, um das Spannungsfeld zwischen den Innovationszyklen der Automobil- und Telekommunikationsindustrie herauszuarbeiten und aufzuzeigen. Zur Realisierung einer zukunftsfähigen, universellen Fahrzeugvernetzung werden ein zentralisierter und ein verteilter Architekturansatz entwickelt und vom heutigen dezentralen System abgegrenzt. Hier erfolgt die wesentliche Erkenntnis, dass insbesondere in der stark diversifizierten Mobilfunklandschaft sowohl das Antennensystem als auch das unmittelbar folgende Frontend zur Digitalisierung der empfangenen Signale ein wesentlicher Flaschenhals sind.

Der zweite Teil fokussiert sich auf die Auslegung und Bewertung von fahrzeugseitigen MIMO Antennensystemen. Ein besonderes Augenmerk liegt hierbei auf den Besonderheiten der automotiven Bauräume, den entsprechenden Integrationseffekten sowie den Auswirkungen auf Funktion und Performance des Antennensystems. Zur Analyse und Bewertung von Mehrantennensystemen werden Kenngrößen auf Systemebene, wie MIMO Effizienz und Kanalkapazität, hergeleitet bzw. weiterentwickelt, um sowohl die erzielbare Datenrate als auch die Ausfallsicherheit bewerten zu können. Auf dieser Grundlage erfolgen die

Untersuchung, die Bewertung und der Vergleich eines verteilten mit einem zentralen, örtlich gemeinsam integrierten Antennensystems. Hierbei werden insbesondere Integrationseffekte auf Gesamtfahrzeugebene herausgearbeitet, die mittels herkömmlicher Antennenkenngößen nur unzureichend erfasst werden können.

Der dritte Teil beschreibt die Entwicklung und simulative Umsetzung eines rekonfigurierbaren, multistandardfähigen  $\Sigma\Delta$ -Modulators zur direkten Digitalisierung von Hochfrequenzsignalen. Hierzu werden zunächst die grundlegenden Funktionsprinzipien von Analog-Digital-Umsetzern (ADC) im Allgemeinen und  $\Sigma\Delta$ -Modulatoren im Speziellen erklärt, um anschließend einen neuartigen zeitkontinuierlichen  $\Sigma\Delta$ -Modulator im Bandpassbereich zu synthetisieren. Zur Erweiterung des Frequenzbereiches wird bewusst hervorgerufenen Aliasing durch Unterabtastung eingesetzt. Es erfolgt eine Untersuchung des Prototypen auf Leistungs- und Bitstromebene durch Betrachtung des Quantisierungsrauschens und der Symbolfehlerrate. Durch Einsatz der Unterabtastung in Verbindung mit dem rekonfigurierbaren  $\Sigma\Delta$ -Modulator wird die Digitalisierung von Signalen zwischen 600 MHz und 6 GHz möglich.

Im vierten Teil werden ergänzend typische Interferenzszenarien im Automobil beschrieben. Anschließend werden Maßnahmen zum frequenzagilen Koexistenzmanagement durch Interferenzunterdrückung mittels Signalauslöschung entwickelt.

**Schlagwörter:** Fahrzeugvernetzung, Mehrelementantenne, Mehrbandantenne, MIMO, Rekonfigurierbare RF Frontends, Direktabtastung, Mobilfunk

# Acknowledgments

This work would not have been possible without the support of many persons:

In particular, I am grateful to Prof. Dr.-Ing. Dirk Manteuffel from the Institute of Microwave and Wireless Systems from Leibniz Universität Hannover for giving me the possibility to work towards a doctoral degree in an industrial environment and of course for acting as a primary reviewer during the review process of this work. His profound interest in the scope of this work and beyond, his continuous and valuable feedback helped me tremendously during my research. I would also like to thank Univ.-Prof. Dr. rer. nat. habil. Matthias Hein for being the secondary reviewer as well as Prof. Dr.-Ing. Markus Fidler for being the chairman of the examination committee. Additionally, I would like to acknowledge apl. Prof. Dr.-Ing. Bernd Geck and Prof. Dr.-Ing. Holger Blume for their support during the initial phase of this work as well as their input about findings and progress.

Furthermore, I would like express my gratitude to my adviser at BMW Group Dr.-Ing. Oliver Klemp for his scientific and personal support during the course of this work. His never-ending motivation, support and the ability to structure even the most complex problems and to ask the right questions at the right time had a significant impact on my doctoral research and this thesis.

I am very thankful all of my colleagues at BMW Group for providing an inspiring research atmosphere, especially Dr.-Ing. Dennis Burgkhardt, Dr. techn. Levent Ekiz, Dr. techn. Peter Fertl and Dr.-Ing. David Gozálvez Serrano for the discussions about various both work and non-work related problems. Additionally, I would like to acknowledge Aline Friedrich from Leibniz Universität Hannover for the always enjoyable collaboration as well as her valuable suggestions during many discussions both in Munich and Hannover. Special thanks go to Christian Arendt for his significant contributions, proofreading and his continuous support as a colleague and dear friend.

I would like to thank all of the talented graduate students for their scientific

contribution through their theses or internships, in particular Christian Arendt, Dominic Berges, Lukas Grundmann, Ingo Heilemann, Marcel Welpot and Florence Vogl. All of these people have provided me with helpful advice, suggestions and discussions.

Moreover, I would really like to appreciate the tremendous love, support, understanding and patience of my wife Kendra-Louise. Thanks a lot for being by my side. Last but not least, I would like to thank my parents for their ongoing and never ending support and that I could always rely on them.



# Contents

<b>Abbreviations and Symbols</b>	<b>xi</b>
<b>1 Introduction</b>	<b>1</b>
1.1 Motivation and Approach . . . . .	2
1.2 Outline . . . . .	5
1.3 List of the Author's Contributions . . . . .	7
<b>2 State of the Art and Evolution of Vehicular Connectivity</b>	<b>11</b>
2.1 Overview of Relevant Wireless Systems and Applications . . . . .	11
2.2 Challenges/Requirements for Future Connectivity Architectures	15
2.2.1 State of the Art and Divergence of Frequency Regulation	15
2.2.2 Ecosystem of Vehicular Connectivity . . . . .	17
2.3 Conceptual Design of a New Connectivity Architecture . . . . .	20
2.3.1 Requirement Specification and State of the Art Discussion	23
2.3.2 Technical-economical interpretation and Summary . . . . .	28
<b>3 Multiservice Multielement Antenna Systems for Automotive Use</b>	<b>31</b>
3.1 Integration Space Analysis . . . . .	31
3.2 Multiservice Antenna Concepts . . . . .	34
3.3 Partitioning and Evaluation of MIMO Antenna Systems . . . . .	38
3.3.1 Preliminaries: Model of a Vehicular MIMO System . . . . .	40
3.3.2 Derivation of Performance Indicators for Automotive MIMO Antennas . . . . .	44
3.3.3 Numerical Evaluation of Performance Indicators . . . . .	51
3.4 Characterization of Multi-Element Vehicular Antenna Systems	57
3.4.1 Simulation of a Distributed MIMO Antenna System . . . . .	58
3.4.2 Measurement of a Distributed MIMO Antenna System	63
<b>4 Digitization by Direct RF Sampling</b>	<b>75</b>
4.1 Architectures for Analog-Digital-Conversion . . . . .	76
4.1.1 Operation of Analog-Digital-Converters . . . . .	78
4.1.2 Performance Evaluation and Limitations of ADCs . . . . .	82

4.2	Design of a Frequency-Agile Multiservice $\Sigma\Delta$ -Modulator . . .	85
4.2.1	Theory and Functional Principles of $\Sigma\Delta$ -modulators . .	87
4.2.2	Design Procedure and Methodology . . . . .	94
4.2.3	Synthesis of a Bandpass-Continuous-Time- $\Sigma\Delta$ -Modulator	97
4.3	Sampling Concepts . . . . .	105
4.4	Evaluation of a Novel Direct RF Sampling $\Sigma\Delta$ -Modulator . . .	111
4.4.1	Assessment of Multiservice Capabilities. . . . .	111
4.4.2	System-Level Assessment based on OFDM Simulation	114
<b>5</b>	<b>RF Signal Processing with Frequency Agile Components in the Analog Domain</b>	<b>121</b>
5.1	Coexistence Management and Interference Mitigation for Vehicular Connectivity . . . . .	122
5.2	Waiving of Frequency Fixed Components . . . . .	128
5.3	Design of a Signal-Canceling-Architecture . . . . .	129
5.3.1	Operation Principle and Theoretical Investigation . . .	129
5.3.2	System Behavior and Sensitivity . . . . .	132
5.4	Prototyping and Realization . . . . .	136
<b>6</b>	<b>Conclusion and Outlook</b>	<b>139</b>
	<b>Bibliography</b>	<b>143</b>

# Abbreviations and Symbols

## Abbreviations

2D	Two Dimensional
2G	2nd Generation
3D	Three Dimensional
3G	3rd Generation
3GPP	3rd Generation Partnership Program
4G	4th Generation
5G	5th Generation
ADAS	Advanced Driver Assistance System
ADC	Analog Digital Converter
AM	Amplitude Modulation
AU	Application Unit
BP	Bandpass
BTS	Base Transceiver Station
CAS	Co-Located Antenna System
CDF	Cumulated Distribution Funktion
CDMA	Code Division Multiple Access
CE	Consumer Electronic
CER	Cost Effectiveness Ratio
CID	Central Information Display
CN	Condition Number
CSI	Channel State Information
CT	Continuous time
DAB	Digital Audio Broadcast
DAC	Digital Analog Converter
DAS	Distributed Antenna System
DL	Downlink
DLC	Delay Limited Capacity
DR	Dynamic Range
DSP	Digital Signal Processor
DSRC	Dedicated Short Range Communication
DT	Discrete time

---

DVB-T	Digital Video Broadcast (Terrestrial)
ECU	Electronic Control Unit
ED	Eigenvalue Distribution
ELD	Excess loop delay
ENOB	Effective Number of Bits
ETSI	European Telecommunications Standards Institute
EVM	Error Vector Magnitude
FDD	Frequency Division Duplex
FDMA	Frequency Division Multiple Access
FFT	Fast Fourier Transform
FIR	Finite Impulse Response
FM	Frequency Modulation
FOM	Figure of Merit
FS	Full Scale
GMSK	Gaussian Minimum Shift Keying
GNSS	Global Navigation Satellite System
GPS	Global Positioning System
GSM	Global System for Mobile Communication
HSPA	High Speed Packet Access
HU	Head Unit
i.i.d.	independent identically distributed
IC	Integrated Circuit
IDC	In-Device Coexistence
IDFT	Inverse Direct Fourier Transform
IEEE	Institute of Electrical and Electronics Engineers
ISM	Industrial Scientific Medical
ITS	Intelligent Transportation System
ITU	International Telecommunication Union
KPI	Key Performance Indicator
LAN	Local Area Network
LDS	Laser Direct Structuring
LOS	Line of Sight
LP	Lowpass
LSB	Least Significant Bit
LTE	Long Term Evolution
MEA	Multiple Element Antenna
MEMS	Microelectromechanical Systems
MIMO	Multiple Input Multiple Output

---

MNO	Mobile Network Operator
MoM	Method of Moments
MOSFET	Metal-Oxide-Semiconductor Field-Effect Transistor
NLOS	Non Line of Sight
OEM	Original Equipment Manufacturer
OFDM	Orthogonal Frequency Division Multiplex
OFDMA	Orthogonal Frequency Division Multiple Access
OSI	Open Systems Interconnection
OSR	Oversampling ratio
PAPR	Peak to Average Power Ratio
PCB	Printed Circuit Board
PDF	Probability Density Function
PEC	Perfect Electric Conductor
PIFA	Planar Inverted F Antenna
PSD	Power Spectrum Density
PSK	Phase Shift Keying
QAM	Quadrature Amplitude Modulation
QoS	Quality of Service
RAN	Radio Access Network
RF	Radio Frequency
RMS	Root Mean Square
rRFFE	Reconfigurable Radio Frequency Front End
RSRP	Receive Signal Received Power
RSRQ	Receive Signal Received Quality
RSSI	Receive Signal Strength Indicator
Rx	Receive
S/H	Sample and hold
SC	Switched Capacity
SDARS	Satellite Digital Audio Radio Services
SDR	Software Defined Radio
SER	Symbol Error Rate
SFDR	Spurious-Free Dynamic Range
SINR	Signal to Interference and Noise Ratio
SISO	Single Input Single Output
SNR	Signal to Noise Ratio
SPI	Serial Peripheral Interface
SQNR	Signal to Quantization Noise Ratio
TDD	Time Division Duplex

TDMA	Time Division Multiple Access
THD	Total Harmonic Distorsion
Tx	Transmit
UE	User Equipment
UL	Uplink
UMTS	Universal Mobile Telecommunication System
USB	Universal Serial Bus
UTM	Universal Telematics Module
V2I	Vehicle to Infrastructure
V2V	Vehicle to Vehicle
V2X	Vehicle to X
VM	Vector Modulator
WLAN	Wireless Local Area Network
XPR	Cross Polarization Ratio

### Symbols

$\delta(t)$	Delta distribution
$f_s$	Sampling frequency
$\gamma$	SNR
$\kappa$	Condition Number
$\lambda$	Wavelength
$\lambda_i$	Subchannel gain and eigenvalue of $HH^\dagger$
H	Channel Matrix
$H_{\text{Kron}}$	Channel matrix based on Kronecker Model
$H_w$	Random fading matrix
$n(t)$	Noise vector
P	Covariance matrix of a signal
$R_H$	Correlation matrix for the channel matrix H
$R_{R_x}$	Receiver side correlation matrix
$R_{T_x}$	Transmitter side correlation matrix
$x(t)$	Transmit signal vector
$y(t)$	Receive signal vector
$\mathcal{F}$	Fourier-transform operator
$\mathcal{H}$	Hilbert-transform operator
$I(\sigma^2, P)$	Mutual information
$\mathcal{L}$	Laplace-transform operator
$\mathcal{Z}$	z-transform operator
ED	Eigenvalue distribution

$NTF$	Noise transfer function
$OSR$	Oversampling ratio
$STF$	Signal transfer function
$\omega$	Angular frequency
$\omega_s$	Angular sampling frequency
$\rho_{m,n}$	Interelement Correlation between antenna $m$ and $n$
$\sigma(x)$	Heaviside function, unit step function
$\sigma^2$	Variance of noise vector
$\tau$	Finite pulse duration or time delay
$\varphi$	Azimuth or general angle
$\vartheta$	Elevation
$\vec{E}(\vartheta, \varphi)$	Electrical field
$C$	Capacity
$C(\vartheta, \varphi)$	Directivity
$C_{\text{erg}}(\sigma^2)$	Ergodic channel capacity
$C_{\text{real},i}(\vartheta, \varphi)$	realized gain
$f$	Frequency
$f_{\text{in}}$	Maximum input signal frequency
$H$	Transfer function
$h(t)$	Impulse response
$h_{ij}$	Entry of the channel matrix
$K$	Number of non-zero eigenvalues
$L$	Inductance or attenuation
$l$	Length
$N$	Number of independent MIMO subchannels
$N_A$	Aperture jitter
$N_H$	Noise due to Heisenberg uncertainty principle
$N_{\text{Rx}}$	Number of receiving antennas
$N_{\text{Tx}}$	Number of transmitting antennas
$N_T$	Thermal noise
$N_U$	Comparator ambiguity
$p(t)$	Impulse response of a vector modulator
$P_H$	Total channel power
$P_{\text{diss}}$	Dissipated power
$R$	Minimum data rate that shall be ensured
$s(t)$	Periodical impulse sequence
$S_e$	Power spectrum density of quantization noise
$S_{m,n}$	Scattering Parameter between antenna $m$ and $n$

$T$	Period, sampling interval
$t$	Time
$v_{\text{ref}}$	Reference voltage
$v_x(n)$	Sampling error
$x_{\text{in}}(t)$	Analog input signal
$x_s(t)$	Sampled signal
$y_{\text{out}}(t)$	Analog output signal



Up until recent years, vehicles have mostly been a matter of transportation to bring passengers conveniently and individually to any destination. Innovations have mostly been based on the introduction of novelties from a mechanical or electromechanical point of view. These innovations usually satisfy one of the demands for faster, more agile, safer, environmentally friendlier and aesthetically pleasing automobiles. In the era of *digitization*, where everything becomes connected, personal mobility appears to be more than simply bridging distances. The vast deployment of cellular networks and the availability of a wireless connection to the internet serves as an enabler for many applications – not only in the domain of consumer electronics but also in the area of automobiles. Connectivity allows for the integration of a vast portfolio of applications and features to offer increased comfort, infotainment and safety. The vehicle serves as the digital interface between passengers and their digital lives, between vehicles and other road users or the infrastructure as well as between the driver as a consumer and the vehicle manufacturer. Providing state of the art connectivity becomes a more and more important criterion in the decision-making process on acquiring a vehicle<sup>1</sup> of a certain type, model or brand [1,2]. So far, the automotive industry has focused on the development of motor vehicles with either an internal combustion or electrical engines. Innovations in the area of connectivity were mostly concentrated to other non-automotive industry sectors. Furthermore, there is a huge discrepancy between the innovation cycles within the automotive industry versus the information and communications industry. A vehicle is not only perceived as hardware any more, its value is mostly determined by software-based functions like advanced driver assistance systems [2]. However, these features always rely on enabling hardware interfaces, like sensors or connectivity systems. In order to provide cutting-edge applications during the long lifetime of a vehicle, the automotive industry has to rely on future-proof technology on the one hand and has to perform a quick but still reliable adaption of consumer electronics technology to serve an enabler within a vehicle.

Current as well as rapidly developing technologies try to fulfill the rising demand for high data rates at high reliability and service availability as well as

---

<sup>1</sup>Given the trend of *sharing economy*, people might rather share vehicles instead of owning them.

mobility [3]. The growing demand for wireless resources in terms of available frequency ranges has led to a highly fragmented frequency spectrum with many different competing and complementary wireless systems in the area of cellular services for mobile applications, nomadic technologies, broadcasting and satellite services. Vehicles in the premium sector usually have all these technologies integrated and must allow concurrent operation while at the same time staying as flexible as possible to keep up with the high pace of the consumer electronics industry.

On an organizational level, the automotive industry transforms from a mechanics and mechatronics focused automobile manufacturer to a highly adaptive technology company, which focuses on customized mobility solutions and services. Besides other trends like electrification and sharing economy, vehicles become highly automated and connected. On a technological level vehicle manufacturers have to employ technology, that increases flexibility, decreases complexity and secures compatibility<sup>2</sup> to overcome the challenges imposed by the goal of reaching what industry calls *future mobility*. It is obvious, that the realization and implementation of *vehicular* connectivity in particular to serve as an enabler technology for most of the upcoming use cases is key for succeeding.

## 1.1 Motivation and Approach

This work pays special attention to the underlying enabler technology and focuses on the bottom-most physical layer [4] of the vehicular connectivity architecture. It analyzes the current state of the art as well as the ecosystem of vehicular connectivity and subsequently derives concepts for system partitioning to ensure compatibility for upcoming connectivity systems while staying in the context of connected mobility.

This multidimensional setup of influencing variables must be considered during vehicle and component development: The performance of a vehicular connectivity platform relies on external influencing factors as well as system-inherent factors which are caused by both by the vehicular (integrational) domain itself as well as the vehicular system partitioning and implementation. The goal of this thesis is to examine both of these performance-influencing factors in order to fully identify the physical-layer bottlenecks of a connectivity architecture capable to serve the needs and requirements of automotive applications and use cases. As a first step, the ecosystem of vehicular

---

<sup>2</sup>This credo is followed up on in Chapter 2.

connectivity is described to derive challenges as well as to allow a classification of findings later on. Based on a segmentation of a general radio system, the key building blocks are then identified and described both qualitatively and quantitatively while at the same time considering the special context of vehicular connectivity in the automotive domain.

The focus of this thesis is set to (1) the antenna system with special emphasis on antenna integration as well as the implementation of multi-element antenna systems, (2) the partitioning and setup of multi-standard transceivers as well as (3) an investigation of the coexistence requirements and concepts for radio frequency interference mitigation in the automotive domain.

Accordingly, three major pillars of vehicular connectivity are identified, analyzed in detail and subsequently improved or advanced on by theoretical concepts, analytical means as well as realization and implementation:

Due to the global fragmentation of wireless communications systems and frequency regulation as well as the variety and increasing number of standards, there are special requirements for the physical layer of the vehicle's connectivity architecture. Cellular communication standards, like Long Term Evolution (LTE) being the fourth generation (4G), and succeeding systems of the fifth generation (5G) use multi-element antenna systems in the context of Multiple-Input-Multiple-Output (MIMO) systems in order to increase both reliability and throughput by fully exploiting the spatial diversity of the communication link.

This work proposes an evaluation method based on a system-level approach by not only considering the impedance and radiation layer with typical performance indicators like return loss and radiation characteristic<sup>3</sup>. The scope is broadened by also integrating the system level with all its influencing factors into the analysis. Even though theory and realization of the presented concepts is generally applicable to any kind of multi-element antenna scenario, particular attention is paid to automotive-specific effects. This thesis analyzes vehicular antenna integration volumes from an electromagnetic perspective and examines the integration effects on antenna system performance. For a proper assessment of vehicular multi-element antenna systems, the typical set of performance indicators based on data on the impedance and radiation layer is extended by introducing additional *system-level* key evaluation indicators assessing the overall system performance and giving an insight about the

---

<sup>3</sup>See Chapter 3 for definitions.

achievable performance both from an engineer's as well as customer's point of view. Of course, this methodology is also applicable to non-automotive scenarios, however the flexibility with regards to integration concepts as well as the influence of the vehicle on the antenna system performance require a dedicated analysis and assessment.

At the same time, multiple coherent and non-coherent systems (like different both active and passive radio services as well as sensor systems) using a highly fragmented and widely spread frequency spectrum between 600 MHz and 6 GHz are integrated into vehicles by the manufacturer. Based on the discussion of the extra- and intra-vehicular connectivity aspects, this thesis develops and discusses different architecture proposals to implement the multitude of both complementary and coherent radio systems into a vehicular connectivity architecture with multi-standard capabilities. The approach followed here resembles a software defined radio like setup. However, the emphasis is set again on the physical layer with focus on frequency agile, multi-standard capable analog to digital conversion with optimization of the noise behavior. The known working principles of sigma-delta modulators are extended for use in direct-sampling of radio frequency (RF) signals. Furthermore, a novel concept of bandpass sigma-delta modulators in combination with undersampling of bandpass signals is proposed, derived analytically as well as implemented and evaluated by simulation. These findings allow the partitioning of a universal telecommunications module with frequency-agile behavior for use in multi-standard telematic control units within vehicles.

To allow for coexistence management and interference mitigation within the proposed multi-standard receiver setup in the vehicular, interference-limited environment, a concept for reducing interference without using any frequency-fixed components like filters<sup>4</sup> is needed. In this context, the concept of signal-canceling is used to reduce the power of interfering signals. This approach is known and used for noise canceling within audio systems like headphones, but also within RF systems like radar to separate received pulses from transmitted pulses or for full duplex applications. However, these applications usually rely on improving the decoupling between receive and transmit stages of a transceiver while the course of this work concentrates on

---

<sup>4</sup>Even though there are concepts of tunable filters known and industrialized, these concepts cannot be seen as frequency-agile like it is required for the concepts discussed within this work.

reducing the susceptibility of a receiving system to the transmitted signals of another wireless system within the vehicle over a broad frequency spectrum.

Due to the author's work in the automotive industry, this thesis covers a broad scope in the field of vehicular connectivity and automotive engineering while at the same time providing an academically motivated, in-depth analysis of the previously stated scientific challenges.

## 1.2 Outline

Chapter 2 introduces the concept as well as applications and underlying technologies of vehicular connectivity. Furthermore, the external influences like other non-automotive industry branches (mostly consumer electronics), regulation and frequency assignments are covered to form the ecosystem of vehicular connectivity. In addition, common architecture concepts for vehicular connectivity are reviewed and extended based on the respective findings to derive requirements and specifications for a new and future-proof, centralized connectivity system with multi-standard capabilities. This system is desired to adapt to upcoming technologies due to its flexibility and serve as an enabler for future applications. The chapter gives an overview of current and upcoming technologies in the context of physical layer vehicular connectivity and serves as the foundation for the following chapters, which cover the three major previously identified bottlenecks for the implementation of a highly performant connectivity platform for use within automobiles. The findings of this chapter are based on passages of [5–7] as well as patent application [8].

Chapter 3 identifies the antenna system as one of the major bottlenecks of the overall communication channel. After an investigation of the automotive domain and the deduction of implications for antenna integration, the previously derived requirement for multi-standard capability is transferred to multi-frequency antenna concepts. Subsequently, the focus is set to multi-element antenna concepts, their positioning and integration in the vehicular domain. A novel approach for partitioning and evaluating multi-element antenna systems is derived based on these findings. After a theoretical and analytical investigation of the proposed performance indicators like condition number, eigenvalue distribution, ergodic channel capacity and zero-outage capacity, the set of parameters is aligned and evaluated by a MIMO system analysis as well as by simulation of the setup's electromagnetic behavior. The methodology is then

used to assess and compare different topologies for the vehicular integration of multi-element antenna systems, again by using simulation but also by performing test drives with different prototypes. Here, the performance of collocated versus distributed antennas is compared. Additionally, the behavior of antenna systems based on a three-dimensional volumetric design approach are compared to a conventional two-dimensional design. The results of this chapter are published within [6, 7, 9–12] as well as patent applications [13–21].

Chapter 4 considers  $\Sigma\Delta$ -modulator analog-to-digital converters which can be used as a reconfigurable radio frequency front end. Ongoing from the current state of the art, lowpass  $\Sigma\Delta$ -modulators are used to introduce the concept of noise shaping for improved signal-to-noise ratio. The transformation from lowpass to bandpass  $\Sigma\Delta$ -modulators yields a flexible digitization and quantization setup, which already fulfills some of the previously defined requirements: the tunability and adaptivity of the notch allows for a reconfigurable and frequency-agile analog-to-digital conversion of directly sampled RF signals. Within this work, the applicability of reconfigurable, continuous-time bandpass  $\Sigma\Delta$ -modulators is expanded even further by following the novel approach of combination the previously synthesized  $\Sigma\Delta$ -modulator with direct undersampling of radio frequency signals in order to increase the operating frequency range. The basic operating principles of  $\Sigma\Delta$ -modulators are briefly introduced following state-of-the art literature. Subsequently, a basic discrete-time lowpass  $\Sigma\Delta$ -modulator is enhanced step-by-step until a continuous-time bandpass  $\Sigma\Delta$ -modulator is synthesized which is then operated in the undersampling mode. All steps are done analytically and are proven by simulations for each stage. Finally, the performance of the previously synthesized analog to digital converter (ADC) is analyzed both on power level with regards to signal-to-noise ratio for multiple wireless systems (e. g. cellular as well as digital broadcasting services of different carrier frequencies and bandwidths) as well as on the bitstream layer within an end-to-end performance simulation for a common digitally modulated multi-carrier signal. These results are available within the publications [5, 22] and patent applications [8, 23] where [8] also includes the concept of simultaneous undersampling and intentional non-overlapping down-aliasing of multiple bandpass signals at the same time.

Based on the findings and limitations mostly due to the resolution and dynamic range of an ADC from the previous investigation, Chapter 5 analyzes typical inference mechanisms and scenarios which are likely to occur in the

automotive environment due to the multitude of installed wireless systems. A concept for a flexible and frequency-agile preconditioning of received radio frequency signals is proposed to make signals compatible to a common direct sampling ADC like the one developed within this work: an architecture based on signal-canceling is introduced and characterized by deriving an analytical description in complete form. The setup is realized as a prototype and characterized by multiple measurements mitigating both inter-subsystem and intra-subsystem interference. While the first kind occurs between different subsystem within a vehicle, the latter one describes the decoupling of the transmitter and the receiver of a (full) duplex transceiver. This concept is published in [24] and patent applications [25, 26].

The results of the simulation and measurement campaigns which have been performed during the work of this thesis are integrated into the respective chapters, where they are discussed in the original context. Finally, an overall interpretation and subsumption of all findings is done in Chapter 6, where a conclusion and outlook is given.

## 1.3 List of the Author's Contributions

### Publications

- A. Posselt, L. Ekiz, O. Klemp, B. Geck, and C. Mecklenbrauker, "System level evaluation for vehicular MIMO antennas in simulated and measured channels," in *Antennas and Propagation (EuCAP), 2014 8th European Conference on*, April 2014, pp. 3051–3054.
- A. Posselt, A. Friedrich, L. Ekiz, O. Klemp, and B. Geck, "System-level assessment of volumetric 3D vehicular MIMO antenna based on measurement," in *2014 International Conference on Connected Vehicles and Expo (ICCVE)*, Nov 2014, pp. 222–226.
- L. Ekiz, A. Posselt, O. Klemp, and C. Mecklenbrauker, "System level assessment of vehicular MIMO antennas in 4G LTE live networks," in *Vehicular Technology Conference (VTC Fall), 2014 IEEE 80th*, Sept 2014, pp. 1–5.
- A. Friedrich, B. Geck, O. Klemp, A. Posselt, and I. Kriebitzsch, "3D-antennensysteme - Design und Validierung," *ATZelektronik*, vol. 9, no. 6,

pp. 44–51, 2014.

- O. Klemp, A. Friedrich, B. Geck, and A. Posselt, “3D-Antennensysteme Anforderungen an die Fahrzeugintegration,” *ATZ-Automobiltechnische Zeitschrift*, vol. 116, no. 12, pp. 60–65, 2014.
- A. Posselt, D. Berges, O. Klemp, and B. Geck, “Design and evaluation of frequency-agile multi-standard direct RF digitizing receivers for automotive use,” in *Vehicular Technology Conference (VTC Spring), 2015 IEEE 81st*, May 2015.
- A. Posselt, D. Berges, O. Klemp, and B. Geck, “Evaluation of a frequency agile direct RF ADC based on mixed-signal OFDM simulation,” in *European Conference on Personal Indoor and Mobile Radio Communications (PIMRC)*, September 2015.
- A. Posselt, M. Welpot, C. Bohm, O. Klemp, and B. Geck, “Evaluation and optimization of active signal canceling for coexistence management in vehicular multistandard transceivers,” in *Microwave Conference (GeMiC), 2015 German*, March 2015, pp. 331–334.
- C. Arendt, A. Posselt, P. Fertl, H. Boche, and J. Nötzel, “Evaluation of vehicular antenna concepts under delay-limited capacity as performance measure for safety critical message transfer,” in *2017 IEEE 28th Annual International Symposium on Personal, Indoor, and Mobile Radio Communications (PIMRC)*, Oct 2017.

## Patent Applications

Note, that only published patent applications are listed here and within the bibliography.

- A. Posselt, O. Klemp, L.-Y. Ekiz, and C. Lottermann, “Method and device for selecting transmission channels in a network radio connection,” Sept. 25 2015, Bayerische Motoren Werke AG, Patent Applications DE102013215855A1, WO002014154576A1, KR102015135254A, CN000105247797A, US020160014793A1, EP000002979371A1.
- A. Posselt, D. Berges, and O. Klemp, “Radio receiver for a motor vehicle, motor vehicle, method and computer program for a radio receiver,” Jan. 28 2016, Bayerische Motoren Werke AG, Patent Applications DE102014214555A1, WO002016012153A1.



- A. Posselt, C. Arendt, and P. Fertl, “Transceiver, Vehicle, Method, and Computer Program for a Transceiver,” Dec. 22 2016, Bayerische Motoren Werke AG, Patent Applications DE102015211336A1, WO002016202496A1, EP000003311498A1, US020180123632A1.
- A. Posselt, D. Gozalvez Serrano, and S. Zimmermann, “Application-controlled geo-beamforming,” Aug. 04 2016, Bayerische Motoren Werke AG, Patent Applications DE102015201641A1, US020170330462A1, WO002016120236A1.
- A. Posselt, A. Friedrich, and O. Klemp, “Antennenelement, Empfänger, Sender, Sendeempfänger, Fahrzeug und Verfahren zum Herstellen eines Antennenelements,” Mar. 02 2017, Bayerische Motoren Werke AG, Patent Application DE102015216147A1.
- A. Posselt and C. Böhm, “A Filter and a Method for Isolating Terminals in a Transceiver Front End,” Aug. 09 2017, Bayerische Motoren Werke AG, Patent Application EP000003203641A1.
- —, “A Filter and a Method for Filtering an Analog Radio-Frequency Input Signal,” Aug. 09 2017, Bayerische Motoren Werke AG, Patent Application EP000003203640A1.
- A. Posselt, D. Gozalvez Serrano, M. Kaindl, and M. Steingruebner, “Vorrichtung für ein Fahrzeug zur drahtlosen Kommunikation und Verfahren zur Einrichtung drahtloser Kommunikation gemäß einem zweiten Kommunikationsstandard ebendieser,” Mar. 29 2018, Bayerische Motoren Werke AG, Patent Application DE102016218580A1.
- A. Posselt, C. Arendt, D. Gozalvez Serrano, M. Kaindl, and M. Steingruebner, “Antennenanordnung für ein Fahrzeug und Fahrzeug,” Apr. 05 2018, Bayerische Motoren Werke AG, Patent Application DE102016219163A1.
- A. Posselt and C. Arendt, “Antennenanordnung für ein Fahrzeug und Fahrzeug,” Apr. 05 2018, Bayerische Motoren Werke AG, Patent Application DE102016219164A1.
- —, “Fahrzeugscheibe und Fahrzeug mit einer Fahrzeugscheibe,” Apr. 05 2018, Bayerische Motoren Werke AG, Patent Application DE102016219167A1.

- A. Posselt, M. Kaindl, M. Steingruebner, and M. Rottelberger, “Antennenanordnung, Karosserieteil und Fahrzeug,” Apr. 19 2018, Bayerische Motoren Werke AG, Patent Application DE102016220238A1.
- A. Posselt, C. Arendt, P. Fertl, and D. Gozalvez Serrano, “Kommunikationssteuergerät für ein Fahrzeug,” Apr. 24 2018, Bayerische Motoren Werke AG, Patent Application DE102016222983A1.

Vehicular connectivity is and will be one of the most important key success factors for the automotive industry both today and especially in the future. Vehicles have to connect to a large number and variety of radio access networks (RAN) to provide reliable services for driver assistance, safety and infotainment applications [6, 10, 22]. The concept of vehicular connectivity includes the driver, the vehicle, its surroundings and the technical environment. Additionally, mobile communication technology in general builds the foundation for future applications which will require pervasive and high-performance connectivity.

This chapter is dedicated to present the general concept of vehicular connectivity and subsequently derives challenges and requirements for future-proof connectivity architectures by presenting aspects of future mobile connectivity. After a brief introduction of the most relevant wireless technologies in Section 2.1, Section 2.2 analyzes challenges of automotive connectivity with special emphasis on upcoming trends and developments, the fast-moving nature of communication technology as well as the potential impact of worldwide changes in frequency regulations. Based on these findings, Section 2.3 discusses different hardware approaches for realizing future-proof automotive connectivity and derives specific hardware requirements. This discussion introduces a paradigm change by suggesting the installation of flexible connectivity hardware at either central or distributed locations inside the vehicle instead of a decentralized, non-coordinated configuration.

## 2.1 Overview of Relevant Wireless Systems and Applications

A sufficient understanding of wireless connectivity standards with relevance for the automotive industry is key for the comprehension of today's connectivity architectures as well as for their partitioning in the vehicular domain. For today's and future infotainment and driver assistance systems, there is a necessity of a variety of fast, reliable and secure number of different means of connectivity as they are for example already deployed in a mobile phone or tablet

computer. These technologies which are considered to fulfill the previously mentioned demands can be grouped into five categories according to Table 2.1: broadcasting, cellular communications, ad-hoc communications, satellite services for positioning and broadcasting and safety technologies [22]. The borders between the mentioned categories can be blurry in some cases, but for automotive applications, the shown classification is valid<sup>5</sup>.

Table 2.1 Relevant wireless services for automotive use with focus on cellular and broadcasting systems [22, 28–32], © 2015 IEEE

Technology	Standard	Channel Access and Modulation Scheme
Broadcasting	AM/FM Radio	AM, FM
	DAB	OFDM, 4–64-QAM
	DVB-T	OFDM, 4–256-QAM
	Sirius Satellite Radio	QPSK
Cellular	2G (3GPP)	CDMA, TDMA, QPSK, GMSK
	3G (3GPP)	TDMA, CDMA, 4–64-QAM
	4G (3GPP)	OFDM, 4–256-QAM
Ad-Hoc	Wi-Fi (IEEE 802.11)	OFDM, 2–4-PSK, 4–256-QAM
	WiMAX (IEEE 802.16)	OFDM, 4–64-QAM
GNSS	GPS	BPSK, CDMA
	Galileo	CDMA, 2–4-PSK
	GLONASS	FDMA, BPSK
Safety	ETSI ITS-G5	OFDM, 2–64-QAM
	DSRC (IEEE 802.11p)	OFDM, 2–64-QAM

*Cellular Communication* is fundamental for the bilateral exchange of information and are therefore important for the interconnection of today’s and future vehicles,

<sup>5</sup>Here, satellite radio is classified as a broadcasting service. However, its technology strongly differs from terrestrial broadcasting services.

both among themselves<sup>6</sup> as well as with the environment. There exist many use cases which are based on bidirectional communication like automatically or manually triggered emergency calls, web services, remote software updates or online entertainment. Many automotive original equipment manufacturers (OEM) envision, that 90 % – 100 % of their newly produced vehicles are equipped with an integrated connectivity module to utilize mobile networks. For BMW Group for example, this holds true for newly produced vehicles from 2015 ongoing [22]. A similar trend can be seen at other premium sector OEMs. The recent developments regarding highly automated driving will require very reliable wireless connectivity [33].

The specification of the Global System for Mobile Communication (GSM), also known as the second generation communication network (2G) was done by the European Telecommunication Standards Institute (ETSI) [28]. In Europe, the main operating frequencies are around 900 MHz and 1800 MHz and allows data rates up to 384 kbit/s [34]. The development of the third generation (3G) mobile network (Universal Mobile Telecommunication System, UMTS) was motivated by new kinds of data services (mostly mobile internet) as well as restrictions from its predecessor 2G wireless technology. At the end of 1990, the first UMTS standard was completed [29]. Together with modifications introduced by High Speed Packet Access (HSPA) concerning modulation, coding and scheduling, data rates up to 14 Mbit/s can be achieved in the downlink and 5.76 Mbit/s in the uplink [35]. With Long Term Evolution (LTE), the 3rd Generation Partnership Program (3GPP) released the fourth generation of cellular communication systems<sup>7</sup>. The motivation for the new standard of mobile wireless networks is based on a simplified flat packet-oriented network architecture, high data rates up to 100 Mbit/s in the downlink, reduced latency, scalable use of bandwidths from 1.25 MHz to 20 MHz and the use of Orthogonal Frequency Division Multiple Access (OFDMA) for downlink [30,35]. In Europe LTE operates at frequencies around 800 MHz, 1800 MHz and 2600 MHz [34]. Other frequencies are used worldwide, cf. Section 2.2.1. Additionally, LTE relies on advantages offered by utilization of Multiple-Input-Multiple-Output (MIMO) systems and thus exploits diversity in space, polarization or radiation pattern of multiple antennas at the same time [30].

*Terrestrial broadcasting services* like Digital Audio or Video Broadcasting

---

<sup>6</sup>Based on cellular Vehicle-to-X (C-V2X), originally LTE V2X, as standardized in Release 14 [30] with Vehicle-to-Vehicle (V2V), Vehicle-to-Infrastructure (V2I), Vehicle-to-Pedestrian (V2P) and Vehicle-to-Network (V2N) operating modes with the latter using traditional cellular links.

<sup>7</sup>3GPP Release 8 is referred to as 3.9G, while 3GPP Release 13 provides real 4G [30,34].

(DAB, DVB-T and DVB-T2 respectively) [32] are deployed in today's vehicles as well as analog broadcasting<sup>8</sup> to provide audio and video reception for passenger entertainment. During the past years, digital technology has been succeeding analog technology and is widely deployed. The digital technology offers advantages like improved audio and video quality, noise immunity and the ability to support added services like advanced traffic information [34]. In addition, the digital systems offer an improved spectral efficiency. The operating frequencies of DVB-T are often positioned closely to those of cellular communication systems. Thus, special attention has to be paid, as broadcasting systems can be subject to interference, especially when deployed in confined integration spaces within a vehicle. Challenges regarding the required coexistence management as well as possible solutions are discussed within Section 2.3 and Chapter 5, respectively.

*Wireless Local Area Networks* (WLAN) have become popular in the last years due to their simple setup and moderate cost. Usually, the infrastructure mode is used to provide connectivity to mobile stations based on the standard IEEE 802.11a/b/g/n [31]. However, WLAN can operate in an ad-hoc fashion to enable data exchange between wireless hosts without the presence of a fixed infrastructure [36]. In the context of vehicular connectivity, this possibility is exploited by the standardization of IEEE 802.11p (11p) [31] to enable Vehicle-to-X (V2X) communication which includes communication between vehicles (Vehicle-to-Vehicle, V2V) as well as between vehicles and infrastructure (Vehicle-to-Infrastructure, V2I). 11p is supposed to be used for safety and commercial real-time applications. The operating frequency is located at 5.9 GHz. The ETSI has standardized an European equivalent technology in [37]. Fig. 2.1 displays the evolution of the cellular communication networks in the framework of the 3GPP and allows comparison and classification with regards to their respective data rate and the aspect of mobility, which is very important especially in the context of vehicular connectivity<sup>9</sup> and connected mobility in general.

**Observation 2.1.** *To provide services for assistance, safety and infotainment, already today vehicles have to connect to a large number of radio services which can be both competing as well as complementary to each other. The*

---

<sup>8</sup>The analog broadcasting services are commonly referred to as FM or AM radio, derived from their modulation technique.

<sup>9</sup>The performance, which can be achieved with moving user equipment (UE) within wireless communications systems is subject to several effects like cell handovers, fading and Doppler effect. This influence is discussed in Chapter 3 where a channel model is introduced to assess the performance of MIMO antenna systems.

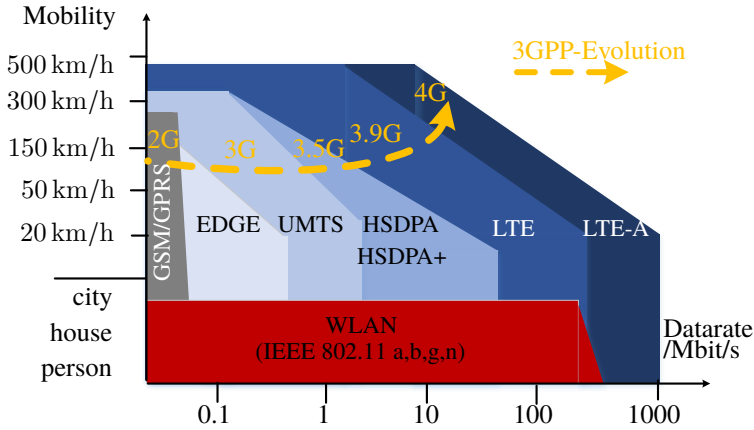


Figure 2.1 Overview of the evolution of cellular radio technologies from GSM to LTE with regards to mobility and maximum data rate. For comparison, WLAN is also included [28–31].

*network between driver, vehicle and the environment consists of wireless systems for cellular and ad-hoc communication as well as broadcasting services and requires the integration of extensive equipment into the vehicle to provide the aforementioned applications at a certain Quality of Service (QoS) level.*

## 2.2 Challenges/Requirements for Future Connectivity Architectures

### 2.2.1 State of the Art and Divergence of Frequency Regulation

Table 2.1 lists wireless services with direct relevance for vehicular connectivity. Each of these radio systems has a dedicated frequency assignment to allow efficient spectrum utilization, guaranteed planning certainty and minimization of interference, generating an incentive to invest into infrastructure and harmonizing with international agreements regarding frequency utilization as well as forward and backward compatibility [38].

Due to an increased demand regarding frequency allocations and increased bandwidths to realize new applications relying on wireless services, changes in frequency assignments become inevitable. Regulatory bodies both within

Europe as well as worldwide handle this demand with spectrum rearming: Strategic reallocation of frequency resources and rededication allows to meet the needs of the customers and the wireless industry. The strategic paper [39] discusses potential new frequency allocations: Right now, within the International Telecommunication Union (ITU) Region 1, frequencies from 470-790 MHz are assigned to broadcasting services. A co-primary assignment of frequencies from 649 MHz to 790 MHz to cellular communication systems instead of broadcasting can be foreseen [22]. In 2015 Europe has been implementing a *Digital Dividend II* which comprises both a rededication of frequencies from previously broadcasting to cellular communications as well as the release of new frequency bands for technology neutral use by mobile network operators (MNO) [40]. Similar efforts are pursued worldwide: many MNOs are discussing or have planned the shutdown of the 2G GSM network to re-purpose the respective frequencies for use by newer wireless services.

**Proposition 2.1.** *In the context of connected mobility, the vehicle serves as a connected device. From an OEM perspective with a rather long life-cycle of connected products of around 15 to 20 years, changes in frequency regulation as well as the discontinuation of certain wireless communication systems can often not be foreseen with sufficient accuracy. Thus, to ensure future compatibility and technological flexibility of its connectivity Electronic Control Units (ECU), all possible frequency bands which have been or are likely to be standardized or regulated by regulatory bodies have to be considered while staying as technologically neutral as possible.*

In the above proposition, the term *technologically neutral* is used to denote the ability of the hardware to work independently of the boundary conditions of a specific communication standard. This approach is also considered in regulation, where frequencies are assigned technologically neutral without specifying a wireless standard to be used, see e. g. [38, 39]. Figure 2.2 shows an overview of today's and future frequency allocations based on the respective standards. Thus, it contains all possibilities for upcoming changes in frequency regulation as only standardized frequency ranges may be regulated reasonably.

Fig. 2.2 is based on the evaluation of the previously cited literature<sup>10</sup> (mostly standards and technical reports) and own investigations partially published in [22, 24]. It leads to:

**Observation 2.2.** *Based on the analysis of wireless services with importance*

<sup>10</sup>In particular: [28–32, 38–40], as well as secondary sources like [34–36].



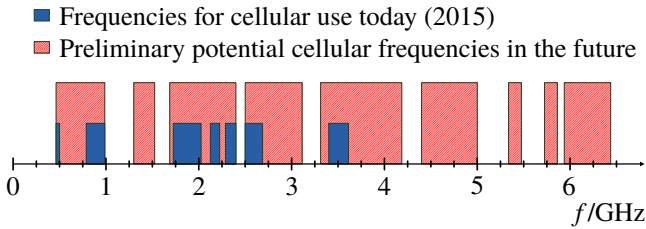


Figure 2.2 Comparison of possible frequency allocations for cellular communications systems both today and in the future based on [22, 24, 28–32, 34–36, 38–40], © 2015 IEEE.

for vehicular connectivity (Table 2.1) and their possibly occupied frequency ranges for operation the required domain is set to the range from 600 MHz to 6 GHz. This range includes all relevant services for the investigations within this work, including broadcasting services at the lower bound at 649 MHz, cellular communications systems (GSM, UMTS, LTE) at various frequencies and vehicular safety radio services (V2X communication) at the upper bound at 5.9 GHz.

**Proposition 2.2.** *The evaluation of relevant services and their utilization of frequency allocations as of today and the future is a relevant prerequisite and gives fundamental information for the design and partitioning of a future-proof and flexible vehicular connectivity architecture.*

## 2.2.2 Ecosystem of Vehicular Connectivity

The goal of vehicular connectivity is the implementation of an interconnected vehicle which links the car to the driver and passengers as well as to the environment. The extra-vehicular connection can include direct communications to other traffic participants as well as communication to back end services providing data for traffic management or comfort functions, see e. g. [41]. In this context, the previously named wireless communication technologies play a decisive role in enabling these functions, both today and especially in the future, where the insatiable demand for high data throughput and the increasing necessity of availability and reliability will increase. Until today, the automotive industry has been focusing on designing, developing and manufacturing of motor vehicles. Most of the innovations have been in the area of mechanical engineering and mechatronics whereas most of the innovations regarding wireless communications have arisen in other industrial sectors which focus primarily on

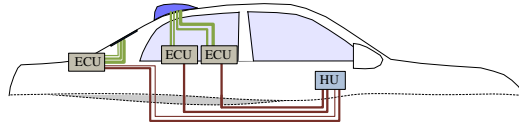


Figure 2.3 Visualization of the historically grown decentralized architecture for bidirectional vehicular connectivity and broadcasting reception.

consumer electronics.

Following this historical development on the one hand, and the necessity of basic connectivity to cellular services and broadcasting services, vehicles are usually equipped with a decentralized connectivity architecture like shown in Fig. 2.3. The roof-top antenna covers cellular communications systems (GSM, UMTS, LTE) as well as satellite systems for positioning (Global Navigation Satellite System, GNSS) and satellite radio (Satellite Digital Audio Radio Services, SDARS). Antennas for reception of lower frequency broadcasting services are usually positioned within fixed windows or rod antennas. The respective ECUs are fed by coaxial cabling. As new communications services kept emerging during the past decades (see Section 2.1), each radio system is served by a dedicated ECU to process the signals received by the antenna and to provide the data to the respective information sink within the vehicle. This could be the head unit (HU) with a central information display (CID) displaying traffic information and maps for navigation or a passenger entertainment system for play-back of audio or video. In order to enable the various wireless services inside the vehicle while at the same time considering the vast diversity of available systems, up to twelve ECUs have to be integrated into the vehicle [22]. During the automotive design and manufacturing process, these ECUs are usually developed and provided by different suppliers but have to be integrated into the overall vehicular architecture by the OEM. Thus the OEM serves as a system's integrator and has to ensure coexistence of all subsystems.

Knowledge from the field of electromagnetic compatibility leads to the observation that systems working in a separated environment usually behave differently in a fully integrated environment and thus can cause interference [42]. Figure 2.4 exemplifies this issue and shows the partitioning of the connectivity architecture.

A prominent example is given in [43] and further discussed in Section 5 and [24] where an impairment of DVB-T reception occurs during an active transmission of the vehicle's LTE transceiver due to little separation of the operating frequencies. Another known issue is parallel operation of multiple cellular transceivers within the vehicle, e.g. one serving the vehicle's connectivity system and one within a passenger's customer device like a cell phone which is physically connected to the vehicle's roof-top antenna<sup>11</sup>. These examples are visualized in Fig. 5.2.

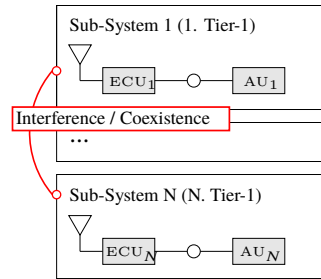


Figure 2.4 Different sub-system from possible different suppliers have to be integrated into the vehicle by the OEM by resolving possible coexistence issues.

In addition to the available and necessary standards according to Table 2.1, which can be both complementary as well as contrary, radio communications systems are subject to rapid changes, especially with focus on terrestrial services. These rapid cycles within the information and communications industry contradict the technology cycles in the automotive domain. New wireless services are emerging rapidly at a rate of only a few years between deployment, for example with the transition from second generation cellular services GSM to the fourth generation with LTE (4G) [28–30]. Within projects like METIS [45] the fifth generation (5G) is already under investigation [46]. Besides the emergence of new generations of communications systems, the respective predecessors are often discontinued (technology sunset, see Section 2.2.1). Taking the product life cycle of a vehicle into account, which is about 10 – 15 years, the automotive industry is forced to take action to withstand the fast developments in consumer electronics and communications technology in general to keep up with the rapid pace of digitization.

The inherent challenges, which have been discussed within the previous paragraphs, lead to the following observations and have to be anticipated to be supported in future vehicles. The importance of the connected car for future applications in the context of mobility will raise steadily [1–3].

**Observation 2.3.** *The ecosystem of vehicular connectivity is subject to rapid changes which contradict the innovation life cycles in the automotive domain.*

<sup>11</sup>To mitigate the attenuation of the car body and metalized windows [44], often coupling devices are offered as optional equipment to connect a mobile phone to the roof-top antenna to provide improved customer connectivity within the vehicle by circumventing the shielding of the vehicle's bodywork.

*The boundary conditions, to which the vehicular connectivity architecture has to adapt, are rapidly changing. The inflexible connection between the function to provide and the respective ECU in a decentralized connectivity architecture will neither be able to facilitate the integration of additional independent sub-systems nor enable effortless adaption to the inevitable changes.*

**Proposition 2.3.** *The transition of car manufacturers from building automobiles as simple means of transportation to a provider of connected mobility and mobility services requires an adaption of the OEM's development process on a general level in terms of speed and flexibility as well as a complete redesign of the connectivity architecture on a technical level resulting in a paradigm change in vehicular connectivity.*

The variety of connectivity services, especially for future services with low latency and high data rates as well as the required support of multiple frequency bands simultaneously poses new challenges to the antenna and system engineer. Ongoing from today's decentralized connectivity architecture, the following proposition is derived for future investigations:

**Proposition 2.4.** *Future vehicular connectivity systems have to enable multiple wireless communications systems, both contrary and complementary. In order to adapt to the previously presented challenges and to facilitate the integration of independent sub-systems a paradigm change is necessary. Moving away from the evolutionary grown connectivity architecture, a new system concept has to be designed to decrease complexity with regards to system integration, to increase flexibility regarding available frequencies and to ensure compatibility for new radio systems during the lifetime of the vehicle [22].*

These three key requirements are detailed in the following section and subsequently solved in the consecutive chapters.

## **2.3 Conceptual Design of a New Connectivity Architecture**

The previous sections introduced the key requirements to enable today's and future connectivity standards in the vehicular domain. Furthermore, a broad understanding for requirements from a hardware perspective has been given. This sections provides an overview of today's connectivity architecture, whose setup is historically driven, and derives two architectural concepts which enable future-proof connectivity.

First, three connectivity system setups are introduced on a macroscopic level. Then, the following subsections provide a detailed partitioning by dividing the overall architecture into key building blocks as well as giving exact and comprehensive hardware requirements.

The hardware architecture of relevance within this investigation are grouped into three categories:

- *Decentralized Architecture*: several different radio services (including broadcasting and cellular systems) are deployed independently inside the vehicle,
- *Centralized Architecture*: central system, which combines multiple decentralized standard-specific ECUs in one flexible and reconfigurable central ECU by using multiservice transceivers close to the port of an appropriately partitioned antenna system and
- *Distributed Architecture*: this hybrid approach consolidates the advantages of a distributed antenna architecture (adapted from the decentralized architecture) together with the centralized signal conversion and processing from the centralized architecture.

The two latter setups have been derived during the work of this thesis and can be seen as a possible answer to Proposition 2.4. They serve as a foundation and provide basic principles for the investigations within the following chapters.

These architectures are now briefly discussed and distinguished to each other.

The *decentralized architecture* has emerged historically [22]: in order to offer new functionality like telematics based on cellular networks or the reception of digital video based on broadcasting, new ECUs have been added to the vehicle to provide these applications to the driver and passengers. The general setup is shown in Fig. 2.3.

The antenna is connected by coaxial cable to the respective ECU which realizes the analog and digital signal processing as well as the baseband processing and provides the information after demodulation and decoding to the information sink. This setup is used for each radio system, e. g. one for cellular services, one for analog or digital audio and video broadcasting each, one for satellite radio and one for positioning purposes.

This architecture concept results in certain disabilities: First, cable losses are introduced leading to a degraded performance due to attenuation of the

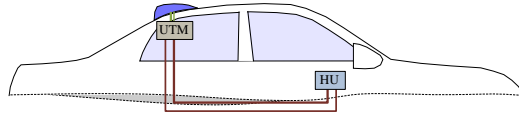


Figure 2.5 Proposition of a centralized connectivity architecture. A Universal Telematics Module (UTM) digitizes the signals close to the feeding point of the antenna, performs baseband processing and then provides the received information to the respective information sink, e. g. the HU of a vehicle, [22], © 2015 IEEE.

received signals<sup>12</sup>. Each of these ECUs as well the respective antenna systems are provided by different suppliers independently and are implemented by the OEM. As all subsystems are required to work jointly in coexistence, system integration by the OEM is a major and resource consuming task. Consider for example coexistence between LTE at lower frequencies (around 600-800 MHz) and DVB-T in the same frequency region [43, 47]. Similar challenges regarding coexistence arise between LTE in band 30 and satellite radio SDARS. The overall performance is limited by the capabilities of its subsystems, thus a joint design process or a different architecture partitioning is desirable and necessary. These impairments of the decentralized architecture lead to the following Observation 2.4 and subsequently to Proposition 2.5 to introduce corrective actions:

**Observation 2.4.** *The inflexible connection between ECU and function within a decentralized connectivity architecture with limited performance will not be able to facilitate the integration of independent sub-systems from an OEM perspective, as no direct coexistence and interference management is possible [22].*

These system inherent disadvantages, namely cable losses, increased effort for integration as well as coexistence challenges and the inflexible connection between function and ECU lead to the second architecture:

**Proposition 2.5.** *To ensure future compatibility, interoperability and facilitated implementation and integration, a centralized connectivity architecture with flexible and reconfigurable characteristics is proposed [22, 24].*

The *centralized connectivity architecture* as shown in Fig. 2.5 comprises a *Universal Telematics Module (UTM)* close the feeding point of the antenna

<sup>12</sup>Of course, the same attenuation is also applied to transmitted signals. This effect can be circumvented by adjusting the transmission power within the regulated limits. This is not possible for in receive mode.

with reconfigurable and frequency agile properties. The aforementioned reconfigurability and agility leads to multiservice capabilities, that is the ability to process different wireless services, like cellular and broadcasting systems, simultaneously within the same module [22]. This architecture serves as the basic concept for the following investigations. Findings based on the detailed analysis of transceiver concepts in Chapter 4 and insights about vehicular MIMO antenna systems in Chapter 3 will lead to the derivation of the third connectivity concept.

### **2.3.1 Requirement Specification and State of the Art Discussion**

The previous section proposed a solution to increase the compatibility, decrease the complexity and at the same time ensuring compatibility of vehicular connectivity architecture in a rapidly changing environment. This somehow contradicts the innovation cycle in the automotive business. The approach uses a centralized hardware to receive and process radio frequency signals as flexibly as possible. In order to react with maximum flexibility on existing and future developments, Mitola has developed the model of a Software Defined Radio (SDR) in [48]. This concept is thoroughly discussed e. g. in [49–52]. A system-level investigation within the vehicular context can be found e. g. in [10, 53–55]. However, the previously cited literature and comparable work keeps a steady focus on sub-systems like the vehicular antenna system itself or digital signal processing and exploiting advantages thereof, while an end-to-end investigation (from the antenna to the ADC) is not available. Furthermore the process of digitizing RF signals steps into the background or the aspects the previously discussed flexibility and agility are neglected.

A canonical transceiver design of an SDR system according to [48] is shown in Fig. 2.6.

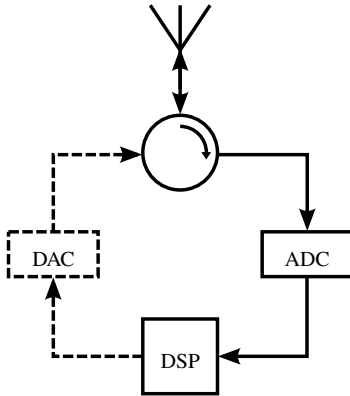


Figure 2.6 General architecture concept of the SDR approach [22], © 2015 IEEE.

It consists of a broadband antenna with receive and transmit capabilities at the relevant frequencies. Subsequently, there is a suitable Analog Digital Converter (ADC) or Digital Analog Converter (DAC) with suitable resolution and RF behavior in the receive or transmit path, respectively. Both paths are connected by a Digital Signal Processor (DSP) which processes the data. The architecture shown in Fig. 2.6 has only theoretical relevance, see [22] and following explanations. A realistic partitioning of the proposed connectivity architecture is visualized in Fig. 2.7. It consists of three building blocks: an antenna system, a signal conditioning stage and the ADC stage, all of which are detailed in the following paragraphs with focus on the receive case. Generally, signals are received by a broadband antenna system and fed into the UTM where they are digitized after preconditioning to allow for correct sampling and quantization. After baseband processing in the digital domain, the extracted information is provided to the information sink within the requesting Application Unit (AU).

The advantage of this technology is evident, since it reduces the general

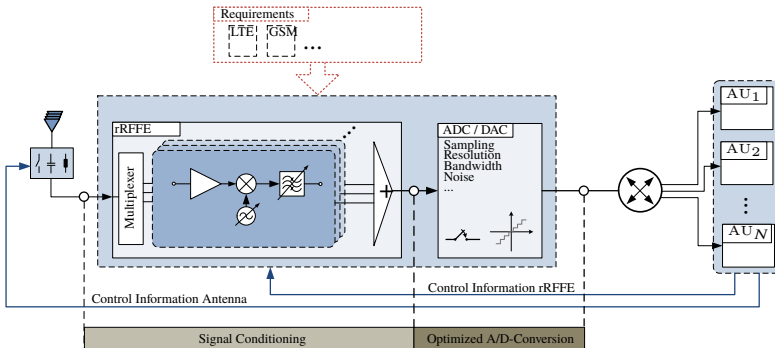


Figure 2.7 Partitioning of the receive system into three major building blocks: it consists of an antenna system, a system unit for signal conditioning to make the signals ADC-compatible and the ADC unit itself for signal digitization and quantization.



complexity of the connectivity system:

**Observation 2.5.** *By eliminating individual ECUs and using an SDR-like system for RF signal processing, it is possible to treat the incoming signals in a centralized fashion and increase compatibility with future systems by providing software updates to the end user instead of having to replace or add ECUs and antennas.*

### 2.3.1.1 Radiofrequency Frontend

As the UTM-concept is closely related to the general software radio concept, it promises a high increase in flexibility. According to Observations 2.1 - 2.5 within this chapter, the following general requirements are derived and detailed later on. To follow the principle *increase flexibility, decrease complexity and secure compatibility*, a reconfigurable architecture with frequency agile properties is needed to cover all of today's and tomorrow's wireless communications systems as well as subsequent customizing and forward compatibility. According to the OSI reference model<sup>13</sup> [4] the physical layer of the system is considered transparent regarding the specific radio system. Thus, only the physical layer is considered within this work.

A suitable RF frontend concept is needed to cover frequencies within the range from 600 MHz to 6 GHz while at the same time enabling multimode support to process multiple radio systems concurrently. Referring to Fig. 2.7, special attention has to be paid to the analog-to-digital conversion stage as well as the RF processing in front of the conversion stage. In order to allow for maximum flexibility, a mostly purely digital SDR-like architecture is foreseen. Nevertheless, this approach is limited by technological as well as physical limits and requires a thorough investigation of the analog-to-digital conversion stage. Even though some processing steps like selection of band and channel can be moved to the digital domain behind the ADC stage [48], measures to ensure coexistence and filtering of interfering signals have to be done in the analog domain in front of the ADC to prevent it from overloading [24].

Now, to be able to sample the highest required frequency of 6 GHz by means of general Nyquist sampling (cf. Chapter 4), a sampling frequency of  $f_s = 1.5 \cdot 2 \cdot 6 \text{ GHz} = 18 \text{ GHz}$  and a resolution of 12 bit [56] would be required. In this example, the sampling frequency is calculated according to the Nyquist

---

<sup>13</sup>The Open Systems Interconnection (OSI) model provides "a common basis for the coordination of standards development." [4]

sampling theorem [57] with an additional factor of 1.5 to account for the bandwidth of the sampled signal and to deal with phase noise of the oscillator providing the sampling clock<sup>14</sup>. This sampling speed cannot be provided with today's ADCs, see Section 4.1. Besides the estimated consumed power of 74 W for 1 pJ per resolution step according to Eq. (4.13) would render a conventional ADC architecture as unsuitable for automotive use. Nevertheless, as the concept of direct RF sampling is very promising for the given requirements, Chapter 4 does an in-depth investigation of the technical requirements and the actual state of technology and subsequently proposes, designs and analyzes a novel concept which unifies a direct sampling ADC with an innovative sampling concept.

At the same time, some preconditioning of the signals is necessary to make the signal *ADC compatible*. This preconditioning stage shall keep the frequency agility and reconfigurability that has been introduced by employing a suitable ADC concept. Chapter 5 introduces a new and highly flexible concept to provide a coexistence and interference management which allows sampling of received signals even in the presence of higher power interfering signals (which would cause blocking of the ADC) while retaining the concept's flexibility and agility.

### 2.3.1.2 Antenna System

The previously introduced UTM concept, which itself relies on an SDR approach, requires a very versatile antenna architecture, being able to send and receive information on many frequencies at the same time. Additionally, it should serve the requirements of the employed wireless services, like matching, radiation characteristics or coupling between antenna elements for all relevant frequencies. For the UTM approach, this requires the antennas to work within the frequency range of 600 MHz - 6 GHz.

Furthermore, the evolution of today's networks towards fifth generation (5G) communications systems includes the combination of human centric communication as well as machine-type communications with a massive amount of communicating nodes. One of the major technical challenges is to integrate the communication of ubiquitous things in mobile networks and to ensure strong availability<sup>15</sup> requirements of up to 99.999 % [45, 46], especially in the context of vehicular connectivity. Communication systems with only one common transmit and receive antenna, also referred to as Single Input Single Output

<sup>14</sup>Otherwise the sampling frequency would have to be *exactly* twice the maximum signal frequency to prevent aliasing.

<sup>15</sup>*Availability* is used as system availability or uptime.

Systems (SISO), fail in exchanging delay-sensitive information in a reliable manner. This system-inherent behavior intensifies in fading limited channels and is investigated in Chapter 3. By increasing the number of antennas within a MIMO system, it is possible to exploit higher data rates and increased reliability of the overall communication link, see e. g. [6, 58].

A vehicular antenna system can be characterized on different layers: On *impedance level*, each deployed antenna element shall be matched within its operating frequency (600 MHz - 6 GHz) range with its reflection coefficient  $S_{11} \leq -10$  dB. Subsequently, on the *radiation level* a certain radiation characteristic (like highly directive antennas versus omnidirectional antennas) may be required depending on the respective application or is evoked by the integration volume and its accompanying electromagnetic boundary conditions. In this work, the radiation characteristic is evaluated based on the realized gain [59], as it also includes losses inside the antenna structure and thus the antenna's efficiency. From a *system-level* point of view, the antenna architecture has to consist of a multiple element antenna (MEA) system to fulfill the need for high data rates and increased reliability<sup>16</sup>. Certain applications in the automotive domain have special requirements regarding these performance indicators, see Section 2.1. Multiple antennas have to be positioned in suitable integration volumes around the vehicle. For more in-depth information consider literature like [60–62]. As certain technical boundary conditions like correlation<sup>17</sup>  $\rho_{m,n}$  or coupling  $S_{m,n}$  between the  $n$ -th and  $m$ -th antenna elements apply especially on the system level, two major observations can be derived with focus on the antenna system:

**Observation 2.6.** *To fulfill the required needs with regards to the broad operating frequencies and simultaneous use for multiple wireless services, multistandard antenna concepts are necessary. These antenna concepts need to be able to be matched in the relevant frequency regions, ideally without a matching network<sup>18</sup>, offer suitable radiation characteristics and be capable of being integrated into or onto a vehicular platform within the automotive environment.*

Possible solutions for the challenges arisen within the observation above are introduced and discussed in Section 3.2 in detail.

<sup>16</sup>Even today, LTE-Advanced (Release 10) [30] already allows up to four antennas for the purpose of multiplexing and diversity.

<sup>17</sup>The correlation indicates, how independent two antenna patterns are. Refer to Section 3.4 for details.

<sup>18</sup>Antenna matching should ideally be done without a matching network, to keep the antenna efficiency as high as possible by avoiding electrical losses from a matching network.

**Observation 2.7.** *The antenna system serves as the air interface of the vehicle to connect to different services and is thus considered as the bottleneck of the overall system. Typical antenna performance indicators gained in a laboratory environment during the design process like return loss, coupling between antenna elements, radiation characteristic do not cover effects from vehicular integration and its impact on overall system performance.*

Since integration space is a scarce good, current vehicular antennas are often positioned close to each other in an antenna compartment on the roof top of the vehicle, possibly close to roof insets or edges of the roof. The low separation between antenna elements results in a strong performance deterioration with regards to the MIMO capabilities. This empirical statement is evaluated both qualitatively and quantitatively in Section 3.3. To the knowledge of the author, there is no evaluation methodology for automotive multi-element antenna systems published, which also comprises systems-level effects besides some general investigation e. g. in [58, 63] which can serve as a foundation, but have to be heavily adapted to the automotive domain by means of consideration of the vehicular integration volumes, high-mobility scenarios as well as special use cases and applications.

### 2.3.2 Technical-economical interpretation and Summary

An evaluation methodology for automotive MIMO antennas is presented in Section 3.3 of this thesis. Together with the results for novel frontend concepts, these findings lead to the new concepts of a distributed connectivity architecture for vehicular applications which is derived in detail in Section 3.4.

Besides the increased functionality and simplified realization, integration and implementation from a technical point of view, the economical angle shall not be neglected: a technical capability increase can of course cause an increase in hardware cost of the affected components. As an at least cost-covering if not even profitable approach is required, all concepts have to be checked for a positive or neutral business case. The function increase in this particular case can hardly be monetized from a customer's point of view. Usually, the customer is only interested in being provided with a certain level of connectivity as agreed beforehand. How that connectivity is achieved in particular is of minor interest for the user. On the other hand, from an OEM perspective especially enabler technologies, which are not directly visible to the customer, are at least of equal interest. A profitability analysis is not a focal point of this thesis, thus this topic is covered very briefly without being exhaustive.

Classical approaches like a cost-benefit analysis cannot be applied to an enabler technology, whereas the toolchain of a *cost-effectiveness* analysis relies on a non-monetary scale to quantify the degree of fulfillment and is thus referred to as *effectiveness* [64]. Identification of alternative architectures (here: centralized, decentralized, distributed), determination of all relevant input costs<sup>19</sup> as well as identification and acquisition of effectivenesses<sup>20</sup> allows for the calculation of the *cost-effectiveness ratio* (CER).

This thesis focuses on the technological aspects of the vehicular connectivity architecture and provides an in-depth investigation from a scientific and technological point of view. These results are presented and discussed in the following chapters.

A first business case analysis based on the presented methodology proved the two novel approaches (centralized and distributed architecture) as worth investigating from an economical perspective. Details are omitted here to focus fully of the technical analysis and to provide technologically novel solutions for the problem at hand.

---

<sup>19</sup>Examples for input costs are: engineering and development, homologation and certification, production, quality and warranty, logistics, packaging and mounting, cable harness

<sup>20</sup>Examples for effectivenesses are: power consumption, weight, volume, flexibility and reconfigurability, multi-standard capability / number of covered communication systems, enabling of forward compatibility, technical performance indicators from Chapters 4 and 3 like condition number, eigenvalue distribution, channel capacity, frequency range, signal-to-noise ratio, resolution



# Multiservice Multielement Antenna Systems for Automotive Use

# | 3

When discussing the ecosystem of vehicular connectivity in Chapter 2, it becomes clear, that realization of a highly-performant vehicular connectivity is subject to influencing factors both within the vehicular ecosystem as well as outside. Nevertheless, it is important to notice, that the area of the OEM's technical influence is limited to the configuration of the vehicular connectivity architecture. This chapter focuses on the antenna subsystem of the overall setup, which is introduced in Section 2.3.1.

Ongoing from Observations 2.6 and 2.7, the antenna system is seen as the air interface of the connectivity architecture and thus serves as one of the major bottlenecks within the overall architecture while at the same time, the integration space is heavily limited due to available space and acceptable weight accumulation in general, technical reasons like electromagnetic compatibility<sup>21</sup> and with growing importance due to aesthetical design constraints. These limiting factors heavily influence the selection of available options for antenna partitioning both with regards to multiservice capabilities as well as with regards to MIMO performance. This chapter first provides an analysis of the automotive integration space. Subsequently, concepts to realize multiservice antennas according to the requirements from Chapter 2 are briefly introduced and analyzed before focusing on partitioning and evaluation of antenna systems consisting of multiple elements for use in wireless MIMO communication systems. These antennas are referred to as multiple element antennas (MEA).

## 3.1 Integration Space Analysis

This section as well as the remainder of this work focuses only on antennas for bidirectional connectivity to and from the vehicle like denoted in Table 2.1 and no receive antennas for broadcasting systems. While sedan type vehicles

---

<sup>21</sup>In a vehicle with extensive special equipment for connectivity in general, broadcasting applications and new on-board networks required by either electromobility (featuring electric motors instead of combustion engines) and/or carbon fiber reinforced car bodies (demanding new conceptions of grounding), electromagnetic compatibility has to be considered carefully in a holistic approach.

usually feature a hard-top roof, which can be provisioned with a roof-top antenna, convertibles or coupés cannot feature an antenna on the roof for mechanical or design reasons respectively. These cars can lack a conductive and permanent roof within their design. This requires antennas to be integrated into other integration volumes than the conventional roof top position. In addition, MIMO antenna systems require a sufficient isolation between each antenna element. Separation of single elements distance-wise is one possible approach to reduce coupling between elements. Other techniques are discussed in Section 3.3.

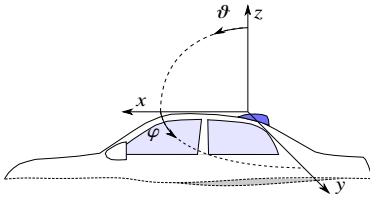


Figure 3.1 Vehicular coordinate system.

Despite these restrictions, the automotive working space allows for a variety of different antenna integration methods and spaces. Fig. 3.1 shows a unified coordinate system for the vehicle which serves as a reference for all further investigations. Table 3.1 summarizes integration spaces across the vehicle, which have been investigated

in the course of this work. The comments for each concept in said table are based on electromagnetic simulations on component, integration space and full vehicle layer. This multilayer approach allows for isolation of effects and model simplification to reduce the complexity of the model and is based on the one used for simulations performed for the results in Section 3.4.1. Further details are omitted here, but are partly published in [6, 7].

The integration volumes from Table 3.1 can be categorized into three major groups: location 7 (front and rear bumper) is close to the ground and proves to be challenging for use in cellular communications systems: the close proximity to the ground as well as the adjacent position to conductive car parts influences the performance of the antenna elements, mostly their matching behavior and the radiation characteristic, see e. g. [60, 62, 65]. The implementation of an omnidirectional system would require several antennas to be deployed around the vehicle due to the limited view of a single antenna in any of the spots 5 - 7. Following the principle, that higher antenna positions provide better performance with regards to omnidirectionality, positions 1 - 3 can serve as predestined antenna locations, whereas position 4 (trunk lid) offers a trade-off between availability (sedan-type cars versus convertibles or coupés) and exclusivity from a product design point of view, as for some vehicles, roof-top antennas might not be desired for aesthetic reasons. Usually, due to packaging



Table 3.1 Comparison of different different vehicular antenna integration volumes with focus on cellular and cellular applications. All visualizations are based on pictures with copyright by BMW Group.

No	Position	Evaluation	Visualization
1	rooftop sharkfin	highest spot on the vehicle, provides perfect omnidirectional / terrestrial as well as upward view, available cross car-line (except convertibles), size of roof or glass inlets must be considered	
2	wind guide / windshield	high spot with little shielding of the vehicular body, good view in driving direction, variety of integration / mounting concepts, e.g. below windguide or roll-over bar, on-screen in blackprint area	
3	spoiler / hang-on plastic parts	high spot with little shielding of the vehicular body, provides upward view, usually occupied by (diversity-) antennas for broadcasting	
4	plastics trunk lid	limited terrestrial and upward view, suitable for cellular services, impaired performance of satellite systems	
5	fixed side windows	covers left/right half-space, combination of left/right side provides high decorrelation, usually occupied by (diversity-) antennas for broadcasting	
6	rear-view mirrors	covers left/right half-space, combination of left/right side provides high decorrelation, very high integrational effort, limited performance (see Sec. 3.4)	
7	front & rear bumper	low position, no terrestrial view, spacious integration volume, impaired performance	

reasons, cellular (GSM, UMTS, LTE) and satellite (GNSS, SDARS) antennas are mounted together, while antennas for (actively transmitting) cellular systems are mounted apart from antennas for the reception of broadcasting systems. Otherwise, these systems would interfere with each other, see Chapter 5. For all positions, besides the arrangement with regards to the vehicle itself, the influence of the integration volume always has to be considered. For example for the otherwise perfect roof-top antenna, the installation of a glass panoramic roof minimizes the available metallic ground plane and thus might change the performance of the mounted antennas<sup>22</sup>.

**Observation 3.1.** *Due to integration onto the vehicle or into the vehicle body, the antenna performance is subject to integration effects [9]. The most dominant effects are roof curvature, cable losses, edge diffraction, the type of vehicle (like sedan or convertible) as well as the size of the roof which is available for use as groundplane.*

These effects have to be taken in account when designing a vehicular antenna system. This can be done either by measurement or by using tools for numerical field simulation.

**Observation 3.2.** *Increasing the spatial separation of single vehicular antenna by moving the elements towards irregular structures of boundaries of the vehicle can cause a deformation of the radiation patterns. This deformation influences the antenna's receive and transmit ability.*

In the context of MIMO antenna systems, a decentralized antenna system consisting of multiple single antenna elements might be desirable - this concept is investigated in Section 3.3. Nevertheless, the automotive antenna engineer has to find the best approach and architecture to fulfill electromagnetic, performance, mechanical and design requirements, as they might contradict each other and setup an area of conflict.

## 3.2 Multiservice Antenna Concepts

This section is introducing and discussing suitable multistandard antenna concepts to fulfill the requirements from Section 2.3.1 which are can be

---

<sup>22</sup>Example: besides cellular antennas, the shark-fin also comprises a patch antenna for GNSS and SDARS services. To create a sufficiently large groundplane, the glass panoramic roof of an exemplary vehicle (2015 BMW 7 series) has been equipped with an indent towards the antenna, see Table 3.1, first row.

generalized to be working working for frequencies between 600 MHz and 6 GHz and thus enabling multistandard operation according to Section 2.1 while at the same time fitting into suitable integration volumes.

In the following, different concepts and techniques for multistandard antennas are presented together with their advantages and disadvantages based on findings within this work as well as literature.

Table 3.2 Comparison of different antenna types potentially capable of providing multistandard functionalities.

Antenna Type	Operating Mode	Properties	References
Reconfigurable Antennas	RF switches (e.g. MEMS) change the behavior of the antenna to fit to the current operating mode.	can be combined with other types of antennas, slow due to switching time between the modes, limited lifetime.	[60, 61, 66]
Logarithmic-periodic Antennas	almost frequency independent antenna with self-complementary structures and artificially elongated edges	very broadband structure, unable to work on a groundplane due to self-complementary operating mode	[61, 67, 68]
Multimode Antennas	Finite conductive surfaces being excited at points corresponding to their eigenmode distribution	facilitated integration possible by reusing already present surfaces, vehicle dependent adjustments necessary	[69–71]
Broadband Monopole Antennas	tapered monopole, the maximum length of the outer edge of metallization determines the lowest possible working frequency	requires sufficiently large conductive surface as groundplane, size is within orders of 0.25λ	[11, 27, 72–76]
Multiresonant Antennas	systems with more than one resonance, made specifically for preselected frequency regions	little flexibility, required frequencies need to be predetermined, miniaturization concepts are applicable	[9, 11, 61, 66, 77]
Single Antennas	status quo of current decentralized antenna architecture, every service is located at a certain position inside the vehicle	all relevant frequencies and systems can be realized in parallel, cross-talk and decentralized system pose inherent challenges (see. Sec. 2.2)	[60, 61]

As previously stated, these antennas have to be integrated into the automotive space and have so fulfill the respective technical requirements. These are in particular:

- broadbanding capability, to cover all necessary frequency bands,
- miniaturization capability, to fit within the respective integration spaces,

- parallel usability, to allow simultaneous processing of different wireless services,
- conformity with the automotive environment, to be able to mount and use the antenna within an automotive environment during the lifetime of the vehicle and
- directional characteristics, to be able to work within the constraints of an omnidirectional, terrestrial coverage.

Polarization purity is neglected here as in all real-life scenarios the polarization is shifted due to scattering effects of the channel [78].

The antenna concepts used within this work are mostly based on hybrid architectures where broadband antenna structures are combined with dedicated resonances, e. g. by adding either resonant length of conductive material or slots to the overall structure. As the focus has been set to interactions of these antennas in MIMO systems, refer to the references cited in Table 3.2 for further general information and [9, 11] as well as Chapter 3.4 for particular information on the antenna concepts used for the analysis within this work.

As a state of the art system, the concept introduced in [11, 27] has been improved and is taken as a reference antenna for all further investigation. In the context of above Table 3.2, the reference antenna is hybrid structure and comprises the operating principles of both multiresonant and broadband antennas. The concept is depicted in Fig. 3.2.

The design process is two-stepped: Firstly, ongoing from the findings in [9, 11], the chosen concept is based on a hybrid approach according to Table 3.2 and combines broadband functionality with multiresonant structures to implement a multistandard antenna prominently for cellular communications. The broadband component is realized with a widened monopole in a V-shape<sup>23</sup>, which allows broadband operation<sup>24</sup> for frequencies above roughly 1.6 GHz. The finite length of the structure limits its broadband behavior [61]. To also cover lower frequencies below 1.6 GHz, two designated resonances at

lower frequencies are appended by adding a shortened topload (roof capacity with parallel inductance by shorting pin) and an additional coupled slot, see Fig 3.2. This first step assures multistandard capabilities by covering all necessary frequencies, either by the broadband or the multiresonant working components of the antenna system. Secondly, the antenna has to be fit into the automotive integration space, thus has to be miniaturized, as the edge length of a monopole-like structure of  $\lambda/4$  at the lower boundary frequency being  $\lambda_{600\text{ MHz}}/4 = 0.125\text{ m}$  already exceeds any available construction space as discussed in Chapter 2. Two different options exist to miniaturize a monopole antenna: there are planar approaches that have the advantage to be printable on a plan printed circuit board (PCB), and there are volumetric approaches, that use the whole three-dimensional space to achieve the set goal. They can be more effective than planar approaches due to an added degree of freedom. Besides miniaturization by deforming the metalized surfaces appropriately, volumetric designs also allow for improved performance on impedance, radiation and system level, e. g. by including parasitic elements for beamshaping, see [11] or improving the arrangement of multiple antenna elements within a MIMO antenna system for



Figure 3.2 Realized prototype of a surface modulated broadband monopole with shorted top-load and additional slot.

<sup>23</sup>Theoretical considerations and simulative investigations show, that the highest surface current density is alongside the resonating edges, thus the inner metallization can be omitted, cf. [60, 79] in general and [11] in particular for the present case.

<sup>24</sup>The operating frequency range of the antenna is determined based on the criteria stated in Section 2.3.1, in short:  $S_{11} \leq -10\text{ dB}$  and omnidirectionality based on the realized gain.

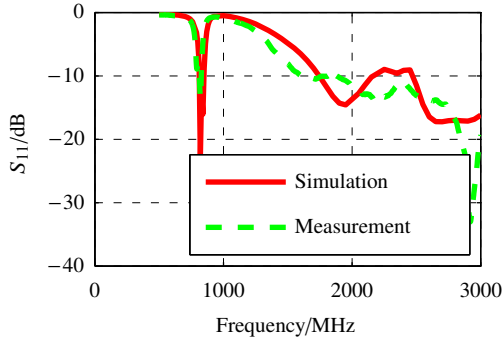


Figure 3.3 Return loss  $S_{11}$  of the reference antenna. Note the two overlain resonances to cover lower frequencies as well as the broadband behavior for higher frequencies.

increased system performance like shown also in [11] and evaluated in [9]. The combination of a broadband component together with two additional resonances to cover lower frequencies is visible in the antenna's return loss as shown in Fig. 3.3. The resonances of the roof capacity and shorting pin (behaving like an LC-circuit) as well as the additional slot are positioned closely to each other and ensure matching of the antenna within band 20. For frequencies above 1.6 GHz the broadband monopole starts to work and ensures matching for mid and high band frequencies. The composition of these operating principles ensures a multiband matching of at least  $-10$  dB for all relevant frequencies. Both the return loss measurement as well as the antenna's realized gain as shown in Fig. 3.4 have been determined for an implementation of the antenna based on a prototype Laser Direct Structuring (LDS) process mounted on a groundplane of  $250 \times 250 \text{ mm}^2$  size.

### 3.3 Partitioning and Evaluation of MIMO Antenna Systems

General requirements for the use of MIMO antenna systems in the automotive domain have been discussed empirically in Section 2.3.1 and have led to Observation 2.7 which states, that the antenna system in general serves as the air interface to between vehicle and radio communications systems and is thus considered as one of the major bottlenecks of the overall connectivity system.

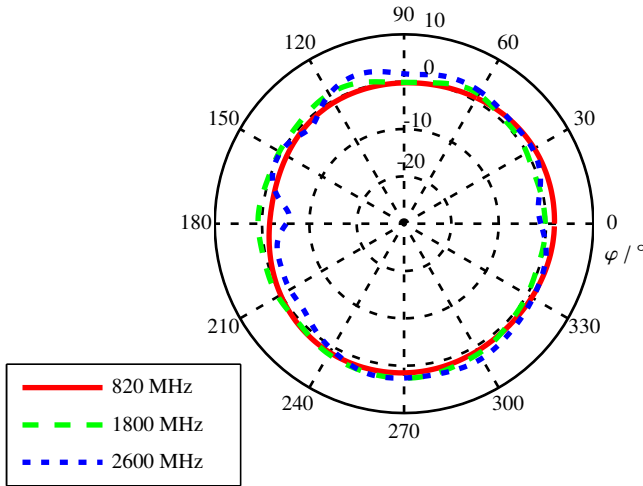


Figure 3.4 Measured realized gain of the 3D surface modulated top-loaded and shorted broadband monopole with an additional slot at an elevation of  $\vartheta = 70^\circ$ .

Summarizing the insights discussed within the previous section as well as the findings from [6, 9], Observation 2.7 can be refined and extended as follows:

**Observation 3.3.** *The physical layer of a wireless communication system with the antenna system being the bottom most part of it (in terms of the ISO OSI reference model [4]), the antenna architecture is considered the bottleneck of the overall architecture. All performance lost here cannot be compensated in higher layers. Thus special attention has to be paid when specifying and partitioning the antenna system. In the context of vehicular connectivity this task can become challenging, as integration space is limited due to mechanical, aesthetic and functional restrictions.*

This observation leads to

**Proposition 3.1.** *To account for the performance not only on component or integration level of the antenna system, an automotive multi-element antenna system has to be evaluated on the system level to account for factors, which influence the overall system performance. The assessment based on key performance indicators determined on impedance and radiation level is not sufficient.*

These limits may lead to an area of conflict between desired requirements and the limits of physics and electromagnetism and call for a methodical prioritization of requirements and careful proceeding. The following section describes the behavior of MEA in general and subsequently derives performance indicators to evaluate antenna systems for use in MIMO applications. Based on these information, a novel and holistic methodology for automotive multi-element antenna systems evaluation, which also comprises systems-level effects is developed and described.

It is the goal of this section to first find a way to describe the influence of a MIMO antenna system on overall system's performance with special regards to the limits and possibilities of the automotive integration domain. During the work of this thesis, besides theoretical analysis, extensive simulation and measurement campaigns have been performed to generate evaluation data. In order to fully lay out the exploitation the problem at hand, again a three step approach for description is chosen to structure the current section: The following Section 3.3.1 describes a system model of a MIMO channel for vehicular use from an analytical point of view and focusses on modeling of both the fading as well as specific MIMO properties of the communication channel while always considering the automotive integration space<sup>25</sup>. Subsequently, Section 3.3.2 introduces novel performance indicators to evaluate an MEA, again with focus on the vehicular domain. Their behavior is briefly evaluated numerically in Section 3.3.3. The application of the derived key performance indicators (KPI) for real-live measurement campaigns is covered in Section 3.4.

### 3.3.1 Preliminaries: Model of a Vehicular MIMO System

The laws of physics strongly dominate the performance of wireless communications systems. Radio systems rely on information transportation by electromagnetic waves from source to sink. The propagation characteristics of these electromagnetic waves directly influence the performance and reliability of the system. These phenomena can be characterized as *free space propagation*, where no objects are influencing the waves as well as *reflection*, *scattering* and

<sup>25</sup>Anticipated information for clarity: Usually, general literature considers MIMO antenna systems either in handheld-like devices like cell phones, tablets and laptops or in the context of array antennas, e. g. for massive MIMO or beamforming. Obviously, the integration volumes of a vehicle differ from the ones of the previously stated devices. The spaces named in Section 3.1 allow to integrate multiple antennas into one volume or to distributed the antennas into different spaces. This thought is followed in this Section and supported by measurements in Section 3.4.



*diffraction* which describe the interaction of electromagnetic waves with objects surrounding the transmitter and receiver respectively. The interaction between impinging waves and these object completely determines wave propagation. Throughout this work, these objects are referred to as *scatterers*. Thus, full knowledge about position and state of these scatterers together with infinite calculating power would allow an exact description of this scenario by solving Maxwell's equations [80] at the transmitter's and receiver's side.

According to the definition in [81] of the radio channel as being the physical medium which is defined by the set of all relevant scatteres and their properties, the radio communication channel can be denoted as a *physical channel* from this point of view. The ultimate goal of the deployment of a vehicular MIMO antenna system and the analysis of its performance within a channel is to provide connectivity for various applications inside the vehicle. Under these circumstances, it is necessary to view the channel as a *bitpipe* which leads to an abstraction of the detailed physical model to a model on system level. This system level model is denoted as *analytical channel*. By considering the analytical point of view, the focus of the evaluation is set on the exchange of information (which can be described e. g. by throughput, latency, reliability etc.) based on signals. Due to the level of abstraction, an exact description of the wave propagation is not necessary and can be neglected [6, 7]. This can be exemplified as follows: within the physical model, the exact positioning and orientation as well as further impedance and radiation level parameters of an antenna are relevant for predicting the behavior of the antenna system, while within the analytical model the correlation between all antenna elements is sufficient to predict the system's performance<sup>26</sup>.

Now, to model a radio channel, the interactions of the electromagnetic waves with the environment (e. g. scatterers) have to be taken into account. Generally, these interactions cause rapid signal fluctuations with dependency on time, space (position) and frequency and are described as *fading* and are separated into large-scale and small-scale fading [85, 86]. Large-scale fading describes the average attenuation of signal power due to the separation of transmitter and receiver over large areas and distances and ignore phase variation e. g. due to waves impinging from different directions due to multipath. When large-scale fading properties cannot be considered as time-invariant and non-stationary, *shadowing* is introduced by using some kind of probability distribution [81, 85]. As the separation between vehicular antennas is short in relation to the propagation

---

<sup>26</sup>Literature like [82–84] shows approaches for this abstraction.

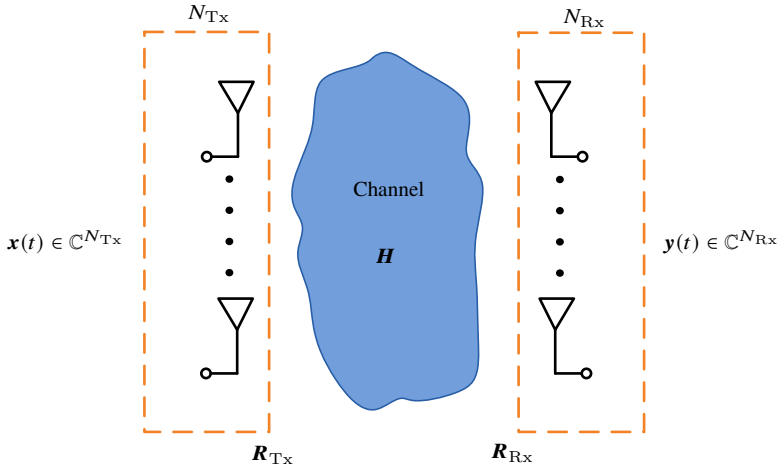


Figure 3.5 Setup of a general MIMO channel with multiple transmitting and receiving antenna elements.

distance, the large-scale fading properties are considered equal. Each antenna experiences the same large-scale fading influence [86]. On the other hand, small-scale fading describes all effects due to rapid changes in amplitude and phase. These changes occur again due to the interaction of the information carrying electromagnetic waves with the object in the channel between transmitter and receiver. These electromagnetic interactions cause multipath propagation, where the superposition of the distinct multipath components leads to rapid fluctuation referred to as small-scale fading. It is mostly characterized by the Doppler spectrum which defines the rate of these random changes. The time in which the channel stays approximately constant is denoted by the coherence time. These values and thus the behavior of the small-scale fading is influenced by e. g. the absolute speed of one terminal, the relative speed to the surroundings, the bandwidth of the signal under investigation and the characteristics of the multipath propagation environment (like a non line of sight rich scattering environment versus a line of sight free space scenario)<sup>27</sup>.

Within this work, the focus is set on the analysis and investigation MIMO

<sup>27</sup>This enumeration gives just general examples to illustrate the channel's influence and is by far not concluding. Refer to general mobile and wireless communications literature like [85–87] for further information on the fading mechanisms and their statistical description.

systems, the general system setup is shown in Fig. 3.5 where  $N_{\text{Tx}}$  antennas are used at a transmitter and  $N_{\text{Rx}}$  antennas are used at a receiver. The channel is considered as a flat-fading, non frequency-selective, narrowband channel<sup>28</sup>. This assumption allows the complex  $N_{\text{Rx}}$ -dimensional receive signal vector  $\mathbf{y}(t) \in \mathbb{C}^{N_{\text{Rx}}}$  to be represented by mapping the complex  $N_{\text{Tx}}$ -dimensional transmit signal vector  $\mathbf{x}(t) \in \mathbb{C}^{N_{\text{Tx}}}$  with a stochastic channel matrix  $\mathbf{H}$ . The channel is considered frequency-flat, is assumed to be linear and can then be modeled at any instant with the complex channel matrix  $\mathbf{H} \in \mathbb{C}^{N_{\text{Rx}} \times N_{\text{Tx}}}$  whose entries  $h_{ij}$  describe the gain from the  $i$ -th transmit antenna to the  $j$ -th receive antenna. The transmission model can be written as

$$\mathbf{y}(t) = \mathbf{H}\mathbf{x}(t) + \sigma^2\mathbf{n}(t), \quad (3.1)$$

where the influence of additive white Gaussian channel noise is denoted by  $\mathbf{n}(t) \in \mathbb{C}^{N_{\text{Rx}}}$  which is represented by complex circularly Gaussian independent identically distributed (i.i.d.) entries with zero mean and variance  $\sigma^2$ .

Now, to model  $\mathbf{H}$  and thus the MIMO channel, one of the most prominent channel models in literature is used: the Kronecker Model, which is presented in [84] and evaluated e. g. in [82, 83]: the Kronecker Model in general appears to slightly underestimate the channel capacity (see Section 3.3.2), mostly for systems with  $N \geq 4$ . Nevertheless, a trade-off has to be made considering the accuracy as well as the simplicity to derive the channel matrix  $\mathbf{H}$ . A detailed derivation of the Kronecker Model is described in [81] based on the theoretical approach of eigenmode tensors. Eigenmodes allow for a description of the channel from different viewpoints, not the overall channel itself. Moving on from this approach, simplifications lead to the Weichselberger Model, which can be seen as a generalized form of the Kronecker Model and introduces a correlation matrix  $\mathbf{R}_{\text{H}}$  which is specific for the channel  $\mathbf{H}$ . Further abstraction finally lead to the Kronecker Model, where the overall channel correlation  $\mathbf{R}_{\text{H}}$  is separated into a transmitter side correlation  $\mathbf{R}_{\text{Tx}}$  and a receiver side correlation

---

<sup>28</sup>This assumption requires, that the propagation delay differences of the multipath components detected at the receiver are negligible compared to the symbol interval [86]. Furthermore frequency-flatness applies especially to radio systems where OFDM is used, as the narrowband subcarriers experience the channel as not frequency selective.

$\mathbf{R}_{\text{Rx}}$  and allows to compute  $\mathbf{H}$  as follows

$$\mathbf{H}_{\text{Kron}} = \frac{1}{\sqrt{P_{\text{H}}}} \mathbf{R}_{\text{Rx}}^{1/2} \mathbf{H}_{\text{w}} \mathbf{R}_{\text{Tx}}^{1/2} \quad (3.2)$$

$$\mathbf{R}_{\text{H,Kron}} = \frac{1}{P_{\text{H}}} \mathbf{R}_{\text{Tx}} \otimes \mathbf{R}_{\text{Rx}}, \quad (3.3)$$

where  $P_{\text{H}}$  is the total channel power and  $\mathbf{H}_{\text{w}}$  is the random fading matrix consisting of independent identically distributed (i.i.d.) random distributed elements. The Kronecker Model is based on the assumption, that the correlation of the overall radio channel can be decomposed into two one-sided receiving and transmitting correlation matrices, which are linked by the Kronecker product (denoted by the symbol  $\otimes$ ). The high level of abstraction and the descriptive nature of the model allow for a more detailed investigation of the performance measure introduced in the following sections and their application for the evaluation of multi-element antenna systems.

### 3.3.2 Derivation of Performance Indicators for Automotive MIMO Antennas

Based on the definition of the linear MIMO transmission channel given in Eq. (3.1) and the description of the channel matrix  $\mathbf{H}$  based on the Kronecker Model, this section introduces a methodology for evaluation of MIMO antennas on the system level of the overall communications system, which includes the influence stated previously in this chapter as well as in Observation 2.7. Note that the concept of the Kronecker Model, namely the separation of the overall channel correlation  $\mathbf{R}_{\text{H}}$  into a transmitter side correlation  $\mathbf{R}_{\text{Tx}}$  and a receiver side correlation  $\mathbf{R}_{\text{Rx}}$ , is key for the following concepts, as it allows to specifically focus on the vehicle side of the transmission channel. Section 2.3.1 has already given a brief overview of the necessity and status quo of (vehicular) antenna evaluation, which is now reprised and subsequently extended.

According to [6], antenna evaluation can be performed on different layers and levels of the overall communications and RF chain, cf. Fig. 3.6. The figure visualizes, on which levels the antenna system can be characterized. Most prominent in the context of antenna evaluation is the radiation and impedance level. Here, characteristic values like return loss  $S_{ii}$ , coupling between elements  $S_{ij}$  and the radiation characteristic e. g. based on realized gain  $C_{\text{real},i}(\vartheta, \varphi)$  can be determined. The IEEE Standard [59] provides an overview of common performance criteria, further information can be found in textbooks

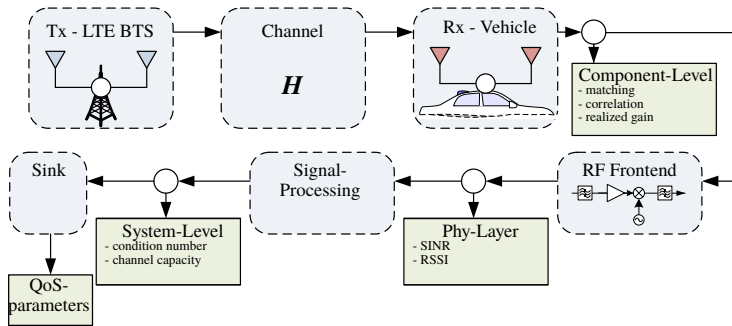


Figure 3.6 Visualization of the receive signal chain including the exploitation of performance indicators on radiation, impedance and system level [6], © 2014 IEEE.

like [60–62, 85, 87]. These performance indicators allow an evaluation of the antennas on component and vehicular level: for example an antenna element can be characterized on a reference groundplane as well as within its vehicular integration volume to make the integration effects visible and to allow for antenna optimization based on the integration domain's influence on component level. However, these performance indicators do not allow to assess the overall system performance, especially when MIMO or diversity techniques are used as shown and discussed in [6, 9]. Here, system level performance indicators are needed. They allow to evaluate the antenna system based on the overall system performance by taking the full communication chain into account. If input values other than the antenna system under test are known or set constant, it is possible to draw conclusions on the performance of the antenna system within its environment. When considering a MIMO communications system like assumed in Fig. 3.6 its performance is mostly characterized by the channel matrix  $H$  which incorporates both the transmit and receive antenna system within the transmit and receive correlation matrices  $R_{Tx}$  and  $R_{Rx}$  respectively when examined in the context of the Kronecker Model. The receive-side antenna system determines the setup of  $R_{Rx}$ . Thus again, based on the assumption of the Kronecker Model, it is possible to investigate an antenna system under test on system level, by evaluating the channel matrix  $H$  as long as all other factors, which influence  $H$  are known for an absolute evaluation or set constant for a relative or comparative evaluation.

**Proposition 3.2.** *Values on impedance and radiation level alone are not sufficient*

to determine the overall performance of a MIMO antenna system, especially in the automotive domain, where challenges with regards to integration and requirements with regards to guaranteed performance like data rate, reliability and availability arise. Thus, further key performance indicators which allow an evaluation on system level need to be considered.

Now, three system level key performance indicators are introduced which firstly determine the overall performance and secondly also incorporate integrational effects as well as typical MIMO performance due to the required decorrelation of the antenna elements, either by spatial separation or other means.

### 3.3.2.1 Ergodic Capacity

The *ergodic capacity* defines the maximum amount of information, which can be reliably<sup>29</sup> transmitted over the channel. This requires perfect channel knowledge (CSI, channel state information), thus knowledge of the entries  $h_{i,j}$  of the channel matrix  $\mathbf{H}$  both at the transmitter and the receiver which can be determined by evaluation of pilot symbols<sup>30</sup> or channel estimation techniques, see e. g. [88, 89].

Based on the assumption, that  $\mathbf{H}$  is constant over a time period which is longer than the transmission time of a given datablock, then the channel capacity  $C_{\text{erg}}(\sigma^2)$  is given as the maximum of the mutual information  $\mathcal{I}(\sigma^2, \mathbf{P})$ :

$$C_{\text{erg}}(\sigma^2) = \max_{\mathbf{P}} \mathcal{I}(\sigma^2, \mathbf{P}) \quad (3.4)$$

with  $\mathbf{P} \in \mathbb{C}^{N_{\text{Tx}} \times N_{\text{Rx}}}$  being the covariance matrix of the transmitted signal. For a Gaussian vector channel, the mutual information is given by

$$\mathcal{I}(\sigma^2, \mathbf{P}) = \log_2 \det \left( \mathbf{I}_{N_{\text{Rx}}} + \frac{1}{\sigma^2} \mathbf{H} \mathbf{P} \mathbf{H}^\dagger \right). \quad (3.5)$$

Note, that  $\text{tr}(\mathbf{P}) \leq P$  and  $\mathbb{E}_{\mathbf{x}}[\mathbf{x} \mathbf{x}^\dagger] = P$  where  $\mathbb{E}[\cdot]$  calculates the expectancy value and  $P$  is the maximum transmit power. Now, if  $P$  is distributed equally over all  $N_{\text{Tx}}$  transmit antennas, thus no techniques like waterfilling are used,

<sup>29</sup>Reliable means, that the probability of error can be minimized.

<sup>30</sup>Transmission of pilot symbols known to the transmitter and receiver and subsequent calculation of the autocorrelation  $S_{x,x}$  and  $S_{y,y}$  of the transmitted and received pilot symbols respectively allow for the determination of the channel matrix based on the Wiener-Lee-Theorem  $S_{y,y} = |\mathbf{H}(j\omega)|^2 \cdot S_{x,x}$ .

then the ergodic capacity can be rewritten as

$$C_{\text{erg}}(\sigma^2) = \mathbb{E}_{\mathbf{H}} \left[ \log_2 \det \left( \mathbf{I}_{N_{R_x}} + \frac{P}{N_{T_x} \sigma^2} \mathbf{H} \mathbf{H}^\dagger \right) \right]. \quad (3.6)$$

If  $\mathbf{H} \mathbf{H}^\dagger$  is diagonalized by performing an eigenvalue decomposition and thus the eigenvalues  $\lambda_i$  of  $\mathbf{H} \mathbf{H}^\dagger$  are computed, then Eq. (3.6) can be simplified to

$$C_{\text{erg}}(\sigma^2) = \mathbb{E}_{\mathbf{H}} \left[ \sum_{i=1}^{N_{\min}} \log_2 \left( 1 + \frac{P}{N_{T_x} \sigma^2} \lambda_i \right) \right], \quad (3.7)$$

where  $N_{\min} = \min(N_{R_x}, N_{T_x})$ , see also [6,58]. As the channel matrix  $\mathbf{H}$  follows a specific probability distribution function, the channel capacity itself becomes a random variable. By taking the expectancy value over the channel realizations, the ergodic capacity delivers the expected value of the mutual information. The eigenvalue decomposition of  $\mathbf{H} \mathbf{H}^\dagger$  represents the decomposition of the MIMO channel into up to  $N_{\min}$  subchannels indexed by  $i$ , each of which has the subchannel-gain  $\lambda_i$ . The overall capacity equals the sum of the subchannel capacities, each of which depend on its respective  $\lambda_i$  as shown in Eq. (3.7). Thus, each non-zero subchannel (or eigenchannel, eigenmode) contributes to the total channel capacity. By employing Jensen's inequality [90], the optimal eigenvalue distribution maximizing the ergodic capacity can be derived, given that still uniform power allocation (and no waterfilling) is used:

$$\frac{1}{N_{\min}} \sum_{i=1}^{N_{\min}} \log_2 \left( 1 + \frac{\gamma}{N_{T_x}} \lambda \right) \leq \log_2 \left( 1 + \frac{\gamma}{N_{T_x}} \left( \frac{1}{N_{\min}} \sum_{i=1}^{N_{\min}} \lambda_i \right) \right), \quad (3.8)$$

where  $\gamma$  corresponds to the signal to noise ratio (SNR) and equality is given only if the eigenvalues  $\lambda_i$  are all equal.

The ergodic capacity can be used to quantify the performance of a communication system. Remember, that the channel capacity denotes the maximum possible transformation of the channel and considers perfect coding, modulation and securing quality of service (QoS) mechanisms. However, if delay-sensitive information needs to be transmitted, the ergodic channel capacity cannot be used as it does not account for outages: with perfect QoS techniques retransmissions guarantee, that all information will be transmitted, if necessary after an unlimited number of retransmissions.

**Proposition 3.3.** *To support delay-sensitive traffic, it is important, that also the physical layer can handle delay requirements. Here, the physical layer is*

again considered the bottleneck of the overall communications system. Thus, performance indicators accounting for these delay-related requirements and constraints have to be introduced and used for system assessment.

### 3.3.2.2 Zero-Outage Capacity

With the increasingly high entry of digitization in the automotive domain and the introduction of corresponding applications, the connectivity of the vehicle as the enabler for these applications is of high importance, see Chapter 2. Besides high data rates, certain applications and use-cases cause delay-sensitive traffic which requires a minimum QoS with regards to reliability and availability. Following the paradigm, that the physical layer is one bottleneck of the wireless communication system connecting the vehicle e. g. to an OEM's backend, it is of special importance, that the lower layers (especially the physical layer) can handle delay requirements<sup>31</sup>.

The previously introduced ergodic capacity describes the information transmission over a channel in average. However, it does not ensure, that a piece of information is transmitted within a fixed a time frame without possibly requiring a certain number of retransmissions. For many automotive-related applications it is necessary to ensure a specific data rate  $R$  for a predefined number of channel realizations. The outage probability is then fixed to a specific value

$$\Pr [C(\mathbf{H}) < R] = \epsilon. \quad (3.9)$$

Setting  $\epsilon = 0$  leads to the definition of the zero-outage capacity as the data rate, that can be *reliably supported in any fading state  $\lambda$  of the channel  $\mathbf{H}$* , cf. [91]:

$$\Pr \left[ \log_2 \left( 1 + \frac{\gamma}{N_{\text{T}_x}} \lambda_i \right) < C^*(\gamma) \right] = 0. \quad (3.10)$$

In order to prove the importance of consideration of the zero-outage capacity as well as the relevance of antenna systems with multiple elements for diversity and multiplexing, the concept of Eq. 3.9 with  $\epsilon = 0$  is applied to a SISO channel which relates to a vehicle with only one antenna for cellular services. In an urban environment with rich scattering an no line of sight between base station

<sup>31</sup>Of course, the appropriate design of higher layers also plays an important role to handle delay requirements. However, higher layers cannot compensate for performance lost in lower layers.



and the vehicle's antenna, the small scale fading can be modeled with a Rayleigh distribution [92].

The channel capacity  $C_{\text{SISO}}$  for a SISO system is defined by the well known Shannon formula [58] and can be derived from Eq. (3.7) by setting  $N_{\text{min}} = 1$ . The resulting equation after channel inversion inversion to include fading properties is given by

$$C_{\text{SISO}} = \log_2 \left( 1 + \frac{\gamma}{\int_0^\infty \frac{f_p(p)}{p} dp} \right). \quad (3.11)$$

The instantaneous power of a rayleigh fading signal<sup>32</sup> is given by the probability density function (PDF)

$$f_p(p) = \frac{1}{\sigma^2} \cdot e^{-\frac{p}{\sigma^2}} \quad (p \geq 0), \quad (3.12)$$

with  $\sigma^2$  being the expected local receive power. Inserted into above equation for  $C_{\text{SISO}}$ , the integration in the denominator tends to infinity causing  $C_{\text{SISO}} = 0$ . Applied to the example of a vehicle with only one antenna for cellular connectivity in an urban environment with non line of sight (NLOS) conditions a SISO operating mode cannot guarantee a non-zero channel capacity.

**Observation 3.4.** *For SISO systems within Rayleigh fading channels, no non-zero capacity can be ensured. This renders single antenna connectivity as not valuable for delay-sensitive applications or any application that requires successful transmission of messages within a finite time. This restriction can be circumvented by employing multiple antennas and thus exploiting the performance gain of MIMO systems in terms of diversity improving reliability and/or multiplexing increasing throughput.*

### 3.3.2.3 MIMO-Efficiency

The channel capacity in general is directly influenced by two factors: the SNR and the distribution of the eigenvalues  $\lambda_i$ . Thus, the channel capacity combines

<sup>32</sup>Rayleigh fading occurs in rich scattering environment with a large number of independent and identically distributed (i.i.d.) impinging waves, whose in-phase and quadrature components are random Gaussian variables with zero mean and variance  $\sigma^2$  and a uniform phase, see Sec.

3.3.1. The probability density of its amplitude is given by  $f_\alpha(\alpha) = \frac{2\alpha}{\sigma^2} \exp\left(-\frac{\alpha}{\sigma^2}\right)$ .

the influence of receive power, noise and possibly interference by considering the SNR as well as the partitioning of the MIMO system by taking the eigenvalues and their distribution into account, cf. Eq. (3.6)-(3.8). MIMO systems usually transmit multiple spatially separated data streams simultaneously. Subsequently it is important to quantitatively evaluate the ability to extract the received data from a noisy signal [63]. The quality of data retrieval is dependent of the *conditioning* of  $\mathbf{H}\mathbf{H}^\dagger$  and can be denoted by the condition number (CN)  $\kappa$  and is defined as the ratio of the maximum and minimum eigenvalue:

$$\kappa = \frac{\lambda_{\max}}{\lambda_{\min}}, \quad (3.13)$$

where  $\lambda_{\max}$  and  $\lambda_{\min}$  are the largest and smallest eigenvalue of  $\mathbf{H}\mathbf{H}^\dagger$  [6,9]. The CN takes values according to  $1 \leq \kappa < \infty$ . For  $\kappa = 1$ , the eigenvalues are equal to each other and maximizes the channel capacity, see Jensen's inequality in Eq. (3.8) which maximizes the capacity for equal eigenvalues  $\lambda_i$ . In contrast, if  $\kappa \rightarrow \infty$ , there exists only one eigenvalue and subsequently only one virtual subchannel. This scenario is equal to a SISO channel.

An additional performance indicator to characterize the MIMO capability of a wireless communication system is the eigenvalue distribution (ED). It is defined as the quotient of the geometric mean and arithmetic mean of the eigenvalues of  $\mathbf{H}\mathbf{H}^\dagger$ :

$$ED = \frac{\left(\prod_{k=1}^K \lambda_k\right)^{1/K}}{\frac{1}{K} \sum_{l=1}^K \lambda_l}, \quad (3.14)$$

where  $K$  equals the number of non-zero eigenvalues [7,93]. The domain of the eigenvalue dispersion ranges from zero to one with  $0 \leq ED \leq 1$ . Here,  $ED = 1$  represents an optimum channel for multistreaming, while  $ED = 0$  disables multistreaming, as only one subchannel is present.

For the channel capacity, the zero-outage capacity serves as a worst-case performance characteristic indicating the minimum throughput which can be guaranteed in any fading state. To quantify the ability to support multistreaming under worst-case MIMO channel conditions, a worst-case condition number  $\kappa_{wc}$  and eigenvalue distribution  $ED_{wc}$  can be calculated as the maximum or minimum

value of Eq. (3.13) and (3.14) respectively over all channel realizations:

$$\kappa_{\text{wc}} = \max \left( \frac{\lambda_{\max}}{\lambda_{\min}} \right), \quad (3.15)$$

$$ED_{\text{wc}} = \min \left( \frac{\left( \prod_{k=1}^K \lambda_k \right)^{1/K}}{\frac{1}{K} \sum_{l=1}^K \lambda_l} \right). \quad (3.16)$$

Before applying these performance indicators for the evaluation of vehicular antenna systems in Section 3.4 the following section analyzes the numerical characteristics of all introduced performance indicators and gives a broad understanding of their behavior and sensitivity. Additionally, a brief comparison between the MIMO capability characterizing condition number and eigenvalue dispersion is given to distinguish them from each other.

### 3.3.3 Numerical Evaluation of Performance Indicators

In the previous section, two measures to characterize the MIMO capability of a wireless MIMO channel have been defined besides the ergodic and zero-outage channel capacity. The condition number only considers two eigenvalues, independently of the order of the MIMO system, while the eigenvalue distribution takes all non-zero eigenvalues into account, not only the largest and smallest eigenvalue. This allows for a more precise gradation, especially when higher order MIMO systems are investigated. Furthermore, the domain of the eigenvalue dispersion is finite. Thus, often linear scaling is used when plotting the eigenvalue dispersion whereas the condition number is usually calculated and displayed in decibel.

Both performance indicators are calculated and plotted in Fig. 3.7 for a  $3 \times 3$  MIMO system. The sum of the eigenvalues is calculated as the trace of a matrix according to  $\text{tr}(\mathbf{H}\mathbf{H}^\dagger) = \lambda_1 + \lambda_2 + \lambda_3$  and is set to a constant value of 3 to have an arrangement of eigenvalues which allows a fair comparison.

The definitions according to Eq. (3.13) for the CN and (3.14) for the ED show, how the ED considers all eigenvalues of the channel, whereas the CN relies on only the smallest and largest eigenvalue. In the plots in Fig. 3.7, this different consideration of the respective subchannel gains results in a different trend when comparing the CN plot with the ED plot: the ED exhibits a round shape, while the CN shows an edged contour as one eigenvalue is always neglected. Note, that the ED is negated to allow a visualization with identically trending colormaps.

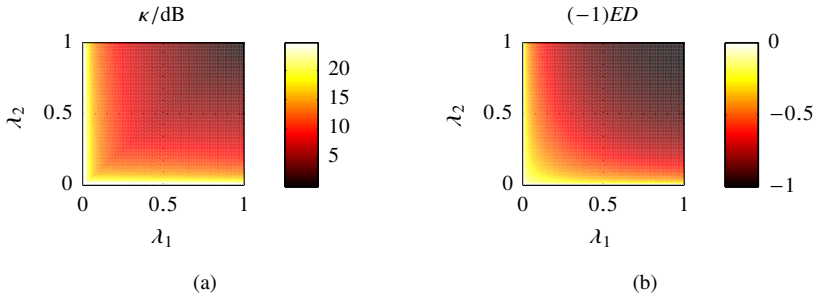


Figure 3.7 Comparison of the calculated condition number  $\kappa$  in (a) and the negative eigenvalue distribution  $ED$  in (b) based on a  $3 \times 3$  MIMO system for variation of the eigenvalues  $\lambda_1$  and  $\lambda_2$ . The sum of the eigenvalues is constant:  $\lambda_1 + \lambda_2 + \lambda_3 = 3$ .

**Observation 3.5.** Besides being applicable to higher order MIMO systems with more than two subchannels, the  $ED$  offers a higher resolution than the condition number.

In the previous Section 3.3.1, where the Kronecker model and the dependency of the channel matrix  $\mathbf{H}$  from the inter-element correlation  $\rho_{ij}$  within the correlation matrices  $\mathbf{R}$  were explained as well as Section 3.3.2, where the condition number, eigenvalue dispersion and two variations of the channel capacity were introduced, the influence of the antenna correlation  $\rho$  becomes obvious, especially in Equations (3.2), (3.7) and (3.9)-(3.14). Now, this observation is evaluated numerically for these performance indicators with focus on the eigenvalue dispersion as well as the ergodic and zero-outage capacity by sweeping the correlation from the fully uncorrelated case with  $\rho = 0$  to the fully correlated case with  $\rho = 1$ . Subsequently, the influence on the performance indicators is visualized and analyzed for different MIMO system configurations ( $2 \times 2$ ,  $4 \times 4$ ,  $6 \times 6$  and  $8 \times 8$ ).

The channel matrix  $\mathbf{H}$  is calculated based on Eq. (3.2) within a simulation covering 10000 Monte-Carlo runs [94] with an accuracy of 0.02 regarding the correlation factor  $\rho$  between the antenna elements of the receive or transmit antenna system. Figure 3.8 shows, that the increase of correlation on both link-ends has qualitatively the same effect - independent of the number of antennas: the ergodic capacity decreases, when the correlation is increased. Not the deviating scale of the colorbar for the  $2 \times 2$  MIMO case in Fig. 3.8a. Hence, a low antenna correlation is a key requirement to achieve a high channel capacity

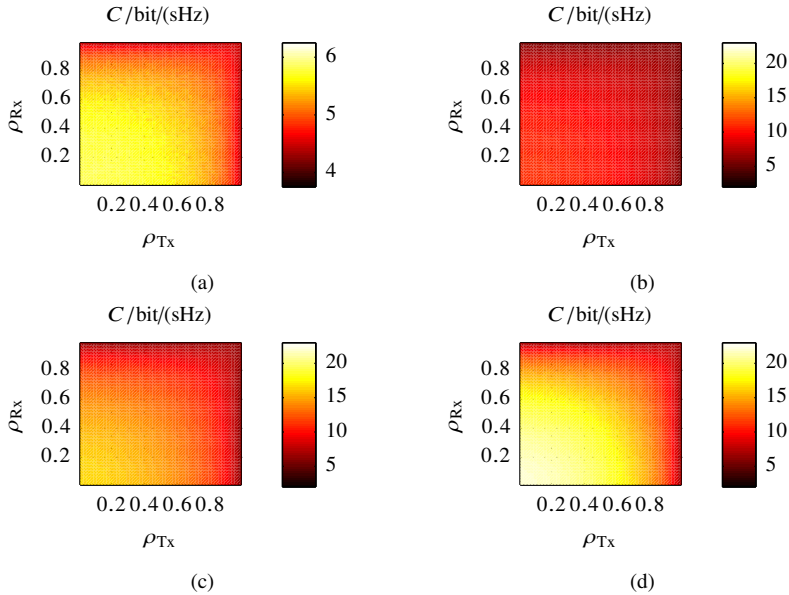


Figure 3.8 Ergodic channel capacity  $C_{\text{erg}}$  under variation of the receive and transmit correlation. The number of antennas at the transmitting and receiving end are changed from (a) two over (b) four and (c) six up to (d) eight elements.

on average. However, a higher number of antennas leads quantitatively to a different behavior as well as different maximum and minimum values which span an increased domain: the more antennas are used, the higher is the relevance of correlation. When a MIMO system with a high number of antennas on both sides of the channels is considered, it is necessary to decorrelate the single antenna elements in order to exploit the potential performance gain due to the increased order of the MIMO system. One of the most efficient ways to lower the inter-element correlation besides polarization diversity is spatial separation<sup>33</sup>. In the vehicular context this requires either an integration volume large enough or a different mounting strategy where antennas are distributed around the vehicle<sup>34</sup>. Comparing a  $2 \times 2$  collocated antenna system ( $\rho = 0.85$ , which matches to the correlation factor of two antenna elements within a typical sharkfin integration

<sup>33</sup>See Section 3.4.1 within this chapter for a theoretical and simulative analysis.

<sup>34</sup>This thought is revisited in Section 3.4, where a distributed antenna system is investigated.

volume) with a  $2 \times 2$  distributed antenna system (with highly separated antennas and thus  $\rho = 0$ ) leads to an increased ergodic capacity of around 141 %, cf. Fig. 3.8a. The higher-order system exhibit similar behavior with qualitative increases within both the theoretical limit ( $N$ -times the throughput with  $N$  being the MIMO rank) and system limit, as impairments like noise have been considered during simulation.

Note, that the results for the channel capacity have been calculated with a fixed SNR of 10 dB. To evaluate the MIMO capability of a communication system exclusively, either the CN or ED have to be used. Within this evaluation, the focus is also set on higher-order MIMO systems, thus here the ED is preferred over the CN, cf. Observation 3.5. Figure 3.9 shows the eigenvalue distribution

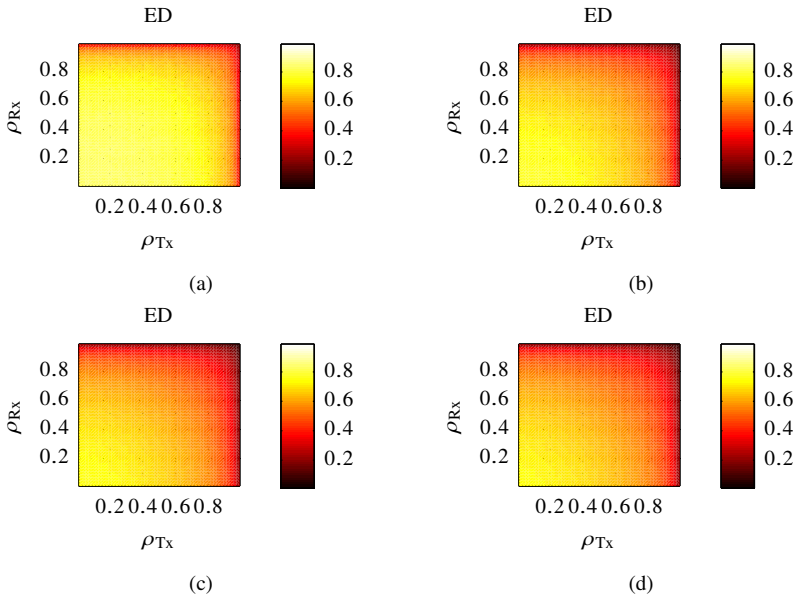


Figure 3.9 Eigenvalue distribution  $ED$  under variation of the receive and transmit correlation. The number of antennas at the transmitting and receiving end are changed from (a) two over (b) four and (c) six up to (d) eight elements.

for different configuration with swept transmit and receive correlations. The qualitative behavior is almost the same for all configurations and is independent of the number of antennas. However, the codomain of the ED for a system with

two antennas is narrower in contrast to the other higher-order configurations. This limit for lower order MIMO systems occurs due to the fact, that a  $2 \times 2$  system cannot circumvent bad reception performance<sup>35</sup> of one of the antennas. Besides, it can be recognized, that the ED shows a progression which is very similar to the ergodic channel capacity as plotted in Fig. 3.8. This leads to the conclusion, that performance indicators like CN or ED which are used to assess the MIMO capabilities of a MIMO channel can be used to estimate the progression of the ergodic capacity for a given system when large-scale fading properties are assumed and the SNR is fixed. This is also somehow visible in Eq. (3.7) stating the ergodic capacity: the two major influencing input values are the sub-channel gains  $\lambda_i$ , which represent the influence of the transmit antennas, channel and receive antennas - thus the MIMO capability as well as the SNR, which reflects the available signal power in a noise and interference limited environment. Hence, based on the general MIMO channel model from Eq. (3.1) where the received signal vector  $\mathbf{y}(t)$  consists of the transmitted signal vector  $\mathbf{x}(t)$  being mapped with channel matrix  $\mathbf{H}$  with additive noise  $\sigma^2 \mathbf{n}(t)$ . The condition number as well as the eigenvalue distribution can be seen as an indicator on how easy the system of equations can be solved for  $\mathbf{x}(t)$  under the influence of noise. This matches the perception, that the condition number specifies how close a matrix is to a weighted unitary matrix, where the weighting factor is determined by the fading properties of the channel [6].

To account for reliability requirements in terms of latency, Eq. (3.9) introduced the zero-outage capacity alongside the previously discussed ergodic capacity. The results of the behavior of the zero-outage capacity for swept correlations for different orders of MIMO systems is plotted in Fig. 3.10. The zero-outage capacity is denoted as DLC, short for delay limited capacity which is used as a synonym for the zero-outage capacity [7, 91]. From a general point of view, the zero-outage capacity is smaller or equal than the ergodic capacity and yields lower values with increasing correlation. Note, that the plots appear to be grainier, even though the same resolution has been used as in Fig. 3.9 and 3.8. Again, the number of antennas influences the maximum achievable value guaranteed throughput: for higher order MIMO systems. Assuming equality in SNR, the distance between the zero-outage capacity for low and high correlation increases for systems with a higher number of antennas. Hence, a low inter-

<sup>35</sup>An antenna can suffer poor reception performance due to e. g. mismatch (because of obstacles in the reactive nearfield of the antenna (see Section 3.2) or a general component fault, positioning of the antenna a deep-fade area or as well a high spatial correlation caused by the channel's scattering properties (see Section 3.3.1).

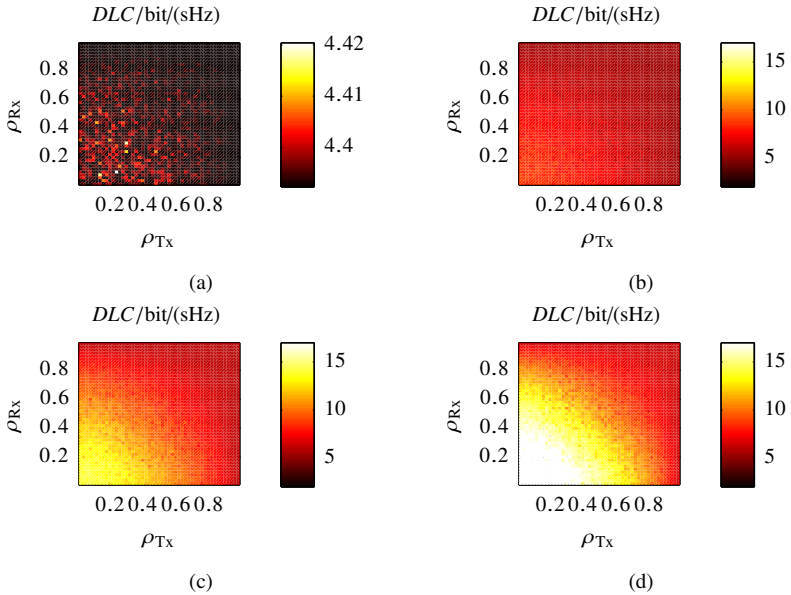


Figure 3.10 Zero-outage capacity under variation of the receive and transmit correlation. The number of antennas at the transmitting and receiving end are changed from (a) two over (b) four and (c) six up to (d) eight elements.

element correlation is fundamentally important, especially for multiple antennas systems with a high number of elements, when considering delay-sensitive traffic [7].

**Observation 3.6.** *In order to evaluate multi-element antenna systems on system level the ergodic channel capacity, zero-outage capacity and eigenvalue dispersion or condition number are introduced. While the ergodic capacity gives an estimation of the mean throughput under ideal conditions with ideal modulation and coding, the zero-outage capacity also considers delay sensitivity and serves as a figure which provides a minimum guaranteed data rate and can be seen as a reliability indicator. While the indicators derived from capacity or throughput always include the channels ability of power transfer and the spatial (MIMO) properties, the eigenvalue dispersion measures the MIMO capabilities independently of the SNR. The eigenvalue dispersion is recommended over the condition number, as it is also applicable on higher order systems and provides*



a higher resolution for  $2 \times 2$  systems.

The condition number and ergodic channel capacity are commonly used as a performance measure for evaluation of MIMO channel measurements in general. Based on the approach introduced within this section, cf. Fig. 3.6, the author has expanded their application with the focus on the assessment of vehicular MIMO antenna systems as shown in [6, 9, 10, 27]. The set of available key performance indicators has been extended mostly within this work and [7] by the introduction of the zero-outage capacity to account for delay sensitive applications as well as by the introduction of the eigenvalue distribution to also consider higher order MIMO systems with more than two non-zero eigenvalues and subchannels.

### 3.4 Characterization of Multi-Element Vehicular Antenna Systems

The previous chapters have analyzed and developed the role of the antenna system to provide reliable vehicular connectivity with a high performance: Observation 3.3 and further remarks in Chapters 2 and 3 have identified the antenna as one of the major bottlenecks of the communications link. To be able to assess the antenna system's performance both qualitatively and quantitatively, Section 3.3 has described the communications link (including the vehicle-sided antenna system) analytically and has derived and evaluated suitable performance indicators. As stated in Observations 3.5 and 3.6, the eigenvalue dispersion (or condition number as an alternative) serves as an indicator to measure and quantify the MIMO efficiency of a system under test, while the ergodic channel capacity and ergodic channel capacity includes additionally the ability of the antenna system to provide a sufficient power level and signal to noise ratio to the receiver.

When considering a communications channel as depicted in Fig. 3.5, it is important to notice, that the vehicle-sided end of the channel is the only parameter, that can be influenced and changed. All other input quantities like fading characteristics, the configuration or transmitting strategy of the base station is usually out of scope of an automotive OEM.

With the findings from Section 3.3.3, which has been used to *calibrate* the absolute and relative behavior (to each other) of the performance indicators, this Section provides detailed results from both simulation and measurement. While Section 3.4 yields findings from a generic evaluation of a general distributed versus a co-located MIMO antenna system, subsequently Section 3.4 evaluates

antenna systems, which have been deployed on or in vehicles for research and series development projects.

It is common knowledge, that the inter-element correlation and coupling can be reduced by increasing the separation between the respective antenna elements [6, 68, 95]. Besides, investigations show, that increasing the number of antennas at the vehicle also improves the overall system performance with regards to capacity (throughput) and reliability. When a limited environment for integration is considered, these two previously mentioned effects are now perfectly decoupled. By increasing the amount of antennas within a finite volume or area, the distance between them decreases automatically.

So far, inter-element correlation was the only input parameter, that has been investigated. This allows for a higher level of abstraction to first understand the behavior of the previously defined performance indicators. This section will focus on also including properties on both component, vehicular and system level. To understand the influence of the vehicular integration environment, the antenna positions from Table 3.1 in Section 3.1 are considered and shall be equipped with an antenna to analyze the system behavior. This investigation is based on a simulative approach for all antenna positions and subsequent measurements for selected antenna positions.

### 3.4.1 Simulation of a Distributed MIMO Antenna System

For the simulation, a box model with the dimensions of a BMW i8 vehicle is used. In comparison to a realistic vehicle model, a box-based model allows for a reductions of complexity, decreases simulation time while keeping sufficient accuracy and thus allows for an efficient comparison of different setups. The windows are modeled as air (thus the real vehicle would not be equipped with metalized windows), the bodywork is setup as a perfect electric conductor (PEC) without losses. Fig. 3.11 shows a visualization of the box-model as well as the respective antenna positions. The antenna positions 1 and 9 correspond to a traditional shark-fin antenna, while the remaining locations have been derived from Table 3.1 and cover the front and rear bumpers, external rear view mirrors as well as plastic covers of the rear roof-supporting pillars. Position 8 is an additional location at the cowl (wind guide).

To focus only on the impact of the vehicular integration and not on any antenna-specific effects, each antenna position is equipped with a point source with the behavior of an ideal dipole. The antenna positions are then analyzed by using the electromagnetic simulations software *Hyperworks FEKO* which

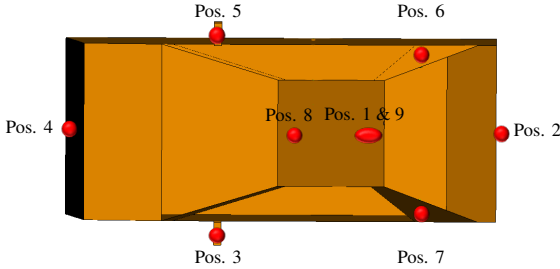


Figure 3.11 Abstracted model of a BMW i8 in top view with nine highlighted antenna positions to be evaluated.

performs an electromagnetic field analysis of 3D structures. In this case, the Method of Moments (MoM) is applied, since it is suitable for the ideal computation of radiation and coupling between antenna elements on metallic and dielectric structures. The Method of Moments is used to perform a full wave solution of Maxwell's equations [96]. With knowledge of the radiation pattern of the  $i$ -th antenna  $C_{\text{rad},i}(\vartheta, \varphi)$  and further parameters of the channel around the antenna under test<sup>36</sup>, the envelope correlation  $\rho_{i,j}$  between two antennas can be calculated as

$$\rho_{i,j} = \frac{\left| \int_{4\pi} C_{\text{rad},i}(\vartheta, \varphi) \cdot C_{\text{rad},j}^*(\vartheta, \varphi) d\Omega \right|}{\sqrt{\int_{4\pi} |C_{\text{rad},i}(\vartheta, \varphi)|^2 d\Omega} \cdot \sqrt{\int_{4\pi} |C_{\text{rad},j}(\vartheta, \varphi)|^2 d\Omega}}, \quad (3.17)$$

with  $\Omega$  being the solid angle<sup>37</sup>,  $|C_{\text{rad},i}(\vartheta, \varphi)|^2 = C_{\text{rad},i}(\vartheta, \varphi) \cdot C_{\text{rad},i}^*(\vartheta, \varphi)$  and  $(\cdot)^*$  denoting the conjugate complex [63, 97].

The numerical results for an evaluation at  $f = 800$  MHz (being one of the longest wavelengths for LTE in Europe<sup>38</sup> in 2016) lead to the following receiver

<sup>36</sup>In this case, the vehicle is positioned in free space, thus no effects due to reflections (modifying the angle-of-arrival distribution of impinging waves) or polarization conversion (XPR) occur.

<sup>37</sup>In Eq. (3.17) the differential of the the solid angle  $d\Omega$  denotes the surface area element of a unit sphere with  $d\Omega = \sin(\vartheta) d\vartheta d\varphi$ . The limit of the surface integral being  $4\pi$  leads to integration over the full surface of the sphere.

<sup>38</sup>3GPP Band 20: Digital Dividend I, Uplink: 832-862 MHz, Downlink: 791-821 MHz,  $\lambda \approx 0.37$  m.

correlation matrix:

$$\mathbf{R}_{\text{Rx}} \approx \begin{pmatrix} 1 & 2.7 \cdot 10^{-6} & 2.3 \cdot 10^{-6} & \cdots & \boxed{0.85} \\ 2.7 \cdot 10^{-6} & 1 & 4.5 \cdot 10^{-5} & \cdots & 1.6 \cdot 10^{-5} \\ 2.3 \cdot 10^{-6} & 4.5 \cdot 10^{-5} & 1 & \cdots & 5.2 \cdot 10^{-5} \\ \vdots & \vdots & \vdots & \ddots & \vdots \\ \boxed{0.85} & 1.6 \cdot 10^{-5} & 5.2 \cdot 10^{-5} & \cdots & 1 \end{pmatrix}. \quad (3.18)$$

$\mathbf{R}_{\text{Rx}}$  is a  $9 \times 9$  matrix with ones on the main diagonal. All correlation coefficients are negligibly small except the antenna correlation for the two antenna elements within the shark-fin antenna, which are positioned closely to each other. Here,  $\rho_{1,9} = \rho_{9,1} = 0.85$ . Thus, within the contour plots of Figures 3.8 to 3.10 is located in the lower part of the diagrams for the distributed antenna locations, whereas the co-located shark-fin antenna system operates at an Rx-correlation of 0.85.

**Observation 3.7.** *The correlation of antennas widely separated within the boundaries of the automotive domain can be neglected. These antenna architecture are referred to as vehicular distributed antenna systems. The correlation of the the co-located antenna system equals 0.85 at 800 MHz and has an influence on MIMO efficiency and thus on the overall system performance.*

Nevertheless, the inter-element correlation is not the only influencing factor. The expressions for the ergodic and zero-outage capacity in Equations (3.7) and (3.9) also show a dependency on the signal to noise ratio, which is mostly limited and determined by antenna integration. It is obvious, that antenna elements on the roof top offer a good surround view whereas antennas which are positioned around the vehicle are always somehow shielded by the car body. These and other integration effects determine the radiations characteristic and influence the antenna matching. Both can result in a variation of the SNR and correlation.

**Observation 3.8.** *Prospective antenna locations as well as the antenna type have to be chose carefully and have to match all requirements, both with regards to the radio communications system but also regarding the mounting volume.*

The latter influence shall be investigated by reusing the previously gained simulation data to discuss an exemplary antenna integration effect. The utilization of perfect electric dipoles still allows to mask out any antenna-type (e. g. monopole, dipoles, PIFA, patch etc.) specific effects. In free space, an electric

dipole has a spatial expansion of zero and features an omnidirectional radiation characteristic in the horizontal plane. It follows that any deformation of the resulting radiation pattern of an integrated source is caused by the interaction of the antenna elements with the chassis of the vehicle.

To be able to quantitatively describe the deformation of the radiation characteristic caused by changing the boundary conditions from free space to typical automotive integration spaces, the directivity  $C(\vartheta, \varphi)$  is used with

$$C(\vartheta, \varphi) = \frac{|\vec{E}(\vartheta, \varphi)|}{|\vec{E}|_{\max}}. \tag{3.19}$$

Due to the shielding properties of the conductive car body<sup>39</sup> two typical scenarios based on the integration volumes from Table 3.1 are investigated in detail. Fig. 3.12 shows the directivity of rooftop antennas in comparison to antennas mounted within rear view mirrors at an exemplary elevation of  $\vartheta = 90^\circ$ . The rooftop antenna exhibit a more omni-directional radiation characteristic

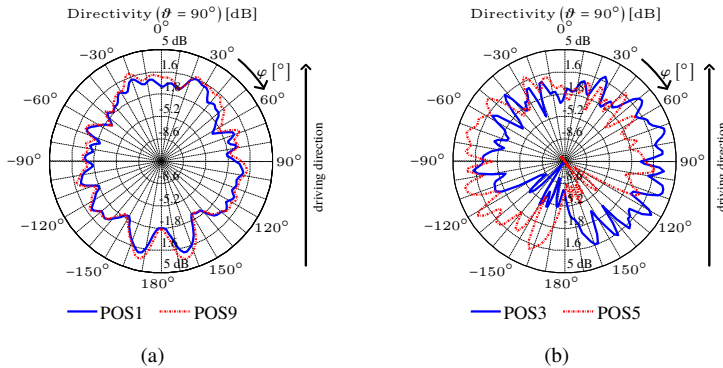


Figure 3.12 Comparison of the combined radiation patterns for both polarizations of (a) a collocated shark-fin like antenna concept and (b) a distributed antenna system with antennas being positioned within the left and right external rear view mirror. Refer to Fig. 3.1 for the coordinate system used.

due to their heavily exposed position on the vehicles roof whereas the mirror antennas positioned at the left and right side of the vehicle feature only radiate

<sup>39</sup>From an RF point of view, both metallic and carbon fiber chassis are considered as conductive with a major influence on RF systems.

and receive in a  $270^\circ$  wide area with a preferred direction to the front of the vehicle left or right side respectively. Even if both antennas were combined (with the correct phase), the direction to the vehicle's rear (at  $\varphi = 180^\circ$ ) end still suffers from a blind spot.

Now, the KPIs discussed within Section 3.3.2 include different characteristic values both dependent of the received power (or a related value) like channel capacity (relying on SINR) and independent of the receives power like the condition number. Focusing on the channel capacity with its proportionality to  $\log_2(\text{SNR})$ , that a good performance (by means of a high maximum data rate) is highly dependent on the antenna system's receive ability and its capability to provide received power at its feeding point, see Eq. (3.7). In this case, an antenna system with a directive behavior or at least with a preferred direction can lead to a performance degradation, if the remote station is positioned within the blind or impaired spot. This effect could be compensated by adding more antenna elements and subsequently increasing complexity as well as material and manufacturing cost. This argumentation leads to a trade-off between complexity, cost and integration space on the one hand versus a reliable performance on the other hand. According to Eq. (3.7), the SNR is weighted with the sub-channel gain  $\lambda_i$ . By applying Jensen's inequality from (3.8) it has been shown, that the channel capacity is maximized if all sub-channel gains are equal which requires all antennas to be perfectly decorrelated (refer to Section 3.3.2 where this coherence is discussed and analyzed in detail). The rooftop antennas offer good omnidirectionality and are thus well-suited to receive waves from any direction but are positioned close to each other and are thus not perfectly decorrelated. This will somehow impair the overall performance.

The following equation restates (3.7) and emphasizes major sensitivities:

$$C_{\text{erg}}(\sigma^2) = \mathbb{E}_{\mathbf{H}} \left[ \sum_{i=1}^{N_{\text{min}}} \log_2 \left( 1 + \underbrace{\frac{P}{N_{\text{Tx}}\sigma^2}}_{\text{power receive ability}} \underbrace{\lambda_i}_{\text{MIMO efficiency}} \right) \right]. \quad (3.20)$$

**Observation 3.9.** *The ergodic channel capacity can assess the overall antenna system performance in includes both the MIMO efficiency (mostly influenced by antenna correlation) as well as the antenna system's reception ability (influenced by the receive power). The optimization of these parameters leads to a trade off in practical realization. The extreme optimizations can be implemented by*

*either a collocated antenna system at a high position (best receive ability) or a distributed antenna system (best MIMO efficiency due to low correlation).*

Of course hybrid solutions are possible in general. Besides, any approach can be optimized. By increasing the number of antennas around the vehicle (to cover blind spots) in combination with an intelligent positioning around the vehicle (for a combined quasi-omnidirectional radiation characteristic but also for decreasing the inter-element correlation) may alleviate the major drawback of a distributed antenna system. However, the increased system complexity and the additional attenuation due to a longer cable harness has to be considered<sup>40</sup>.

**Proposition 3.4.** *The positioning of antenna elements in, on or around a vehicle has a significant influence on a single antenna element's performance as well as on the overall system performance of the combination of all antenna elements serving as a MIMO antenna system.*

Following the remarks in Section 3.3.2 about suitable KPIs for evaluation of (automotive) antenna systems, the influence of different antenna integration strategies and its influence on performance has been investigated. The real-life implementation usually tends to either one of the above scenarios (distributed vs. collocated antennas), both extreme cases are investigated by measurement in the next section additionally to the above simulation

### 3.4.2 Measurement of a Distributed MIMO Antenna System

Two different exemplary setups shall be evaluated by utilizing the KPIs presented in Section 3.3.2 while picking up the previous findings. The performance indicators are collected during test drives within live LTE networks with the respective antennas under test being mounted onto a vehicle.

#### 3.4.2.1 Setup

A BMW X5 (model year 2014) is equipped with a radio network analyzer (Type Rohde & Schwarz TSMW) which includes a narrow band scanner for determination of parameters like SNR, Reference Signal Received Power (RSRP) and Reference Signal Received Quality (RSRQ) as well as a wideband scanner for channel estimation and calculation of the channel matrix based on known

<sup>40</sup>The additional attenuation due to feeding lines from the transceiver to the antennas can be circumvented by moving the digitization stage close to the feeding point of the antenna, see Section 4. This concept is often implemented within base stations.

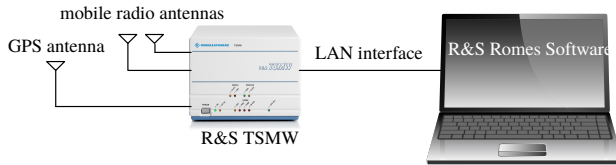


Figure 3.13 Measurement setup for the evaluation of automotive MIMO antenna setups via test drives and determination of system-level KPIs.

pilot signals (refer to Section 3.3.2 for further information). These parameters can be determined for all automotive-relevant cellular services (GSM, UMTS, LTE). The TSMW is connected to the antenna system under test as well as an additional GNSS antenna for precise georeferencing all measurement values. This measurement setup is shown in Fig. 3.13 and has already been used in similar and comparable setups in [6, 9].

The antennas are integrated into the external rearview mirrors and onto the roof at the position of the shark-fin antenna as shown in Fig. 3.14.

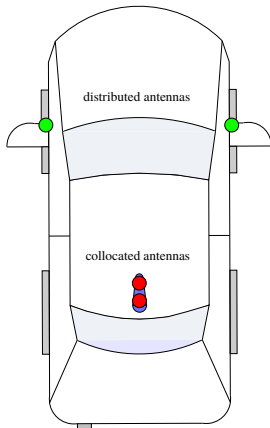


Figure 3.14 Antennas positions.

Details regarding these positions are given in Table 3.1.

The scattering parameters for both antenna concepts have been measured with a calibrated network analyzer (calibration layer at feeding point of the respective antenna) are depicted in Fig. 3.15. To calculate the channel capacity later on, the SNR is used. It is important to ensure that both antennas do not suffer from any location or mounting specific mismatch losses. For this evaluation, the focus is set to the downlink frequencies of band 20, precisely at 796 MHz. In this range, all antenna elements within both concepts are sufficiently matched ( $S_{11} < -10$  dB). However, the difference in matching between the collocated and distributed antenna system yield a matching difference<sup>41</sup> of

<sup>41</sup>Magnet mounted monopole antennas are used for this evaluation. At the mirror position / A-pillar, the available groundplane is smaller than for the roof-top position where the roof itself serves as a groundplane. This leads to a mismatch and subsequently to a difference in matching of both



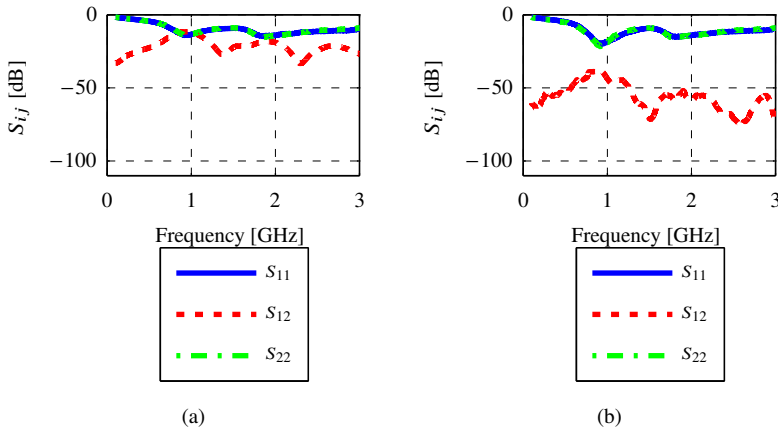


Figure 3.15 Comparison of the scattering parameters (matching  $S_{ii}$  and isolation  $S_{ij}$ ) of two antennas with (a) collocated positioning on the rooftop and (b) distributed positioning within the external rear-view mirrors.

3.62 dB which is not negligible and will be compensated during post processing to allow for a fair comparison. The isolation shows a significant difference of approximately 26 dB. In combination with the results from the numerical field simulations from above, these results indicate that the distributed antennas may be considered as decorrelated. There are approaches available in literature to calculate the inter-element correlation of a MIMO antenna system based on its scattering parameters. However, these approaches are based on the assumption of lossless antennas as well as isotropic channel properties (uniform angle-of arrival distribution over azimuth and elevation) and consider only the antenna properties at the feeding point, whereas the antenna performance is dependent on the surface current of the complete structure and its implications and any related influences, cf. [97].

### 3.4.2.2 Approach

The test drives are done on a 8.9 km long test track in Munich, Germany which includes all possible propagation scenarios that can occur in vehicular communication situations, namely urban, suburban and rich scattering environments as

---

setups.

well as line of sight (LOS) and non line of sight (NLOS) areas [6]. A map of the measurement track is shown in Fig. 3.16 The starting point of the measurement

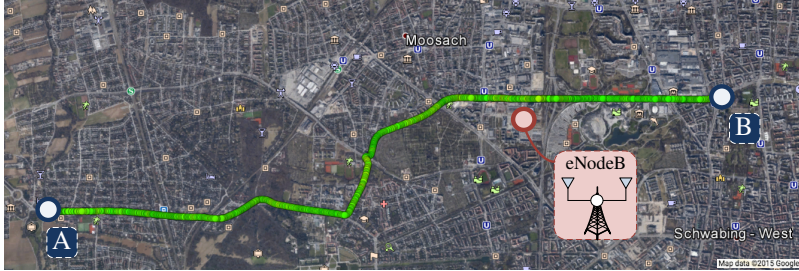


Figure 3.16 Specification of the measurement track for the evaluation of multi-element antenna systems.

track is located at the office of BMW Car IT at Petuelring 146 and ends at the JET gas station at Verdistrasse 142. The basestation (eNodeB) at 796 MHz DL is located close to the Olympiapark and is equipped with dual cross-polarized ( $\pm 45^\circ$ ) antennas. In [6, 9, 10] it was shown that the chosen measurement track allows for reproducibility in propagation characteristics. Nevertheless, each measurement is conducted three times and care is taken, that measurements are conducted at a time with little traffic on the road. As the test vehicles are regular motorists, they are subject to different traffic conditions (e. g. red light, traffic jams, shielding by larger vehicles / trucks). During the stop in front of a red light or within a traffic jam, multiple values would be recorded for one spatial spot. This would cause a bias in the statistical evaluation. To prevent any distortion within the measured values, all data is processed as follows. The setup from Fig. 3.13 collects 25 values per second reliably<sup>42</sup>. At a speed of 60 km/h this results in one measurement value per 0.67 m. Now, to mask out small-scale fading effects, *spatial binning* is conducted like shown in [6, 10]. To ensure that each bin contains at least one value, its size has to be 0.67 m at a speed of 60 km/h. In order to allow for inaccuracies of the speedometer as well as positioning inaccuracies (based on GPS), the binning size (distance) is set to 0.8 m which would allow a maximum speed of 72 km/h (without GPS inaccuracies).

The channel matrix  $\mathbf{H}$  and the wideband SNR are recorded at 0.25 Hz. The

<sup>42</sup>Own observation, the number of reliably collected values is influenced by the laptop, the maximum writing speed to the data storage medium and other external factors.

coefficients of the channel matrix as well as an additional narrowband SNR are recorded at that rate for every subband of the LTE pilot signals. These parameters are used to calculate the MIMO efficiency (condition number or eigenvalue distribution) and channel capacity after doing the spatial binning.

### 3.4.2.3 Results

In this section selected results of the measurement campaign are presented while following two goals: (i) implementing the methodology introduced within Section 3.3.2 (as already partly shown in [6, 9]) and (ii) comparing a collocated versus a distributed MIMO antenna system. The shown results are restricted to one exemplary but insightful test drive from point A to point B (cf. Fig. 3.16).

During the measurement and analysis of the scattering parameters of the antenna systems under test a matching difference between both systems was observed, which would penalize the collocated antenna system. To compensate this effect, an offset of 3.62 dB is subtracted from measured SNR values of the distributed antenna system.

From the simulation-based analysis in Section 3.4.1 where an integration volume specific radiation characteristic has been identified, the following observation can be derived:

**Observation 3.10.** *The positioning of antenna elements in, on or around a vehicle has a significant influence on a single antenna element's performance as well as on the overall system performance of the combination of all antenna elements serving as a multielement antenna system for MIMO applications.*

The radiation pattern derived from simulation of the electromagnetic fields at 796 MHz shows the manipulative influence of the vehicle chassis which gives the antenna system a preferred direction. Thus, the *combined* SNR is evaluated first for both antenna concepts. Figures 3.17 and 3.18 show the SNR plotted over the driven distance as well as a histogram for both the co-located and distributed antenna system after averaging over resource blocks of the LTE signal. The overall large-scale behavior shown in Fig. 3.17 over the driven distance show the same course for both setups, however, an offset is visible which yields generally higher SNR values for the collocated system which offers an omnidirectional radiation characteristic due to its rooftop position. This behavior results in the histogram plot in Fig. 3.18 which is oriented to higher SNR values for the collocated system versus the distributed system. This result is consistent to the simulations results from Section 3.4.1. The SNR evaluation gives an insight

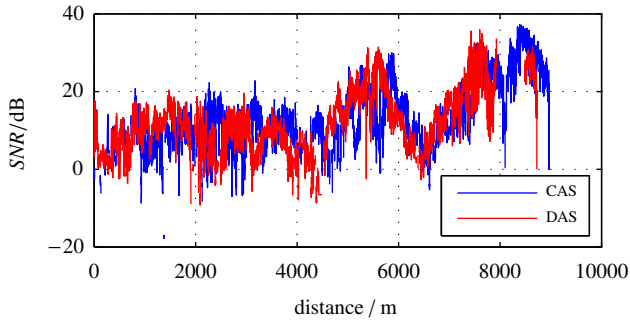


Figure 3.17 Recorded SNR over the measurement track.

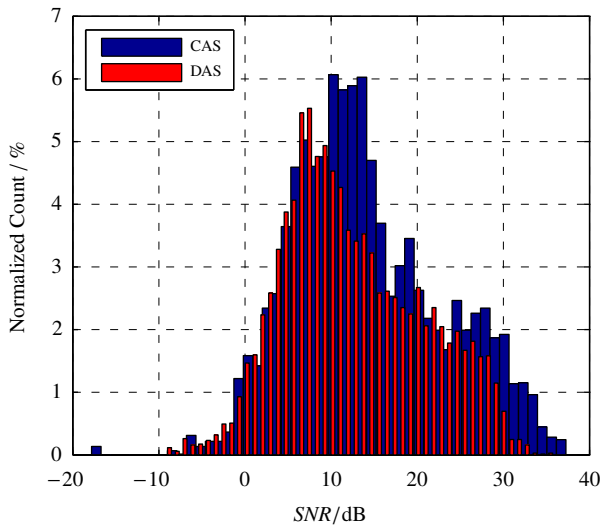


Figure 3.18 Histogram of the recorded SNR in percent.

about the antenna's *receive ability* and to provide the received power<sup>43</sup> at its

<sup>43</sup>As the channel as well as the antenna behave reciprocal, this also holds true for the transmit case, cf. [63, 80, 85, 87].

feeding point (given that the interference stays constant). This leads to

**Observation 3.11.** *Due to the exposed position on the vehicle’s roof, the co-located antenna system delivers a better performance concerning the receiving SNR. The position of the antenna system allows for an omnidirectional radiation characteristic of each antenna and allows the antenna to receive impinging waves from any (terrestrial) direction.*

As stated in Observation 3.9 and Eq. (3.20), the MIMO performance is a second dominant influencing factor for the overall performance. Thus the eigenvalue dispersion according to Eq. (3.14) in Section 3.3.2 is calculated from the channel matrix and displayed in Fig. 3.19 as a histogram and cumulative density function to quantify the MIMO capabilities of both configurations. The antenna systems yields best MIMO performance, if the values of the ED

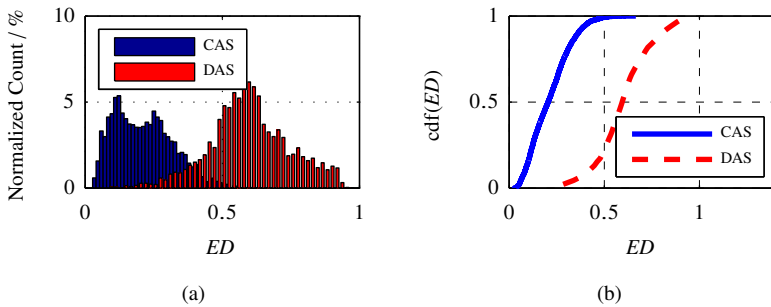


Figure 3.19 Diagram showing the measured ED for both the co-located and distributed antenna system plotted (a) as a histogram and (b) as a CDF.

approach one, see Eq. (3.14) and the discussion within Section 3.3.2. When  $ED = 1$ , the subchannels are uncorrelated which maximizes the capacity of the MIMO channel, cf. Jensen’s Inequality in Eq. (3.8). According to Fig. 3.19 the advantages of a distributed antenna architecture in contrast to a co-located system becomes obvious: the distributed antenna system (DAS) with spatially separated antennas (cf. Fig. 3.14) yields higher values for the ED and offers an enhanced MIMO capability which can be concluded to

**Observation 3.12.** *Due to the low and thus negligible correlation between the single antennas the antenna system has a higher ability to exploit the multipath behavior of the MIMO channel. This ability is captured by the eigenvalue dispersion.*

The low antenna correlation is in line with the measured coupling between both antenna elements of  $-26$  dB (see Fig. 3.15). However, this shall only be seen as an indication. In [97], the authors discuss two different approaches to compute the correlation coefficient based on either the scattering parameters or the radiation characteristic of the respective antenna elements. As already stated above, the calculation based on scattering parameters over-simplifies the existing boundary conditions<sup>44</sup> and introduces errors and inaccuracies.

The expected value for the ED lies between 0.2 for the co-located concept and 0.6 for the distributed approach. The results yield the behavior expected from the evaluations of the isolation between the antenna elements or the simulated correlation coefficient respectively. For a comprehensive statement, the influence of the conditioning of the channel matrix as well as the system's reception abilities have to be merged. The conditioning of the channel matrix is analyzed based on inter-element correlation and evaluation of the eigenvalue based on the ED, the reception abilities are expressed by the SNR.

As stated previously, the channel capacity comprised both of the just mentioned influencing factors. Since the measurement provides a representation of  $\mathbf{H}$  at a temporal instant, Eq. (3.7) can be rewritten by omitting the expectancy operation and inserting measured values  $\gamma_m$  for the SNR:

$$C = \sum_{i=1}^K \log_2(1 + \lambda_i \cdot \gamma_m), \quad (3.21)$$

where  $K$  denotes the number of subchannels, which here is smaller than or equal to two since a  $2 \times 2$  MIMO system is evaluated. The case  $K = 1$  corresponds to the SISO case in which the channel matrix  $\mathbf{H}$  is not of full rank. Still,  $\lambda_i$  represents the  $i$ -th eigenvalue of  $\mathbf{H}$ .

To evaluate under which circumstances one of the major influencing factors (SNR and condition of the channel matrix) has the largest influence, the channel capacities for the co-located antenna system (CAS), DAS and the respective SISO systems are plotted in Fig. 3.20. For computation of the SISO capacity the antenna with a highest SNR is selected (like in a switching diversity system). There is a slight gap visible between the CAS and DAS capacity, but there is a crossing point between both curves at approximately 3.9 bit/(s Hz). This effect shows the shift of influence between the measured SNR and the conditioning of the channel matrix. Distributed antennas can only exploit their advantages of

<sup>44</sup>Summarized from p. 65: assumption of lossless antennas and an isotropic channel, reduction of effects within the antenna to its feeding point by neglecting the actual surface current.

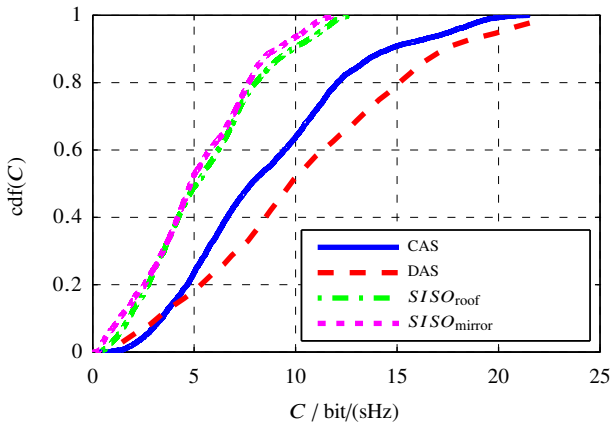


Figure 3.20 Comparison of channel capacity based on CDFs for DAS, CAS and the respective SISO configurations.

better channel conditioning in the high SNR regime. Both the well conditioned channel matrix as well as the high SNR result in a high channel capacity. In the low SNR regime, the superior antenna positioning of the co-located approach cause superior performance in comparison. Fig. 3.20 shows additionally the SISO capacities of both concepts: both MIMO approaches can clearly outperform the SISO setup. For single antenna setups, the channel capacity is directly dependent of the SNR without any influence of (sub-) channel gains. The CAS with roof-top antenna positioning is superior to the DAS due to its better reception ability which can be observed in the higher SNR values as indicated in Fig. 3.17 and 3.18. In order to better understand the influence of different SNR magnitudes due to antenna positioning around the vehicle, the effect of the SNR is masked out by replacing the measured value  $\gamma_m$  by fixed value  $\gamma$  which is set to 10 dB divided by the number of transmitting antennas  $N_{Tx}$  to account for the maximum transmit power constraint given by regulation and standardization, cf. Eq. (3.7). The results are depicted in Fig. 3.21a. Because of the spatially separated antennas, the MIMO channel matrix is well conditioned. With a fixed SNR, the capacity yields higher values for the DAS. These advantages are caused by less antenna correlation. The SISO capacity would be a line parallel to the y-axis at a capacity of 3.46 bit(sHz). Note that

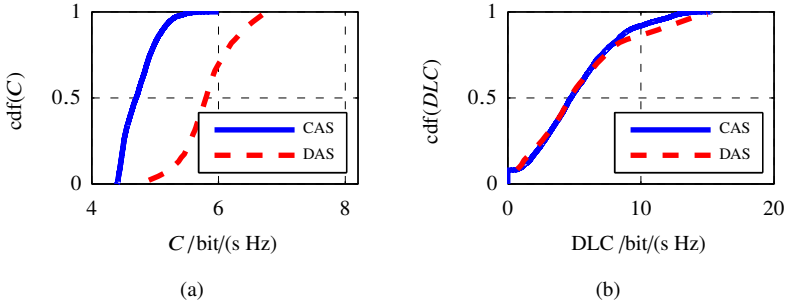


Figure 3.21 Comparison of (a) the channel capacity for a fixed SNR of 10 dB and (b) the zero-outage capacity for measured SNR values for DAS and CAS.

mean value (being equal to the ergodic channel capacity) of the distributed antenna approach (with almost perfectly decorrelated antennas) is related to the SISO capacity by factor 1.7 which is less than the only theoretically achievable doubling of the channel capacity. This observation matches with the findings from evaluation of Jensen's Inequality within Eq. (3.8) about maximization of the channel capacity due to optimal eigenvalue distribution in the case of uniform power allocation as explained in Sec. 3.3.2.

Fig. 3.21b displays the zero-outage capacity for measured SNR values  $\gamma_m$ . The DAS outperforms the CAS slightly, especially towards higher capacity values which are most likely generated within high SNR sections of the measurement track. Besides this effect, the SNR dependency as well as the influence of the channel condition (in terms of receive antenna correlation) seems to be balanced.

Besides the setup-specific quantitative insights gained during the comparative evaluation of a distributed and a co-located vehicular antenna architecture, two further observations can be derived:

**Observation 3.13.** *For a comprehensive antenna assessment and evaluation of the influence of correlation on channel capacity, it is not sufficient to consider a fixed SNR or a normalized channel matrix. For practical relevance both the receive SNR and influence of the channel matrix must be taken into account.*

**Observation 3.14.** *In most automotive scenarios in general and in combination with typical vehicular channel scenarios and antenna integration concepts, a trade-off exists between minimizing antenna correlation and maximizing the receive SNR by employing omnidirectional antenna. A fair comparison of*



*concepts is only possible by examining both effects.*

Within this section two totally different antenna setups based on different integration volumes were assessed and compared to each other. At the same time, the methodology introduced within Section 3.3 of this thesis as well as within the author's publications [6, 7, 9, 10, 27] was applied to measured data to demonstrate its behavior as well as sensitivities for an antenna architecture with totally different integration aspects and effects due the vehicular environment. The same methodology was used by the author of this thesis in [9] to analyze the influence of three dimensional (3D) volumetric antenna design approaches in comparison to conventional planar two dimensional (2D) methods within the same confined integration space of a vehicular sharkfin-like roof-top antenna. The system-level based evaluation methodology clearly showed the superiority of a volumetric design approach with regards to MIMO performance: the exploitation of the third dimension to generate an appropriate surface current allowed the implementation of a lower inter-element correlation which leads to a well conditioned channel matrix, good MIMO efficiency and ultimately to increased data rate and reliability. For further information refer to [11] for the antenna under test and to [9] for the evaluation of the MIMO capabilities.



As described in the previous section, both modern and future vehicles shall be able to support multiple wireless systems at the same time to enable advanced driver assistance systems (ADAS) for increased comfort and safety as well as services and applications for convenience and infotainment. The connectivity architecture and interface concept introduced in Chapter 2 relies on an approach where the RF signals are converted as close to the feeding point of the antenna as possible. This includes the analog-to-digital conversion in a receive mode as well as digital-to-analog conversion in transmit mode. This approach leads to

**Observation 4.1.** *Future trends in vehicular connectivity require flexible, re-configurable and frequency-agile RF frontends. Digitization of received signals close to the feeding point of the antenna appears to be a promising solution and requires suitable analog-to-digital converters (ADC) for sampling and quantization. It shall cover an operating frequency range from 600 MHz to 6 GHz with maximized dynamic range [22].*

Following this concept, it is possible to cover requirements regarding frequency agility and reconfigurability within a vehicular connectivity architecture by employing suitable architectures for analog-to-digital conversion. The ADC which defines a bottleneck of a future-proof connectivity architecture is thus thoroughly investigated within this work.

This chapter introduces the fundamentals for converting analog antenna signals to digital data including common ADC architectures, their operating principle as well as performance limitations of state-of-the-art ADCs in Section 4.1. Subsequently, based on this knowledge a suitable ADC topology for use in agile and reconfigurable vehicular connectivity platforms is identified and synthesized in Section 4.2. Finally, Section 4.3 describes ongoing from the well known Nyquist sampling an innovative sampling concept based on undersampling to increase the ADC's maximum operating frequency with special regards to use within a multiservice receiver.

## 4.1 Architectures for Analog-Digital-Conversion

Radio frequency signals being received by an antenna are a physical signal of analog nature and thus continuous in time and value [98]. To be processed by digital means these signals need to be converted into the digital domain. The ADC serves as the interface between the analog and digital domain and performs the signal conversion. This section identifies the fundamental building blocks of an ADC and analyzes their major properties.

From a conceptual point of view, the process of conversion of a continuous-time and continuous-value signal to a signal discrete in both time and value can be divided in three steps [98]: *sampling* to obtain a discrete-time signal by taking samples of a time-continuous signal at a sampling rate  $f_s$ , *quantization* by selecting a value from a finite set of possible values as close as possible to the actual value for each of the previously taken samples and finally *coding* where each discrete value is represented by a digital word. As there are many different ADC architectures presented in literature to implement these tasks, it is suitable to perform all following investigation and analysis on system level. Thus, the ADC will be considered as a system according to system theory [99] whose input and output values are examined.

Generally, two types of ADCs can be differentiated depending on their sampling speed of the input signals [22, 100]:

- Nyquist rate analog-to-digital converters,
- oversampling analog-to-digital converters.

The Nyquist rate ADC features a one-to-one correspondence between the input and output signal. The input signal is quantized within  $N$  steps, thus each input value within an interval is assigned to a fixed value in the output signal. The signal is sampled with at least two times the maximum input signal frequency  $f_{in}$  to allow proper reconstruction of the signal [57]:

$$f_s = 2f_{in}. \quad (4.1)$$

The Nyquist approach in general usually allows a low to medium resolution of the signals, except for ADCs based on an Integrating Architecture, where a high resolution for low sampling rates can be achieved. The major advantage of Nyquist rate ADCs is the straightforward availability of the output signals without any further signal processing. In the literature, e. g. [100, 101], different

Table 4.1 Qualitative overview of different architectures for realization of Nyquist rate ADC and their qualitative characteristics regarding sampling rate and resolution based on findings in [100, 101]. Note that these architectures cannot provide high sampling speeds and a high resolution at the same time.

Architecture	Sampling rate	Resolution
Integrating	low – mid	high
Successive – Approximation	low – mid	mid – high
Algorithmic	mid	mid
Parallel	high	low – mid
Two – Step	high	low – mid
Folding	high	mid
Pipelined	mid – high	mid – high
Time – Interleaved	high	low – mid

architectures are discussed that allow for different resolutions at different sampling speeds. These architectures as well as their major properties are summarized in Table 4.1. According to this comparison, there always exists a trade-off between resolution on the one hand and sampling speed on the other hand.

An oversampling ADC samples a signal between 20 to 512 times the highest frequency component of the signal referred to the maximum frequency  $f_{\max}$  of a baseband signal and to the signal bandwidth  $f_B$  of a bandpass signal [22, 100]. Due to the high sampling speed, the signal is quantized at a low resolution. First, this deteriorates the signal-to-noise ratio (SNR). In the course of a following signal processing (e. g. filtering) the quantization error can be reduced or affected positively in terms of SNR. With the reduction to a relevant frequency range by filtering, a high resolution as well as a high sampling speed in relation to the signal can be achieved. This makes the oversampling ADC architecture especially interesting for application in a multiservice connectivity architecture like proposed in Chapter 2 as well as for software radio concepts in general [48]. In contrast, Nyquist rate ADCs only offer a trade-off between either fast sampling or a high resolution.

The categorization into Nyquist rate ADCs and oversampling ADC serves

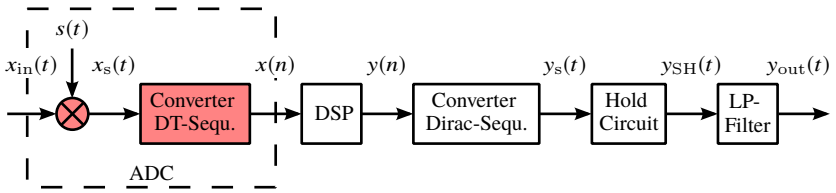


Figure 4.1 Generalized Structure of a mixed-signal system for reception and processing of analog signals.

as a fundamental classification based on different sampling techniques<sup>45</sup>. The fundamental steps regarding sampling and quantization are always done and will be analyzed in more detail in order to allow proper understanding and partitioning of a suitable ADC architecture for the problem at hand later on.

#### 4.1.1 Operation of Analog-Digital-Converters

Within this section, a general ADC will be analyzed as a mixed-signal system to investigate the relevant building blocks with special emphasis on sampling and quantization.

The setup of a common mixed-signal system with analog input and a sink for information including an ADC on system level is shown in Fig. 4.1. A representation as a mixed-signal system is suitable, as the processed signal exists in analog and discrete, both in the domains of time and value, cf. Fig. 4.1. An input signal  $x_{in}(t)$  is digitized and processed within a DSP and finally converted to an analog output signal  $y_{out}(t)$ , e. g. voice. The focus of the following is set to the analog-to-digital conversion.

The input signal  $x_{in}(t)$  is processed by a periodical impulse sequence  $s(t)$  and subsequently expressed as  $x_s(t)$  as a sampled signal:

$$x_s(t) = x_{in}(t)s(t). \quad (4.2)$$

For equidistant sampling with a sampling interval  $T$ , a delta distribution  $\delta(t)$  is

<sup>45</sup>For high-performance applications, the second architecture seems more appropriate, as it allows for implementation of an improved behavior in a noise-limited environment. This is explained in Section 4.2.

used for  $s(t)$ . The sampled signal becomes

$$x_s(t) = x_{in}(t) \sum_{n=-\infty}^{\infty} \delta(t - nT) \quad (4.3a)$$

$$= \sum_{n=-\infty}^{\infty} \underbrace{x_{in}(nT)}_{:=x_{in}(n)} \delta(t - nT). \quad (4.3b)$$

To obtain a representation of the sampling operation in frequency domain, the Fourier transform  $\mathcal{F}\{\cdot\}$  of Eq. (4.3) is calculated according to

$$\mathcal{F}\{x_s(t)\} = \int_{-\infty}^{\infty} \sum_{n=-\infty}^{\infty} x_{in}(n) \delta(t - nT) e^{-j\omega t} dt \quad (4.4a)$$

$$= \sum_{n=-\infty}^{\infty} x_{in}(n) e^{-j\omega nT} \quad (4.4b)$$

$$= \frac{1}{T} \sum_{n=-\infty}^{\infty} X_{in}(\omega - n\omega_s) \quad (4.4c)$$

with  $\omega_s = 2\pi f_s = 2\pi/T$  being the angular sampling frequency. Spectra replica of  $X_{in}$  will appear at multiples of the sampling angular frequency  $\omega_s$ . Eq. (4.4c) also shows the requirement for  $f_s \geq 2f_{max}$ , as otherwise, the copies of the spectrum will overlap and cause aliasing. This theorem is usually referred to as *Nyquist-Shannon sampling theorem* [57, 98, 102].

Real signals in general have a finite slope, finite impulse width, finite bandwidth and finite amplitudes. To represent real signals, the ideal Delta distribution within the sampling operation has to be replaced by a real sample-and-hold circuit according to Fig. 4.2.

The finite impulse function  $h(t)$  can be expressed by two Heaviside functions (also called unit step function [90]) with  $\sigma(x) = 0$  for  $x < 0$  and  $\sigma(x) = 1$  for  $x \geq 0$ .  $h(t)$  can then be written as  $h(t) = \sigma(t - nT) - \sigma(t - nT - \tau)$  with the finite pulse duration  $\tau$ . The

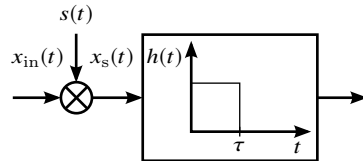


Figure 4.2 Sample-and-hold circuit

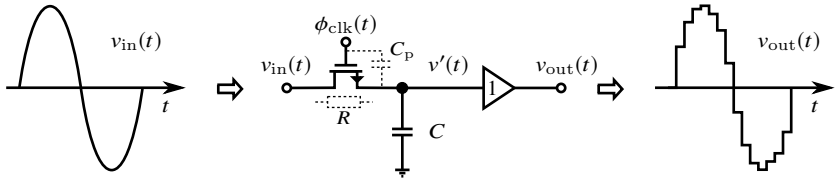


Figure 4.3 Exemplary realization of a sample-and-hold circuit, adapted from [103].

spectrum of  $x_{\text{SH}}(t)$  is calculated equivalently to Eq. (4.4b)-(4.4c) to be

$$\mathcal{F}\{x_{\text{SH}}(t)\} = \frac{1}{\tau} \int_{-\infty}^{\infty} \sum_{n=-\infty}^{\infty} x_{\text{in}}(n)h(t)e^{-j\omega t} dt \quad (4.5a)$$

$$= \underbrace{\sum_{n=-\infty}^{\infty} x_{\text{in}}(n)e^{-j\omega nT}}_{=X_s(\omega) \text{ (Sample-Effect)}} \underbrace{\frac{1}{j\omega\tau} (1 - e^{-j\omega\tau})}_{\text{(Hold-Effect)}} \quad (4.5b)$$

$$= X_s(\omega)e^{-j0.5\omega\tau} \frac{\sin(0.5\omega\tau)}{0.5\omega\tau}. \quad (4.5c)$$

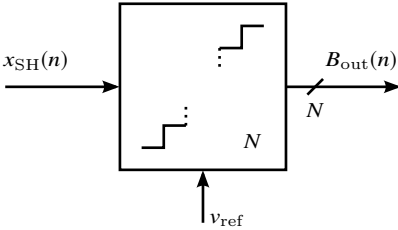
In Eq. (4.5c) both the already known sampling term due to ideal sampling as well as a new holding term due to  $h(t)$  appear. An exemplary realization of a non-ideal sample-and-hold circuit is shown in Fig. 4.3. A time-continuous signal  $v_{\text{in}}(t)$  passes a switch which is controlled by a clock  $\phi_{\text{clk}}(t)$ . Once the switch is closed,  $v'(t)$  follows  $v_{\text{in}}(t)$  and charges the capacitor  $C$ . When the switch is opened,  $v'(t)$  stays constant due to the charged capacitor and is passed via an amplifier (here set to 1) to the output voltage  $v_{\text{out}}(t)$ . The output voltage and therefore the circuit clearly show a sample-and-hold behavior. In Fig. 4.3, the switch is exemplarily implemented by a  $n$ -type MOSFET<sup>46</sup>. The depiction indicates several effects, which have to be considered for a more detailed analysis on transistor level, e. g. finite slope of  $v_{\text{out}}(t)$  for a sample due to an  $RC$ -element behavior, current injection within the transistor which leads to a voltage error of  $v'(t)$  or leakage current through  $C$  in hold mode. A more comprehensive investigation of these and other effects exceeds the system-level analysis within this section, they are discussed thoroughly in literature like e. g. [100, 103].

After sampling based on a viable sample-and-hold operation,  $x_{\text{SH}}(n)$  exists

<sup>46</sup>MOSFET: metal-oxide-semiconductor field-effect transistor.



as a discrete-time continuous-value signal. The second step for digitization is quantization. This task is performed by a quantizer as shown in Fig. 4.4.



Input signals are the continuous-value signal  $x_{SH}(n)$  and an analog reference voltage  $v_{ref}$ , the output signal equals a digital  $N$ -sized word

$$B_{out}(n) = \sum_{t=1}^N b_t(n) 2^{-t} \quad (4.6)$$

Figure 4.4 Quantizer with  $N$  steps to convert  $x_{SH}(n)$  to a discrete-value signal  $B_{out}(n)$ .

with binary values  $b_t(n) \in \{0,1\}$  whereas the bit  $b_N(n)$  with the least significance<sup>47</sup> is called  $b_{LSB}(n)$  and leads

to the smallest possible change in voltage  $v_{LSB}(n) = v_{ref}/2^N$ . The dependency between input and output can be expressed as

$$v_{ref}(n)B_{out}(n) = x_{SH}(n) \pm v_x(n) \quad \text{with} \quad -\frac{v_{LSB}(n)}{2} \leq v_x(n) < \frac{v_{LSB}(n)}{2}. \quad (4.7)$$

The error  $v_x(n)$  at the output decreases for higher values of  $N$ . Fig. 4.5 shows the characteristic of a 2 bit quantizer with the output  $\{00,01,10,11\}$ . As an example,

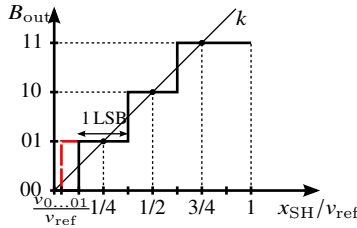


Figure 4.5 Characteristic of a quantizer with  $N = 4$  steps.

the output changes from 10 to 11 at an input value of  $x_{SH}/v_{ref} = 5/8$ . In order to limit the resolution error to the maximum quantization error of  $v_{LSB}/2$ , the relative input values of the quantizer have to stay between  $-1/8$  and  $5/8$ . The maximum input amplitude is often referred to as *Full Scale* (FS). If these values are exceeded, the error also exceeds the unavoidable quantization error. This exceedance of the maximum level is called *clipping* and has direct impact on

<sup>47</sup>LSB: Least Significant Bit.

the ADC's performance, for instance with regards to its dynamic range. Based on the identification and description of the fundamental building blocks within an ADC, sampling and quantization, performance indicators are introduced in the next Section 4.1.2 to allow an assessment of the multiservice ADC within this chapter.

### 4.1.2 Performance Evaluation and Limitations of ADCs

Based on the principles for the analog-to-digital conversion by sampling and quantization of analog signals, several parameters for performance evaluation can be derived. Within this work, the focus is set on dynamic testing instead of static or quasi-static testing like discussed in [100, 103, 104]. As dynamic tests usually have more significance [5, 22], technical KPIs related to maximum sampling ratio, quantization resolution and noise are investigated within this section. In Section 4.4.2, a system-level approach for evaluation on the bitstream layer will be used to evaluate an ADC-architecture.

A mono-frequency signal, e. g. a sinusoid is fed into the ADC under test. Its output is evaluated in frequency domain and allows for the investigation of the input signal (sine) in relation to quantization noise or possibly occurring harmonics. To investigate the impact on the performance of the quantization, a stochastic approach like in [100] is used: The input signal is considered as a rapidly changing signal, thus the quantization error  $v_x$  is an evenly distributed random variable between  $|v_{\text{LSB}}/2|$ . Thus, its probability density function  $f_x$  is constant within this range with  $f_x = 1/v_{\text{LSB}}$  with the result that  $\int_{-\infty}^{\infty} f_x dx = 1$ . The expectation value is calculated with the first moment with

$$\overline{v_x} = \int_{-\infty}^{\infty} x f_x dx = \frac{1}{v_{\text{LSB}}} \int_{-v_{\text{LSB}}/2}^{v_{\text{LSB}}/2} x dx = 0. \quad (4.8)$$

Its root mean square (RMS) is

$$\sqrt{v_x^2} = \left( \int_{-v_{\text{LSB}}/2}^{v_{\text{LSB}}/2} x^2 dx \right)^{1/2} = \frac{v_{\text{LSB}}}{\sqrt{12}} := v_{\text{Q, RMS}}. \quad (4.9)$$

It is unequal to zero and proportional to the resolution of the quantizer. Now, to calculate the signal to noise ratio, the sinusoid's RMS is required alongside the RMS of the quantization error from Eq. (4.9). For an amplitude

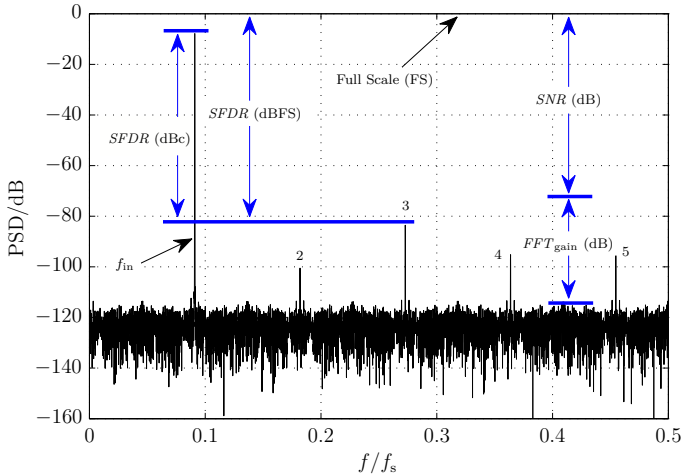


Figure 4.6 Spectral Power Density (PSD) Plot of a Nyquist rate ADC. The input sine signal is positioned at  $f_{in}/f_s = 0.09$ . After sampling with  $f_s = 10$  MHz several harmonics appear due to nonlinearities. Different characteristic parameters for performance description are shown.

between 0 and  $v_{ref}$  (no clipping, see Section 4.1.1) the RMS of a sine equals  $v_{sin, RMS} = v_{ref}/(2\sqrt{2})$ . The  $SNR$  is calculated according to

$$SNR/dB = 20 \log \left( \frac{v_{sin, RMS}}{v_{Q, RMS}} \right) = 20 \log \left( \sqrt{\frac{3}{2}} 2^N \right) \approx 6.02N + 1.76. \quad (4.10)$$

It describes the ratio of the input signal and the inevitable quantization noise. The higher the resolution  $N$  of the quantizer, the lower is the quantization noise which leads to a large  $SNR$ . As the  $SNR$  in Eq. (4.10) is solely limited due to the quantization noise, it is also labeled as *Signal-to-Quantization-Noise Ratio*,  $SQNR$ .

To illustrate these performance indicators, an exemplary 12 bit-ADC with an input sine signal at  $f_{in} = 0.91$  MHz and a sampling rate of  $f_s = 10$  MHz is simulated with Matlab Simulink [105]. Subsequently, the output spectrum is calculated for  $N_{FFT} = 2^{14}$  points and is shown in Fig. 4.6. The input signal can be seen at  $f_{in}/f_s = 0.09$ . For this configuration, the theoretical  $SNR$  from Eq. (4.10) yields to  $SNR = 74$  dB. However, the noise floor is located around  $-116$  dB. This shift of the noise floor occurs due to the processing gain of the

fast Fourier transform (FFT)<sup>48</sup> which was used to transform the converted signal from time domain to frequency domain [98]. The gain

$$FFT_{\text{gain}} = 10 \cdot \log(N_{\text{FFT}}/2) \quad (4.11)$$

offsets the noise floor from around  $-74$  dB to  $-116$  dB. Thus, the calculated theoretical  $SNR$  from Eq. (4.10) matches well to the simulated  $SNR$  at  $SNR_{\text{sim}} = 76.62$  dB.

Further peaks arise from the noise. These peaks are harmonics positioned at  $n \cdot f_{\text{in}}$  with  $n = 2,3,4,5$  due to nonlinearities, e. g. within the quantizer as depicted in Fig. 4.4. The Spurious-Free Dynamic Range  $SFDR$  is the ratio of the input signal to the strongest spurious signal and describes range between the peak of the spectral power density of the input signal and the largest interferer in the first Nyquist zone between  $0$  Hz and  $f_s/2$ . In the given example the third harmonic sets  $SFDR = 75.83$  dBc when related to the carrier (input signal) or  $83.26$  dBFS when related to the maximum full scale input. Due to the occurrence of harmonics as interfering signals, additional parameters are defined:

- Signal-to-Noise-and-Distortion Ratio:  
 $SNDR/\text{dB} = 10 \log(P_{\text{sig}}/(P_{\text{noise}} + P_{\text{harm}})),$
- Total Harmonic Distortion:  
 $THD/\text{dB} = 10 \log(P_{\text{sig}}/(P_{\text{harm}})),$
- Effective Number of Bit:  
 $ENOB = (SNDR/\text{dB} - 1.76)/6.02.$

$ENOB$  is calculated based on Eq. (4.10) where the  $SNR$  is replaced by  $SNDR$  to represent the ADC's resolution in a realistic environment.

To objectify a comparison between different ADCs even further, two *Figure-of-Merits* (FOM) are introduced which combine some of the previously stated parameters to generate comparative benchmark figures. The authors of [107] define

$$FOM_1 = 2^{ENOB} f_s, \quad (4.12)$$

<sup>48</sup>The processing gain can be explained based on effects during execution of the FFT: an FFT bin's amplitude response behaves like  $\sin(x)/x$  (sinc-function). By increasing the FFT-points, the width of the main lobe of the sinc-function within a bin decreases, thus less noise in relation to signal energy is located within the respective bin which leads to an improved  $SNR$ . For further explanation refer to [98, 106].

which connotes that an increase of  $ENOB$  by 1 bit is comparable to doubling the sampling rate  $f_s$ . The dissipated power  $P_{\text{diss}}$  in Joule of an ADC is considered in

$$FOM_2/J = \frac{P_{\text{diss}}}{2^{ENOB} f_s}. \quad (4.13)$$

Eq. (4.13) illustrates the dissipated energy per resolution step. Increasing the  $ENOB$  by 1 bit comes along with doubling of  $P_{\text{diss}}$ . At the same time the increase of the resolution by 1 bit causes an increase of the  $SNR$  by 6 dB, cf. Eq. (4.10).

Besides these indicators describing the ADC's performance, other limits apply. It is not possible to implement any arbitrary combination of sampling rate and resolution as the practical realization of an ADC is subject to limits from a physical and technological perspective. In [107], four major characteristic values are defined: thermal noise  $N_T$  at the input of the ADC, aperture jitter  $N_A$  as well as noise due to comparator ambiguity  $N_U$  and the Heisenberg uncertainty principle  $N_H$ . The limiting nature of these items is shown in Fig. 4.7 by deriving a relation between resolution and its respective impact in dependency to sampling frequency  $f_s$ . Refer to [107] for a detailed derivation and discussion. Only the most important limits are shown, their independency is assumed for this evaluation. Furthermore, some selected commercially available ADCs are included into the figure. For sampling speeds from 60 MHz to 40 GHz the resolution limit shifts from thermal noise to aperture jitter as a dominant, performance limiting effect. Above 40 GHz, restrictions occur due to wrong decisions within the quantizer which are only of minor importance for today's ADCs. Nevertheless, it is not possible to maximize both sampling speed and resolution. In the following sections we first try to maximize the sampling rate and the ADC's resolution. Later on, a proficient sampling technique is introduced to enable sampling of signals at higher frequencies than the Nyquist cutoff frequency at  $f_s/2$ .

## 4.2 Design of a Frequency-Agile Multiservice $\Sigma\Delta$ -Modulator

In this section, a  $\Sigma\Delta$ -modulator suitable for use as a direct RF digitizing ADC in the vehicular connectivity architecture proposed in Chapter 2 will be designed and evaluated based on its quantization noise behavior. First, theory and basic functional principles are introduced to justify the suitability of  $\Sigma\Delta$ -modulators

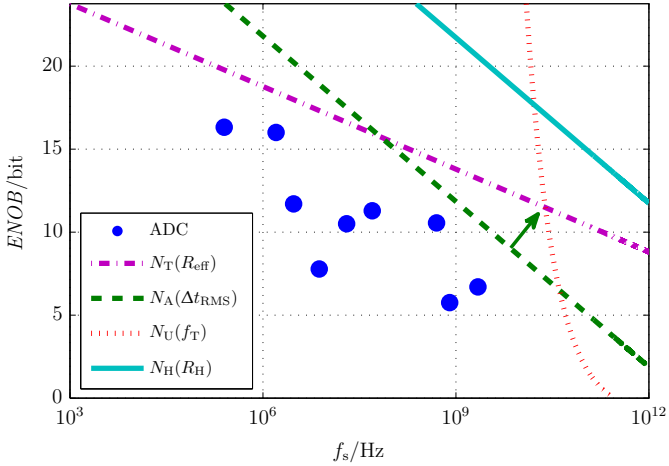


Figure 4.7 Visualization of physical and technological limits regarding resolution and sampling rate of an ADC. Furthermore, the performance of typical ADCs is shown within the plot.

in the given use case. After integration of a modulator into a complete ADC, discrete-time systems of first and second order are investigated. Subsequently, a novel three step approach for the design of a frequency-agile multiservice ADC is developed including the models and transformations in system theory. Finally, as a first proof of concept of the proposed architecture, the performance of direct RF digitization of signals of different bandwidths and carrier frequencies is evaluated based on the previously introduced performance metrics.

**Proposition 4.1.** *Utilization of bandpass continuous-time  $\Sigma\Delta$ -modulators with reconfigurable properties enables direct and frequency-agile digitization of signals from 600 MHz to 6 GHz and with signal bandwidths between 10 MHz and 150 MHz with a resolution between 10 bit and 14 bit. Design of higher order  $\Sigma\Delta$ -modulators and usage of oversampling allow for noise shaping and improved signal-to-noise behavior with increased dynamic range [5, 22].*

As discussed in the preceding chapter, the main characteristics of the radio frequency front end of a future connectivity architecture consider the ability to directly digitize signals at bandpass frequencies up to 6 GHz including the

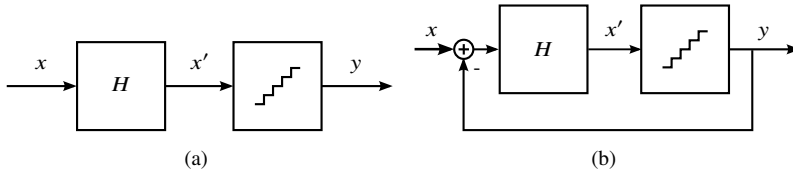


Figure 4.8 System setup (a) without feedback (open loop) and (b) a closed loop system achieving noise shaping, adapted from [22], © 2015 IEEE.

reconfigurability for frequency agility<sup>49</sup> and support of multiple standards and bandwidths.

### 4.2.1 Theory and Functional Principles of $\Sigma\Delta$ -modulators

In section 4.1, operation and performance assessment of ADCs has been discussed based on a general system model and by investigating the main tasks of an ADC: sampling, quantizing and coding. The quantization error from Eq. (4.9) leads to a performance degradation, which can be expressed by the *Signal-to-Quantization-Noise Ratio*,  $SQNR$  and influences the general  $SNR$ -behavior and dynamic range according to Eq. (4.10). In the context of control systems engineering, common Nyquist rate ADCs are usually carried out as an *open loop system* without a feedback loop [100]. However, to influence the quantization noise, a feedback loop with a filter in the forward pass can be used. By positioning the filter (usually an integrator) in the forward path instead of the feedback path, some disadvantages like limited linearity and limited accuracy due to nonidealities can be avoided, as all nonidealities are combined within the quantization error. The digital output signal then consists of a delayed copy of the original input signal and a differentiated version of the quantization error [108]. Fig. 4.8a shows an open loop implementation of a Nyquist rate ADC. The input signal passes a filter  $H$  and reaches the quantizer which links the output signal to a limited resolution to a certain error. The closed loop realization in Fig. 4.8b allows for noise shaping as the quantization noise is not evenly distributed within the investigated spectrum.

ADCs based on  $\Sigma\Delta$ -modulators usually oversample the input signals, thus they sample faster than the Nyquist frequency. The combination of oversampling and

<sup>49</sup>In this context, frequency agility defines the ability to directly digitize signals at different frequencies, e. g. by reconfiguration of certain hardware components.

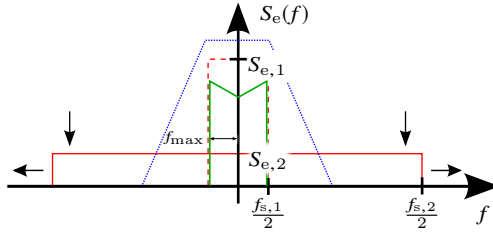


Figure 4.9 Reduction of quantization noise within the interval  $[-f_{s,1}/2, f_{s,1}/2]$  by oversampling the signal at a higher rate  $f_{s,2}$  and thus reducing the noise by spreading it within the broader interval  $[-f_{s,2}/2, f_{s,2}/2]$  and subsequent filtering of the relevant frequency domain.

subsequently constraining the sampled signal to the relevant frequency band by a filter allows for further reduction of quantization noise, cf. Fig. 4.9. Assuming the linear model of the quantizer from Section 4.1.1, the power spectrum density (PSD)  $S_e$  of the quantization noise within the frequency domain  $[-f_s/2, f_s/2]$  is equally distributed over the quantization step  $\Delta$  [100]

$$S_e = \frac{\Delta}{2\sqrt{3}f_s}. \quad (4.14)$$

The PSD  $S_{e,1}$  of the signal sampled with  $f_{s,1}$  is distributed within the interval  $[-f_{s,1}/2, f_{s,1}/2]$ . When sampling with another  $f_{s,2}$ , while  $f_{s,2} > f_{s,1}$ , the quantization noise density is spread within the broader interval  $[-f_{s,2}/2, f_{s,2}/2]$ . While the noise power related to the respective interval stays constant, the absolute value at a given position is smaller as  $S_{e,2} < S_{e,1}$ , as  $S_e \propto 1/\sqrt{f_s}$  see Eq. (4.14). This phenomenon can be exploited to improve the performance of a  $\Sigma\Delta$ -modulator ADC: if a lowpass signal with its maximum frequency  $f_{\max}$  equaling the sampling frequency  $f_{s,1}$  is sampled with  $f_{s,1}$ , the ADC behaves like a Nyquist rate ADC where the quantization noise is positioned within the bandwidth of the signal. However, if the signal is sampled at a higher rate  $f_{s,2}$  with  $f_{s,2} > f_{s,1}$ , the quantization noise is distributed within the interval  $[-f_{s,2}/2, f_{s,2}/2]$  and is thus less in the relevant interval  $[-f_{s,1}/2, f_{s,1}/2]$ . After filtering within this relevant interval, the signal exists with reduced quantization noise compared to the configuration where Nyquist sampling was used. This effect is visualized in Fig. 4.9 and leads to the definition of the oversampling ratio *OSR*

$$OSR = \frac{f_s}{2f_{\max}} \quad (4.15)$$



with  $f_{\max}$  being the frequency of a bandwidth limited input signal which has to be sampled with  $2f_{\max}$  to avoid aliasing and  $f_s$  being the rate at which the input signal is actually sampled. For  $OSR > 1$ , the signal is oversampled, for  $OSR = 1$  Nyquist sampling is used.

The signal-to-noise ratio of an oversampling ADC can now be calculated in correspondence to the  $SNR$  of a Nyquist rate ADC, cf. Eq. (4.10). The power of the input sine signal equals  $P_s = \Delta^2 2^{2N} / 8$  according to Section 4.1.2. The noise power  $P_e$  is calculated by integrating its spectral power density from Eq. (4.14) within the interval  $[-f_{s,2}/2, f_{s,2}/2]$  and performing ideal lowpass filtering with a sectionwise defined transfer function  $|H(f)| = 1$  for  $[-f_{s,1}/2, f_{s,1}/2]$  and else  $|H(f)| = 0$  afterwards:

$$P_e = \int_{-f_{s,2}/2}^{f_{s,2}/2} S_{e,2}^2(f) |H(f)|^2 df = \int_{-f_{s,1}/2}^{f_{s,1}/2} \frac{\Delta^2}{12f_{s,2}} df = \frac{2f_{\max}\Delta^2}{12f_{s,2}} = \frac{\Delta^2}{12OSR}. \quad (4.16)$$

By taking the ratio of the power of a sine input signal and the quantization noise the  $SNR$  reads as

$$\begin{aligned} SNR_{\max}/\text{dB} &= 10 \log \left( \frac{P_s}{P_e} \right) = 10 \log \left( 2^{2N} \frac{3}{2} OSR \right) \\ &\approx 6.02N + 1.76 + 10 \log(OSR). \end{aligned} \quad (4.17)$$

By setting  $OSR = 1$ , Eq. (4.17) is converted to the  $SNR$  of a Nyquist rate ADC.

**Observation 4.2.** *Oversampling of signals leads to an increased signal-to-noise ratio and thus allows an improved dynamic range when used within noise shaping  $\Sigma\Delta$ -modulators. Doubling the sampling rate  $f_s$  and thus doubling the  $OSR$  yields an increased  $SNR$  of 3 dB.*

So far, only the improvement of  $SNR$  due to oversampling has been investigated. Now the performance of a general  $\Sigma\Delta$ -modulator is derived by investigating the feedback loop, which has been previously introduced. For the moment, a  $\Sigma\Delta$ -modulator can be seen as a discrete-time system, as a bandwidth-limited input signal is sampled before the modulator at a rate  $f_s$  which results in the signal  $x_{\text{SH}}(nT_s) = x_{\text{SH}}(n)$ . As the sample-and-hold circuit is positioned in front of the modulator and its feedback loop, the performance of the overall system is influenced by an inevitable sampling error. In Section 4.2.3 a continuous time  $\Sigma\Delta$ -modulator is synthesized which allows the sample-and-hold

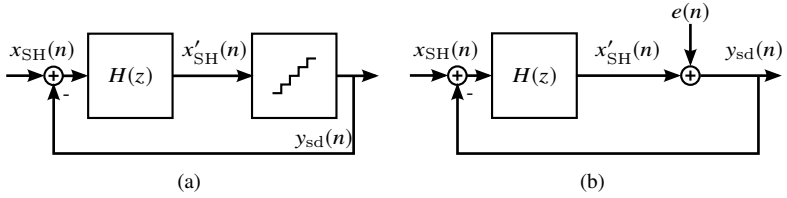


Figure 4.10 (a) Original model of a first order  $\Sigma\Delta$ -modulator with transfer function  $H(z)$  and a quantizer, whereas (b) represents a linear model thereof. The quantizer is represented by an additive signal  $e(n) = y_{sd}(n) - x_{SH}(n)$ .

circuit to be positioned within the modulator and enables consideration of the sampling error. According to Fig. 4.10a, a discrete-time signal  $x_{SH}(n)$  passes the filter  $H(z)$  and is quantized in the following block which results in  $y_{sd}(n)$ . This signal is now fed back to the input of the  $\Sigma\Delta$ -modulator and is subtracted. In order to further investigate this setup with regards to its performance, a linear equivalent circuit model is employed like depicted in Fig. 4.10b. The quantizer is replaced by  $e(n)$  [100, 108] with  $e(n)$  satisfying  $e(n) = y_{sd}(n) - x_{SH}(n)$  and thus representing the quantization error between  $y_{sd}(n)$  and  $x_{SH}(n)$ . This model is an idealized environment but is accurate if all input values  $x_{SH}(n)$  and  $e(n)$  are linearly independent. Based on the interpolative setup in Fig. 4.10b and due to linear independence of the input values the output  $y_{sd}(z)$  can be written as

$$\begin{aligned} y_{sd}(z) &= H(z)[x_{SH}(n) - y_{sd}(z)] + e(n) \\ &= \frac{H(z)x_{SH}(z)}{1 + H(z)} + \frac{e(z)}{1 + H(z)} \end{aligned} \quad (4.18)$$

By defining the signal transfer function  $STF(z)$  as

$$STF(z) \equiv \left. \frac{y_{sd}(z)}{x_{sh}(n)} \right|_{e(n)=0} = \frac{H(z)}{1 + H(z)} \quad (4.19)$$

and the noise transfer function

$$NTF(z) \equiv \left. \frac{y_{sd}(z)}{e(n)} \right|_{x_{sh}(n)=0} = \frac{1}{1 + H(z)}, \quad (4.20)$$

the output signal can be simplified in the following way:

$$y_{sd}(z) = STF(z)x_{sh}(n) + NTF(z)e(z). \quad (4.21)$$

For obvious reasons and according to [100] the transfer function  $H(z)$  of the filter shall be defined so that  $|STF| = 1$  and  $|NTF| = 0$  for  $f = 0$  Hz. The  $\Sigma\Delta$ -modulator has a lowpass characteristic. A possible solution is an integrator with the transfer function

$$H(z) = \frac{1}{z-1} = \frac{z^{-1}}{1-z^{-1}}. \quad (4.22)$$

With Eq. (4.19) and (4.20) the transfer functions becomes

$$STF(z) = z^{-1}, \quad NTF(z) = 1 - z^{-1}, \quad (4.23)$$

where  $STF(z)$  represents a delay element. For analysis of the system's behavior, the transfer functions are transformed from  $z$ -domain into  $f$ -domain<sup>50</sup> which leads to

$$|STF(\omega)|^2 = 1, \quad |NTF(\omega)|^2 = 4 \sin^2\left(\frac{\omega T}{2}\right). \quad (4.24)$$

The output signal  $y_{sd}(n)$  is not changed for any frequency by the  $STF$  but is influenced by the  $NTF$  for higher frequencies. Subsequently, lowpass signals can only be processed up to a certain cutoff frequency depending on the transfer functions  $STF$ ,  $NTF$  and the sampling rate  $f_s$ . This behavior can be analyzed by again computing the  $SNR$ . The maximum possible  $SNR$  is determined in analogy to Eq. (4.16) and (4.17):

$$SNR_{\max}/\text{dB} \approx 6.02N + 1.76 - 5.17 + 30 \log(OSR), \quad (4.25)$$

which yields a significant improvement by increasing the  $SNR$  even further compared to the  $SNR$  without noise shaping (only oversampling was applied) from Eq. (4.17).

The performance of a  $\Sigma\Delta$ -modulator can be improved even further, by applying higher order modulators. So far, only first order setups have been investigated. Fig. 4.11 shows a second order  $\Sigma\Delta$ -modulator. This modulator comprises two feedback loops of the output  $y_{sd}(n)$  to the inputs of the transfer functions  $H_1(z)$  and  $H_2(z)$ , respectively. Just as within the first order setup, they are configured as integrators, cf. [100],

$$H_1(z) = \frac{1}{1-z^{-1}}, \quad H_2(z) = \frac{z^{-1}}{1-z^{-1}}. \quad (4.26)$$

<sup>50</sup>The transformation is done by using  $z = e^{j\omega T} = e^{j2\pi f/f_s}$  based on the relation of  $z$ -transformation to the Fourier and Laplace transformation like shown in [90, 98].

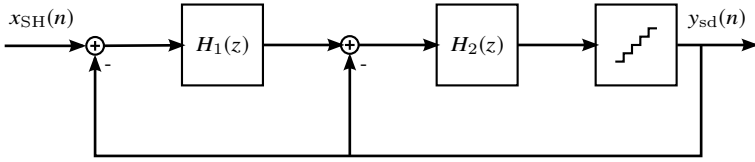


Figure 4.11 Block diagram of a second order  $\Sigma\Delta$ -modulator with two signal transfer functions  $H_1(z)$  and  $H_2(z)$  for improved noise shaping.

The transfer functions are calculated accordingly to be

$$STF(z) = z^{-1}, \quad NTF(z) = (1 - z^{-1})^2 \quad (4.27)$$

with their absolute values in frequency domain

$$|STF(\omega)|^2 = 1, \quad |NTF(\omega)|^2 = 16 \sin^4 \left( \frac{\omega T}{2} \right). \quad (4.28)$$

Now, the maximum possible  $SNR$  for a second order  $\Sigma\Delta$ -modulator yields

$$SNR_{\max}/\text{dB} \approx 6.02N + 1.76 - 12.9 + 50 \log(OSR), \quad (4.29)$$

which results once again in a performance improvement, when compared to setups that only rely on oversampling and no noise shaping at all, cf. Eq. (4.17) or both oversampling and first order noise shaping like shown previously in Eq. (4.25).

**Observation 4.3.** *By changing the order of the  $\Sigma\Delta$ -modulator, the improvement due to oversampling is again scaled by factors depending on the order of the modulator.*

To investigate the effects of oversampling and noise shaping, a second order  $\Sigma\Delta$ -modulator is realized with Matlab Simulink [105]: An input sine signal at 8 kHz is sampled at  $f_s = 8.192$  MHz and thus with an  $OSR = 512$ . The output spectrum is depicted in Fig. 4.12 and shows the input signal at the relative frequency  $9.77 \cdot 10^{-4}$ . The theoretical maximum signal-to-noise ratio is calculated according to Eq. (4.29) to be  $SNR_{\max} = 130$  dB which matches the results from Fig. 4.12. A third order harmonic is present at  $2.93 \cdot 10^{-3}$ . This phenomenon occurs because the input signal and the noise signal are not totally linearly independent within the model implemented for this simulation.

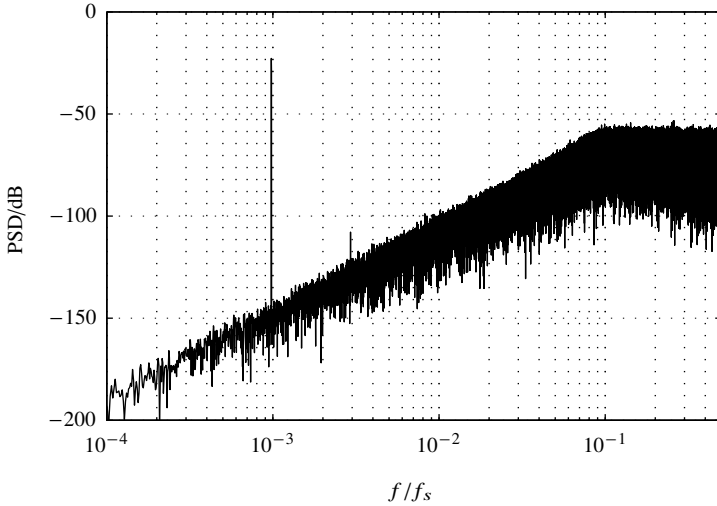


Figure 4.12 Power spectrum density (PSD) of the output signal of the second order  $\Sigma\Delta$ -modulator from Fig. 4.11. A sine at 8 kHz is fed into the input. The desired noise shaping with lowpass behavior is clearly visible. The noise level increased at 40 dB per decade, matching Eq. (4.28).

However, the assumption of linearity was an requirement during the previous investigations<sup>51</sup>. Due to the appearance of the harmonic, the  $SDNR$  at 85.6 dB is more relevant then the previously calculated  $SNR_{\max}$ , see Section 4.1.2.

From a theoretical perspective, the number of feedback loops can be increased infinitely with the result that the  $\Sigma\Delta$ -modulator comprises  $n$  integrators and  $n$  feedback loops. In practice, higher order transfer functions for  $STF$  and  $NTF$  are difficult to realize as the modulator can become unstable [100, 104]. Close attention to stability for second order  $\Sigma\Delta$ -modulators must be paid. All setups investigated within this work consider Lee's rule

$$\max_{\omega} |NTF(e^{j\omega})| \leq 1.5 \quad (4.30)$$

as an indicator for stability of  $\Sigma\Delta$ -modulators [100, 104].

<sup>51</sup>In practical realizations low-power noise can be added in front of the quantizer to increase and ensure linear independence. This procedure is called *dithering* and is investigated e.g. in [104].

## 4.2.2 Design Procedure and Methodology

The previous section introduced the basic operating principles of  $\Sigma\Delta$ -modulators including the influence of oversampling and architecture design (order) of the modulator as well as its impact on  $SNR$  for baseband signals. Now, this Section introduces an architecture which allows digitization and processing of RF signals without preceding mixers for down-conversion including suitable noise shaping. On the one hand, this requires high sampling rates to satisfy the Nyquist theorem as the input signals are positioned in the bandpass region. On the other hand broadband signals with several MHz bandwidth shall be processed. This also requires high sampling rates to ensure a sufficient  $OSR$ .

**Proposition 4.2.** *A conventional discrete-time  $\Sigma\Delta$ -modulator with lowpass noise shaping can be transformed to a continuous-time architecture with bandpass noise shaping formed like a notch to allow direct RF sampling with an improved  $SNR$ -performance.*

In [109] over 300  $\Sigma\Delta$ -modulators have been analyzed including architectures like *Switched Capacitor* (SC)  $\Sigma\Delta$ -modulators, *Continuous-Time* (CT)  $\Sigma\Delta$ -modulators, Hybrid  $\Sigma\Delta$ -modulators and reconfigurable  $\Sigma\Delta$ -modulators. Some trends evolve: The bandwidth of input signal of continuous time (CT) architecture can vary between 10 MHz to 150 MHz with a resolution between 10 bit to 14 bit [22]. These properties are ideal for handling large bandwidths like LTE or WLAN with over 20 MHz [30, 31]. Furthermore, CT-architectures based on integrated circuits (IC) will benefit from technology scaling which will enable higher transit frequencies among other things, cf. Fig. 4.7. Section 4.1.2 discussed physical limits, including the impact of transit frequency. If the CT-architecture is implemented in a reconfigurable manner, it is a highly suitable candidate to get close to the proposed SDR-like approach. Due to the direct digitization of the RF signals, it offers enhanced flexibility by adapting to different RF-signals. Up to now, the transfer function of the forward path of the  $\Sigma\Delta$ -modulator was implemented as an integrator with lowpass behavior. It can be transferred to a transfer function with a bandpass characteristic. In continuous domain, this can be a resonator which can be realized in  $g_m$ -C technique or LC-filter based [110] and is able to respond to different signal positions as long as it is realized tunable. Within the following investigation, the focus is set on the LC-filter model which can be realized with on-chip inductors [22, 110].

The steps to obtain a continuous-time  $\Sigma\Delta$ -modulator in the bandpass domain are the following [22]:

1. Design of a lowpass converter prototype in discrete time (DT).
2. Transformation to a bandpass converter prototype in DT to be able to operate for bandpass signals.
3. Transformation of the bandpass converter DT to CT by the so called *impulse invariant transformation* to benefit from reconfigurability, high sampling speed and wide bandwidth implementation methods.

As shown in [22], these steps lead to a multistandard and frequency-agile architecture. Step 1 is already thoroughly explained in Section 4.2.1. The following remarks will focus on steps 2 and 3 based on the previous findings starting from the discrete time  $\Sigma\Delta$ -modulator shown in Fig. 4.11.

#### 4.2.2.1 Transformation from a Lowpass $\Sigma\Delta$ -Modulator to a Bandpass $\Sigma\Delta$ -Modulator

Starting from a lowpass  $\Sigma\Delta$ -modulator whose *NTF* behaves like a highpass, now a *NTF* with bandstop characteristic is needed. This allows efficient processing of the input signal as the noise forms a *notch* [104] at the zero of *NTF* at  $f_n$  instead of decreasing the noise all over the frequency range from DC to  $2f_{\max}$ .

The transformation from a lowpass prototype to a bandpass architecture can be done by  $z$ -mapping in DT domain according to [109] with

$$z \mapsto -z^{-2}. \quad (4.31)$$

This transformation is carried out with the second order noise transfer function of the lowpass  $\Sigma\Delta$ -modulator from Eq. (4.27) which leads to the new transfer function  $NTF = (1 + z^{-2})^2$ . After the transformation, BP-*NTF* has a double zero at  $z_{0,BP} = \pm j$  instead of  $z_{0,LP} = \pm 1$ . The modulator doubles its order. Its transfer function can be calculated in analogy to Eq. (4.22) and yields to  $H(z) = -z^{-2}/(1 + z^{-2})$ . It acts as a perfect resonator with infinite gain at  $z = \pm j = e^{\pm j 2\pi f_n / f_s} = e^{\pm j \pi / 2}$  with the notch being positioned at  $f_n = f_s / 4$ .

#### 4.2.2.2 Transformation of the Bandpass Converter from DT to CT

Research in [109] shows, that  $\Sigma\Delta$ -modulators in continuous-time domain enable broadband signal processing. This leads to a hybrid architecture in which analog signals are generated with a DAC and fed back into the system. Quantization is done behind the filter and in front of the quantizer like shown in Fig. 4.13.

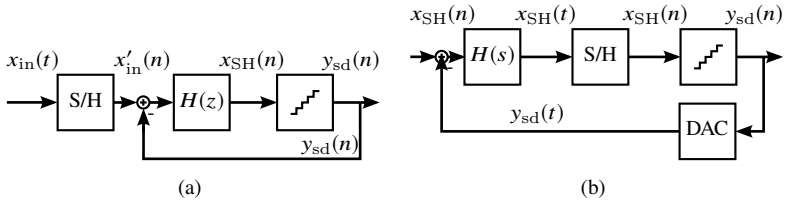


Figure 4.13 Change in the  $\Sigma\Delta$ -modulator-architecture from (a) discrete time (DT) to (b) continuous time (CT). The system blocks are resorted and the sample and hold block is positioned in front of the quantizer.

This kind of setup allows implementation of the filter transfer function in CT instead of DT: The signal is filtered in the analog domain which is easier to realize and faster [22]. Furthermore, sampling errors caused by the S/H stage can now be corrected by the feedback loop. No anti-aliasing filter (AAF) is needed [104, 111]. The digital signal  $y_{sd}(n)$  is now fed back via the DAC into the analog input of the modulator like shown in 4.13. It is not discrete any more, but continuous. Suitable design of the DAC and  $H(S)$  ensures, that

$$x_{SH}(t) = x_{SH}(n) \quad (4.32)$$

for all sampling instants  $t = nT_s$ . This ensures that the CT- $\Sigma\Delta$ -modulator has the same properties as the DT- $\Sigma\Delta$ -modulator, especially regarding its *NTF* and *STF*. Knowledge from [104, 108] can be employed to setup a CT- $\Sigma\Delta$ -modulator. To ensure equality of the DT and CT setup according to Eq. (4.32),  $x_{SH}(n)$  of the DT configuration as well as  $x_{SH}(t)$  from the CT architecture are transformed into time domain based on the open loop configuration according to Fig. 4.14. This transformation relies on the impulse invariant transform [104, 108, 112]

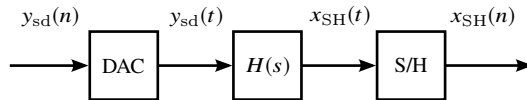


Figure 4.14 Setup of the  $\Sigma\Delta$ -modulator from Fig. 4.13b in open loop configuration.

$$H_{DT}(z) = \mathcal{Z} \left\{ \mathcal{L}^{-1} \left\{ H_{DAC, CT}(s)H(s) \right\} \right\} \quad (4.33)$$

where  $\mathcal{Z}$  is the  $z$ -transform operator and  $\mathcal{L}$  is the Laplace-transform operator. The right side of Eq. (4.33) is mostly influenced by  $H_{DAC}$ . Thus the process for DT-CT-conversion can be described by the following steps:



1. Design of a  $\Sigma\Delta$ -modulator with the desired properties like  $OSR$ ,  $SNR$ -requirements, order of the system and frequency response (lowpass, bandpass) and sampling rate  $f_s$  as a discrete time setup.
2. Application of the impulse invariant transform from Eq. (4.33) under consideration of the utilized DAC and filter  $H(s)$  within the CT-setup.
3. Identification of coefficients in dependency of frequency within the feedback loop by coefficient comparison to match the DT- and CT-architecture and ensure that the condition from Eq. (4.32) holds.

This section described the advantages of a continuous-time bandpass  $\Sigma\Delta$ -modulator (CT-BP- $\Sigma\Delta$ -modulator) and proposed a three step approach on how to design such a modulator. Starting from a prototype in discrete time, the architecture was transformed from the lowpass into the bandpass frequency domain to allow processing of signals in the RF band without preceding mixer stages. The application of the impulse invariant transform (DT-CT-transform) enables simple realization with widely available  $LC$ -circuits and enables processing of broadband signals of up to 150 MHz. By calculation of frequency dependent feedback coefficients, it is possible to realize an agile notch which allows frequency agile processing of signals at different positions within the RF spectrum.

A bandpass continuous time  $\Sigma\Delta$ -modulator (BP-CT- $\Sigma\Delta$ -modulator) is able to meet the requirements for flexible processing of future wireless communication systems. Chapter 2 proposed an architecture close to a software radio concept first introduced by Mitola in [48] in 1995. A concept for direct digitization of RF signals without using mixer stages for downconversion in the frequency domain was introduced within this section. Especially the utilization of  $\Sigma\Delta$ -modulators enables noise shaping and improvement of the signal-to-noise behavior of an ADC as well as direct sampling of bandpass signals by using undersampling with regards to the maximal signal frequency  $f_{\max}$  while at the same time adhering to a sufficient oversampling ratio  $OSR$  with regards to the signal's bandwidth  $f_B$  at moderate sampling frequencies  $f_s$  [22]. The following Section 4.2.3 deals with the specific synthesis of a BP-CT- $\Sigma\Delta$ -modulator based on the introduced and theoretically discussed methodology.

### 4.2.3 Synthesis of a Bandpass-Continuous-Time- $\Sigma\Delta$ -Modulator

The necessary steps for the synthesis of a BP-CT- $\Sigma\Delta$ -modulator are generally described in Section 4.2.2 and are now applied for synthesis of a 4th-order

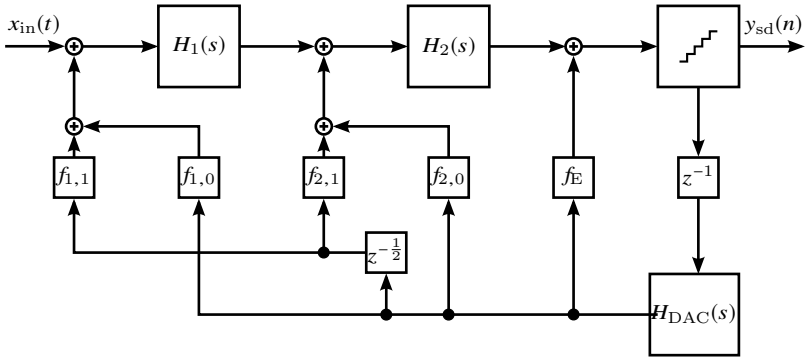


Figure 4.15 Architecture of the proposed BP-CT- $\Sigma\Delta$ -modulator with  $LC$ -resonators  $H_1$  and  $H_2$  and a FIR-DAC feedback loop based on an ideal DAC and the feedback coefficients  $f_{m,n}$  and  $f_E$  [22], © 2015 IEEE.

BP-CT- $\Sigma\Delta$ -modulator with  $LC$ -resonators.

The setup of the modulator is chosen according to Fig. 4.15 and is adapted from [113–116]. The input signal  $x_{in}(t)$  passes a second-order resonator consisting of a capacity and inductance with the general transfer function

$$H'_1(s) = \frac{a_2 s^2 + a_1 s + a_0}{s^2 + (\omega_0/Q)s + \omega_0^2}, \quad (4.34)$$

with the resonance frequency at  $\omega_0 = 1/\sqrt{LC}$ , quality factor  $Q$  and the coefficients  $a_i$  and  $b_i$ , see [117]. An ideal configuration with  $Q \rightarrow \infty$  and setting the coefficients to be  $a_2 = a_0 = 0$  and  $a_1 = \omega_0$  results in

$$H_1(s) = \frac{\omega_0 s}{s^2 + \omega_0^2}. \quad (4.35)$$

If the second resonator  $H_2$  is laid out as the first one, then  $H_2(s) = H_1(s)$ . Now, after passing both resonators, the signal is quantized by a 1 bit quantizer. This allows high sampling frequencies, as the quantizer can be setup as a comparator<sup>52</sup>, cf. [110]. The feedback of the output signal  $y_{sd}(n)$  is accomplished by a DAC with a finite impulse response (FIR-DAC). It consists of a DAC with the same number of bits as the quantizer (1 bit) and weighting coefficients  $f_{m,n}$  with

<sup>52</sup>The input signal is compared to a reference signal: depending on the sign of the difference, the output bit is set to either 0 or 1.

$m \in \{1,2\}$  and  $n \in \{0,1\}$  which are separated by a  $z^{-1/2}$  delay (half sampling rate  $T_s/2$ ). In order to obtain the same *NTF* as for the DT-system, at least four coefficients are necessary. The order of the transfer functions is doubled during the transformation from a lowpass modulator to a bandpass modulator, like shown in Eq. (4.31) and the following calculations in Section 4.2.2. The number of needed coefficients justifies the utilization of a FIR-DAC instead of a single feedback path with only one possible weighting coefficient like shown previously, e. g. in Fig. 4.13. The transfer function of the FIR-DAC in the Laplace space is given by

$$H_{\text{FIR-DAC},m}(s) = \sum_{n=0}^1 f_{m,n} e^{-nsT/2} H_{\text{DAC}}(s) \quad (4.36)$$

for  $m = 1,2$ . The factor  $e^{-nsT/2}$  is used to map the half delay element  $z^{-1/2}$  [99]. In order to minimize intersymbol interference, a return-to-zero DAC with a response like shown in Fig. 4.16 is used.

Intersymbol interference can occur at changes between  $-1$ ,  $0$  and  $+1$ . Interference is reduced when the DAC returns to zero within the period  $T_s$  [22, 110]. The return-to-zero DAC has the impulse response

$$H_{\text{DAC}}(t) = \begin{cases} \pm 1, & 0 \leq t \leq T_s/2 \\ 0, & \text{else,} \end{cases} \quad (4.37)$$

and can be transformed into the Laplace space based on a shifted Heaviside function [99] to be

$$\mathcal{L}\{H_{\text{DAC}}(t)\} = \frac{1 - e^{-sT_s/2}}{s}. \quad (4.38)$$

An additional path with a full delay element  $z^{-1}$  and the coefficient  $f_E$  is used to eliminate excess-loop-delay (ELD) due a non-ideal DAC which responds with a delay  $\tau_d$  as depicted in Fig. 4.16.

The generated finite impulse response of the DAC from the quantizer's output signal  $y_{\text{sd}}(n)$  is weighted by different coefficients and is injected in front of

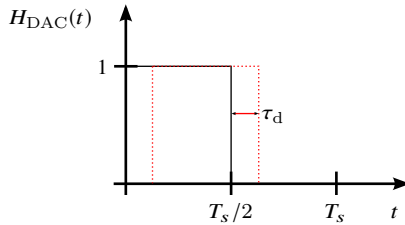


Figure 4.16 Response of a return-to-zero DAC to reduce intersymbol interference by ensuring, that the DAC returns to zero within the period  $T_s$  before again changing its value. A non-ideal DAC can delay the response by  $\tau_d$ .

the resonators  $H_1$  and  $H_2$  to generate the desired noise shaping. Now, the coefficients  $f_{m,n}$  and  $f_E$  are computed in dependency of the position of the notch at frequency  $f_n$ .

Starting with the impulse invariant transform from Eq. (4.33) and solving for the transfer function in  $z$ -domain yields

$$H_S(z) = \mathcal{Z}\{\mathcal{L}^{-1}\{H_{DAC}(s)H(s)\}\}. \quad (4.39)$$

At the same time with Eq. (4.20)

$$H_S(z) = NTF^{-1} - 1 \quad (4.40)$$

applies for the  $z$ -domain transfer function. Now a respective function for  $NTF$  is calculated based on the work of SCHREIER in [108] in dependency of the  $\Sigma\Delta$ -modulator's order,  $OSR$ , the position of the notch frequency  $f_n$  and the maximal out-of-band gain  $H_{inf}$ . As a modulator in the bandpass domain (instead of lowpass domain) is synthesized and as the order doubles during the lowpass to bandpass transformation, the order must be even and is set to four<sup>53</sup>. In this case, the oversampling ratio is preliminary and can be freely selected to be  $OSR = 128$ . The out-of-band gain is set to 1.5 according to Eq. (4.30) by applying *Lee's rule* for stability, see Section 4.2.1. Based on [108] a set of noise transfer functions is generated with Matlab [105] for different positions of the notch at  $f_n$  [22]. Thus together with Eq. (4.40) the left side of Eq. (4.39) is known. Based on the right side of this equation, the inverse Laplace transform followed by a  $z$ -transform is computed of the  $\Sigma\Delta$ -modulator depicted in Fig. 4.15. The result comprises the FIR-DAC coefficients. The overall transfer function can be composed by adding the additional path for excess-loop-delay (ELD) elimination to Eq. (4.36) and including dependency to the normalized sampling frequency<sup>54</sup>  $\nu = f_s/(2f_n)$ :

$$H(s,\nu) = \sum_{m=1}^2 H_{FIR-DAC,m}(s) + f_E e^{-s}. \quad (4.41)$$

This superposition is possible, as all subsystems are considered as linear time-invariant systems. As the equation is a function of  $\nu$ , a set of FIR-DAC coefficients can be calculated depending on the notch's position [22]. The first

<sup>53</sup>The equivalent lowpass  $\Sigma\Delta$ -modulator is thus a second order architecture.

<sup>54</sup>Frequency dependency was introduced during the calculation of multiple noise transfer functions  $NTF$ , each of which is dependent to the respective position of the notch within the noise at  $f_n$ .

four summands comprise the direct feedback paths to the resonators, the last part of the above equation is the ELD elimination paths, c. p. Fig. 4.15. After inserting Eq. (4.36) and (4.38),  $H(s, \nu)$  becomes

$$H(s, \nu) = \sum_{m=1}^2 \sum_{n=0}^1 f_{m,n} e^{-nsT/2} \frac{1 - e^{-sT_s/2}}{s} + f_E e^{-s}. \quad (4.42)$$

To allow a comparison of coefficients between the representation of the transfer function in DT and CT, Eq. 4.42 has to be converted into  $z$ -domain. Due to the delay term  $e^{-sT/2}$ , an additional sampling instant occurs for  $n = 1$  between two adjacent samples. This kind of non-integer sampling cannot be processed by the regular  $z$ -transform. In [99], the author proposes a modified  $z$ -transform, which allows the acquisition of the output signal at any time between two consecutive samples. It is based on insertion of an additional delay element at the output with  $(1 - m)T_s$  with  $\{m \in \mathbb{R} | 0 \leq m \leq 1\}$  and addition of an auxiliary sampler with  $T_s$ . Then [99] defines the  $z$ -transform of a function  $X(s)$  with non-integer sampling to be

$$X(z, m) = z^{-1} \sum \left[ \text{res} \left( \frac{X(s) e^{mT_s s} z}{z - e^{T_s s}} \right) \Big|_{\text{pole}(X(s))} \right], \quad (4.43)$$

where  $\text{res}(\cdot)$  defines the residue and  $\text{pole}(\cdot)$  the pole of the respective function. This modified  $z$ -transform can handle non-integer samples like the 0.5 sample from Eq. (4.42) and allows its transformation into a discrete-time form. Now a system of linear equations can be set up by equalization

$$H_S(s) = H(z, \nu) \quad (4.44)$$

of the discrete-time transfer function based on the generated *NTF* (left side) and the discrete-time version of the CT- $\Sigma\Delta$ -modulator (right side of above equation). Now, like shown in [22], the coefficients  $f_{m,n}$  and  $f_E$  of the FIR-DAC can be easily determined by comparison of coefficients in Eq. (4.44).

To briefly analyze and prove its functionality, the previously synthesized bandpass continuous-time  $\Sigma\Delta$ -modulator is now fully implemented in Simulink and Matlab [105]. The approach presented beforehand allows computation of FIR-DAC coefficients for any notch frequency  $f_n$  and hence enables frequency agile digitization in the RF band while still depending on sampling frequency  $f_s$ . The relevant frequency range of a bandpass modulator reaches from 0 Hz (DC) to  $f_s/2$ . As the frequency range is directly dependent on  $f_s$ , a

high sampling frequency is chosen. Analysis of state of the art publications like [107, 110, 118–120] shows, that sampling frequencies around 4 GHz are feasible, see also Section 4.1.2 where physical limits have been briefly discussed. Thus, the first Nyquist zone starts at 0 Hz and ends at 2 GHz. The quantizer has a resolution of 1 bit with amplitudes  $-1$  V and  $1$  V. Depending on the frequency of the input signal  $f_{in}$  the notch frequency  $f_n = f_{in}/f_s$  is calculated to compute the coefficients of the FIR-DAC for the respective notch frequency. The coefficients  $f_{m,n}$  and  $f_E$  for notch frequencies within the first Nyquist zone

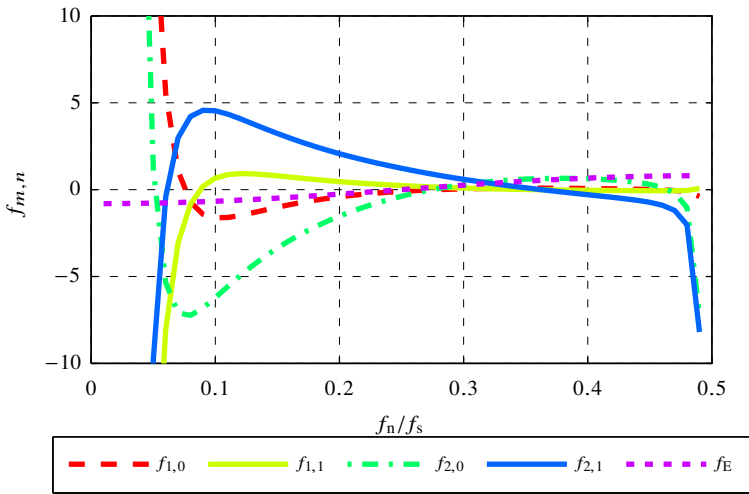


Figure 4.17 Evaluation of coefficients  $f_{m,n}$  of the FIR-DAC for different relative notch frequencies  $f_n/f_s$ . Due to the behavior of the coefficients at the beginning and end of the first Nyquist zone, the operating range of the  $\Sigma\Delta$ -modulator is constrained to  $f_n/f_s \in [0.1; 0.4]$ , © 2015 IEEE.

are plotted in Fig. 4.17. Note, that the modulator cannot be used within the complete range from 0 Hz to 2 GHz. The absolute values of  $f_{m,n}$  increase towards the ends of the first Nyquist zone and diverge towards infinity. This would lead the feedback path to overdrive the input of the modulator and cause clipping, as the input values are not any more within the range from  $-1$  V to  $1$  V, see Section 4.1.2 and [121]. On the one hand, setting the maximum allowed gain to 10 allows the notch to be positioned between 0.1 and 0.4 [22]. On the other hand, the gain is very low for notches around 0.3, this requires a very exact

realization of the feedback coefficients.

Figure 4.18 shows exemplary the behavior of the synthesized  $\Sigma\Delta$ -modulator for a sine input signal at  $f_{in} = 400$  MHz at the lower bound and at  $f_{in} = 1.6$  GHz at the upper bound respectively with a sampling rate of  $f_s = 4$  GHz and an input amplitude of  $-10$  dBFS. The PSD of  $y_{sd}(n)$  is plotted. Both the sine signal and the desired noise shaping around the input signal appear as expected. The used

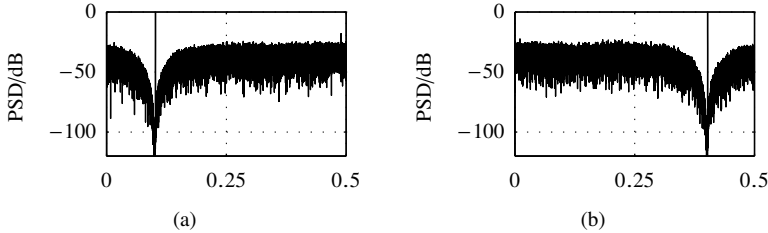


Figure 4.18 PSD plots of  $y_{sd}(n)$  for selected notch frequencies. The relative notches are positioned at (a)  $f_{in}/f_s = 0.1$  and (b)  $f_{in}/f_s = 0.4$ . With a sampling rate of 4 GHz the input sine signals at 400 MHz and 1.6 GHz respectively. The noise shaping around the input signals is clearly visible in both cases.

FIR-DAC coefficients are taken from Fig. 4.17. Note, that the position of the notch is moved in frequency by applying the suitable feedback coefficients. At the same time the required frequency agility is shown.

**Observation 4.4.** *By calculating and setting appropriate feedback coefficients within the feedback loop of the  $\Sigma\Delta$ -modulator, it is possible to realize frequency agility and reconfigurability by moving the notch within the first Nyquist zone. The overall operating range can be limited towards the lower and upper bound of the first Nyquist zones due to diverging behavior of the feedback coefficients, whereas the end of the first Nyquist zone is limited by the sampling frequency.*

To allow further quantitative investigation regarding the modulator's noise behavior with regards to its SNR, the  $SQNR$  is evaluated next like shown in Fig. 4.19. As illustrated, the  $SQNR$  is evaluated for different input amplitudes between  $-60$  dB  $\equiv 0.001$  V and  $0$  dBFS  $\equiv 1$  V for three notch frequencies with a fixed  $OSR = 100$ . For sampling frequency  $f_s = 4$  GHz this yields a 20 MHz wide signal, like commonly used for LTE- or WiFi-systems [30, 31, 34]. Independent of the notch position, a minimum  $SQNR$  of 70.77 dB is achieved if the input amplitude is set slightly lower than the maximum allowed input (full

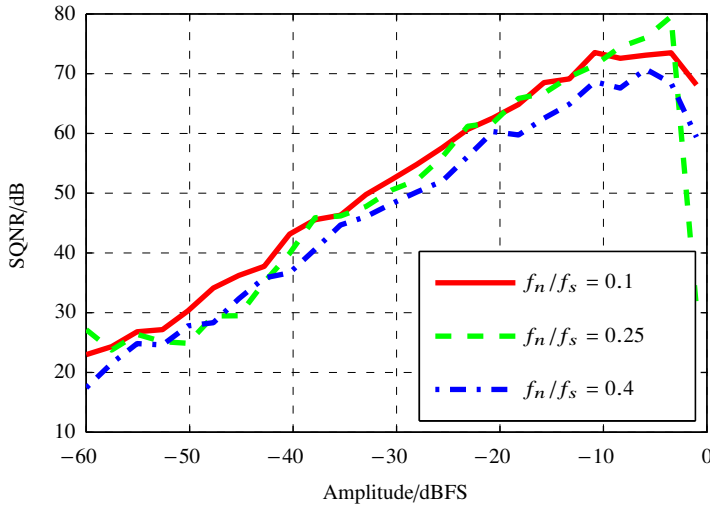


Figure 4.19 Analysis of the  $SQNR$  for relative notches at the beginning, in the middle and at the end of the  $\Sigma\Delta$ -modulator's operating range in dependency of the input amplitude.

scale). This is equivalent to a resolution of  $ENOB = 11.37$  bit based on Eq. (4.10). For notch in the middle of the operating range at 0.25 a best case  $SQNR$  of 79.57 dB with a related resolution of 12.9 bit is reached.

The presented architecture is capable of direct digitization of RF signals positioned within the first Nyquist zone. The investigation of the feedback coefficients lead to the restriction of the operating frequency range from 0.1 to 0.4 (relative notch positions  $f_n/f_s$ ) instead of the full first Nyquist zone. Thus, for a sampling frequency  $f_s = 4$  GHz it is possible to digitize signals between 0.4 GHz and 1.6 GHz. This frequency range is obviously not sufficient to sample and quantize signals up to 6 GHz, as previously derived in Section 2.2.1.

The next section introduces and evaluates a concept for further extension of the operating frequency range by increasing the upper limit by processing signals which are positioned in higher order Nyquist zones.



### 4.3 Sampling Concepts

**Proposition 4.3.** *The concept of undersampling allows digitization of signals in higher Nyquist zones and can thus increase the  $\Sigma\Delta$ -modulator's operating frequency range [22].*

This concept of undersampling allows the negligence of mixer stages which downconvert signals from higher order Nyquist zones into the first Nyquist zone and thus avoidance of their respective performance impairments [122]. The terms *undersampling*, *bandpass sampling* and *subsampling* are used as synonyms within this thesis.

Starting with the Nyquist sampling theorem from Eq. (4.1) [57, 102], a signal is subsampled if  $2f_{\text{in}} > f_s$ . Note, that within a  $\Sigma\Delta$ -modulator a signal can be undersampled and oversampled at the same time. It is subsampled, if the Nyquist theorem is violated with respect to the input signal's frequency (see above). At the same, a signal is oversampled, if it is sampled with the factor  $OSR = f_s/(2f_B)$  with  $f_s \gg f_B$  considering the signal's information carrying bandwidth  $f_B$ .

The occurring aliasing effects due to undersampling are used intentionally to shift the signal into the first Nyquist zone at  $f_{\text{IF}}$  based on the following equations and inequalities [123]:

$$f_{\text{IF}} = \begin{cases} \text{rem}(f_{\text{in}}, f_s) & \text{if } \text{fix}(f_{\text{in}}/(0.5f_s)) \text{ is even} \\ f_s - \text{rem}(f_{\text{in}}, f_s) & \text{if } \text{fix}(f_{\text{in}}/(0.5f_s)) \text{ is odd} \end{cases} \quad (4.45)$$

and

$$0 < f_{\text{IF}} - \frac{f_B}{2}, \quad f_{\text{IF}} + \frac{f_B}{2} < \frac{f_s}{2}. \quad (4.46)$$

The function  $\text{rem}(x,y)$  determines the remainder of division  $x/y$  and  $\text{fix}(x)$  performs a rounding operation of  $x$  to zero. Under certain circumstances, Eq. (4.45) can cause negative intermediate frequencies  $f_{\text{IF}}$ , e. g. if  $f_{\text{IF}} < 2f_B$ . To eliminate the superposition of negative frequencies within the first Nyquist zone and thus reduce unwanted interference, Eq. (4.46) is introduced. At the same time, it sets the minimum sampling rate to  $f_s = 2f_B$  to allow sampling without loss of information. The coherence to the general Nyquist theorem is obvious. Fig. 4.20 visualizes the operation of down-aliasing. A given signal in a higher order even Nyquist zone is mapped into the first Nyquist zone in inverted position whereas a signal in an odd Nyquist zone is aliased into the first Nyquist zone in normal position, cf. Eq. (4.45). The minimum size of the

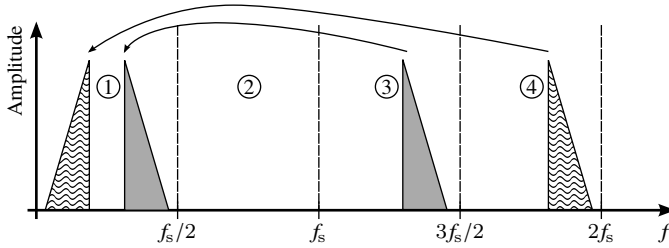


Figure 4.20 Visualization of the undersampling process: intentional exploitation of the aliasing for downshifting of higher Nyquist zone signals into the first Nyquist zone. Depending on the parity of the order of the Nyquist zone (being even or odd), the signals are undersampled by  $f_s$  into the first Nyquist zone, either in inverted or normal positions respectively.

first Nyquist zone within  $[0 \text{ Hz}; f_s/2]$  has to be sufficiently large to fit the whole input signal. This yields  $f_s/2 = f_B$  to fulfill the Nyquist theorem [57, 102].

To clarify the operating principle of the bandpass sampling, the  $\Sigma\Delta$ -modulator from Fig. 4.15 is fed with a signal commonly used for LTE in Band 7 [30] at 2.63 GHz. Considering the modulator's original sampling frequency at  $f_s = 4 \text{ GHz}$  and the upper bound of its first Nyquist zone at 1.6 GHz (limited due to the feedback coefficients, see Fig. 4.17), the test signal is outside the operational frequency range. Now, to employ subsampling with the previously synthesized architecture, the new sampling frequency is set to 1.5 GHz which causes the test signal to be positioned in the fourth Nyquist zone, as  $N_{\text{Nyq}} = \text{ceil}(2f_{\text{in}}/f_s) = 4$ . The ceiling-function  $\text{ceil}(x)$  rounds its argument to the smallest integer which is greater or equal to  $x$ . The FIR-DAC coefficients are chosen appropriately to generate a notch at

$$f_n = (-1)^{N_{\text{Nyq}}} \left( \frac{N_{\text{Nyq}}}{2} - \frac{f_{\text{in}}}{f_s} - \frac{1}{4} \right) + \frac{1}{4} \approx 0.247. \quad (4.47)$$

Eq. (4.47) also considers the parity of the Nyquist zone, in which the input signal is positioned. In the given example, it is within an even Nyquist zone is thus downsampled to an inverted position. The resulting power spectrum density is plotted in Fig. 4.21. Qualitatively, an elevated noise level compared to regular sampling<sup>55</sup> is visible, see Fig. 4.18 and 4.19 for comparison. A

<sup>55</sup>The term *regular sampling* refers to the general Nyquist theorem, cf. Eq. (4.1), where the maximum input frequency is relevant. The signal is still oversampled within the  $\Sigma\Delta$ -modulator with regards to the signal's bandwidth  $f_B$ .

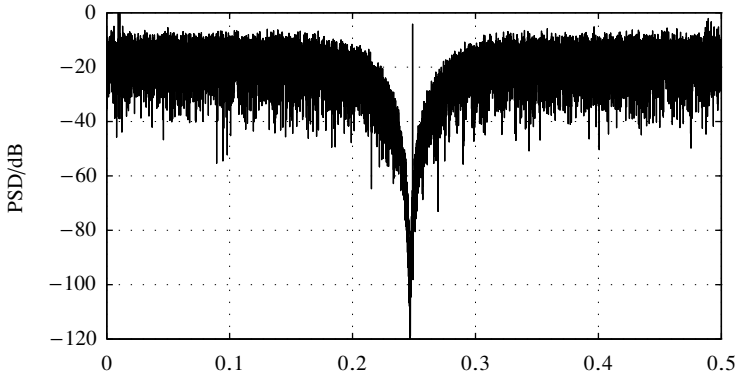


Figure 4.21 PSD plot of  $y_{sd}(n)$  for a signal with  $N_{Nyq} = 4$  being downsampled into the first Nyquist zone. The elevated noise floor is clearly visible when compared to the PSD of a not oversampled signal.

quantitative investigation of the quantization noise is conducted based on the  $SQNR$  for signal processing in different Nyquist zones in dependency of the input amplitude. The results are depicted in Fig. 4.22. For reference the  $SQNR$  of a signal at 0.37 GHz within the first Nyquist zone has been calculated. The selection of the input frequency causes the relative notch frequency  $f_n = 0.247$  to be at the same relative position as for the following setups with the LTE signal at 2.63 GHz. This setup is compared to a configuration that employs undersampling of the 2.63 GHz signal with  $OSR = 37.5$  and  $OSR = 70$  respectively. For an input amplitude between  $-35$  dBFS and  $0$  dBFS, a reduced  $SQNR$  can be determined [22]. This impairment of the ADC's  $SQNR$  occurs, as the quantization noise of each Nyquist zone is additively overlying within the first Nyquist zone [122, 124].

The noise power is a function of the *undersampling ratio*  $USR = f_{in}/f_s$ . The higher  $USR$ , which is equivalent to a higher order Nyquist zone, the higher is also the noise level: This impairment of the ADC's  $SQNR$  occurs, as the quantization noise of each Nyquist zone is additively overlying within the first Nyquist zone. The authors in [110] state an approximate value of 3-5 dB per Nyquist zone. This behavior can be seen in Fig. 4.22. The highest  $SQNR$  value of a subsampled signal reaches 50.83 dB, whereas the respective signal in the first Nyquist zone is sampled with an  $SQNR$  of 74.13 dB. This requires to

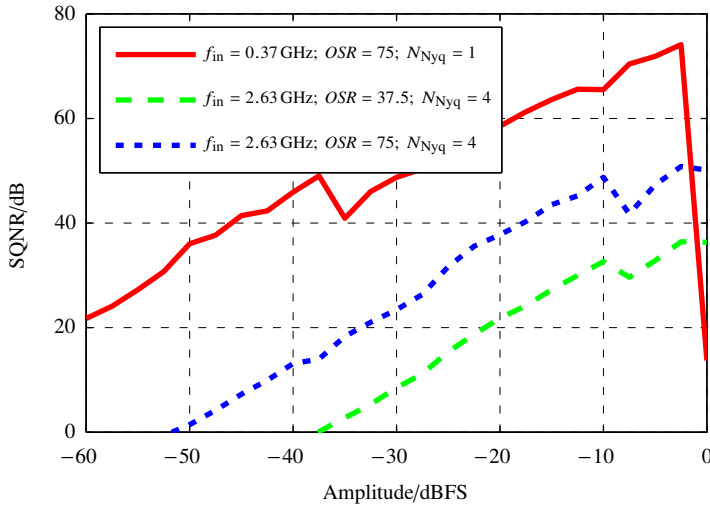


Figure 4.22 Analysis of the  $SQNR$  in dependency of the input amplitude for different setups for different Nyquist zones and oversampling ratios. All setups have the same relative notch position, but the signals at 2.63 GHz are subsampled which causes a performance degradation with regards to  $SQNR$  when compared to a signal at the same relative notch but within the first Nyquist zone at 0.37 GHz, © 2015 IEEE.

design the first Nyquist zone as large as possible to limit the influence of this performance degradation due to aliasing of the noise. As already described in Section 4.2.2 and 4.2.3, the first Nyquist zone's size is dependent of the sampling frequency  $f_s$  and the stability of the architecture due to the FIR-DAC coefficients.

The improvement of the  $SQNR$  by 10 dB around  $-37$  dBFS is linked to a critical selection of feedback coefficients. The input signal is positioned at the relative frequency  $f/f_{in} = 0.247$ . For this frequency, the feedback signal is almost not influenced by small changes of the frequency, as the feedback coefficients are very small, cf. Fig. 4.17. This also causes harmonics to appear at the edges of the spectrum shown in Fig. 4.21. According to [108] this effect can be solved by intentionally adding low power noise. This method has not been used for the work shown here.

Furthermore, Fig. 4.22 also shows how the changed sampling frequency

(from previously 4 GHz to now 1.5 GHz for the analysis of undersampling) reduces the  $OSR$  and thus evokes an additional decrease of  $SQNR$  besides the decrease due to noise aliasing. The  $OSR$  is calculated adapted from Eq. (4.15) for a bandpass  $\Sigma\Delta$ -modulator by setting  $OSR = f_s/(2f)$ . For a 20 MHz wide signal as commonly used in LTE systems, the oversampling ratio drops from 100 to 37.5 by changing the sampling frequency from 4 GHz to 1.5 GHz. The maximum  $SQNR$  for this configuration yields 36.43 dB. For further reference, an additional curve is shown for a doubled  $OSR$  of 70, a constant input and sampling frequency but changed bandwidth of the signal (now 10 MHz) which yields a better performance due to a higher oversampling ratio.

The utilization of undersampling within a  $\Sigma\Delta$ -modulator ADC allows processing and digitization (sampling and quantization) of signals positioned at higher frequencies than the upper bound of the first Nyquist zone and thus increases the ADC's operating range. As already layed out in Sec. 2.2.1, the previously synthesized ADC shall be used to cover frequencies between 600 MHz and 6 GHz. If a  $\Sigma\Delta$ -modulator with a sampling rate of 4 GHz is chosen, almost all signals within the first Nyquist zone can be sampled without using undersampling. Remember, the operating range within the first Nyquist zone is limited to the range from  $0.1f_s = 400$  MHz to  $0.4f_s = 1.6$  GHz. Subsampling is used for signals with an input frequency of at least 1.6 GHz. Investigations in [22] based on a systematic evaluation of the output spectrum of the  $\Sigma\Delta$ -modulator for sampling frequencies between 1 GHz and 4 GHz reveal that the architecture shown in Fig. 4.15 only operates in Nyquist zones according to

$$N_{\text{Nyq}} = \frac{1}{2}(4n - (-1)^n + 3) \text{ with } n \in \mathbb{N}, \quad (4.48)$$

as within all other Nyquist zones, the signal is heavily attenuated.

Now, to use bandpass sampling as a technique to increase the operating range of the ADC, the sampling frequency has to be chosen appropriately to firstly satisfy Eq. (4.48) and secondly to maximize the oversampling ratio [22]. Thus, the sampling rate is chosen *variably* to ensure subsampling within the fourth Nyquist zone according to Eq. (4.45) and (4.46). Fig. 4.23 shows both  $OSR$  and appropriate sampling frequency  $f_s$  in dependency of the input frequency  $f_{\text{in}}$ . The  $OSR$  stays constant within the first Nyquist zone and increases within Nyquist zones of higher order. For performance reasons, the first Nyquist zone is preferred. Thus, a rather high possible sampling frequency is used to increase the size of the first zone as much as possible. If the signal's input frequency is too high, the fourth Nyquist zone is preferred for undersampling, cf. Eq. (4.48).

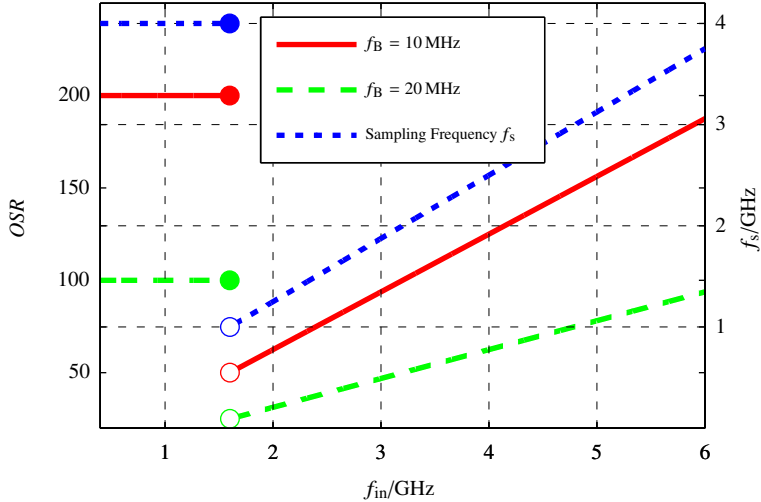


Figure 4.23 Plot of the oversampling rate  $OSR$  and the selected sampling frequency  $f_s$  in dependency of input frequency  $f_{in}$ . For  $f_{in} \leq 1.6 \text{ GHz}$  the signal is sampled at  $4 \text{ GHz}$  within the operating range in the first Nyquist zone. For  $f_{in} > 1.6 \text{ GHz}$ , subsampling is used with an appropriately chosen sampling frequency, © 2015 IEEE.

**Observation 4.5.** *To increase the operating range of a  $\Sigma\Delta$ -modulator, undersampling with regards to the maximum input frequency can be used. Signals in higher order Nyquist zones are intentionally aliased into the first Nyquist zone. This process decreases the signal-to-noise ratio, as the noise of adjacent Nyquist zones is superposed. To maximize the size of the first Nyquist zone, a high sampling frequency  $f_s$  can be used. The sampling rate for undersampling has to be chosen considering both the order of the Nyquist zone in which the original signal is positioned as well as the oversampling ratio to fully exploit the benefits of oversampling with regards to signal band [22].*

By vertically duplicating  $\Sigma\Delta$ -modulators like shown in Fig. 4.15 and [114, 116, 117, 125] and equipping each modulator with a dedicated frequency synthesis to create an appropriate sampling frequency, it becomes possible to increase the overall architecture's frequency range and digitize multiple signals in the range from  $600 \text{ MHz}$  to  $6 \text{ GHz}$  *simultaneously* [22].

## 4.4 Evaluation of a Novel Direct RF Sampling $\Sigma\Delta$ -Modulator

Within Section 4.2 a novel bandpass continuous-time  $\Sigma\Delta$ -modulator with frequency-agile properties is designed and preliminary evaluated with regards to its quantization noise behavior. The concept of undersampling is used for the first time within this particular ADC as shown in Section 4.3. The following sections provide an assessment of the ADCs capabilities both with regards to frequency agility and applicability to multiple wireless services as well as its behavior with focus its performance on bitstream layer.

### 4.4.1 Assessment of Multiservice Capabilities.

According to Observation 4.5 the frequency-agile configuration of the designed ADC allows for multiservice operation by being able to adapt to different boundary conditions like signal frequency  $f_s$  or bandwidth  $f_B$ . Simultaneous processing can be achieved by cascading multiple  $\Sigma\Delta$ -modulators and equipping each with a dedicated frequency synthesis as sampling clock [22, 114, 125]. The coefficients of the FIR-DAC are set individually in each branch. This would generate multiple notches on the output spectrum of the overall architecture which would enable processing of multiple signals at the same time at different frequencies. This approach is also used in [126], not with the same goal but for avoidance of transceiver malfunctions.

To evaluate the simultaneous multistandard capabilities of the architecture designed within this work, see Chapter 4 and [22], an example like shown in Table 4.2 is considered. The carrier frequencies and bandwidths are chosen arbitrarily to cover the frequency range of interest (600 MHz to 6 GHz) with suitable configurations but according to the respective standards, see Section 2.2.1 for derivation of the frequency range of interest and [28–31] for the particular wireless standards. The architecture under test is based on the continuous-time bandpass  $\Sigma\Delta$ -modulator which can be operated in an undersampling mode. Like already shown in Fig. 4.23, signals with  $f_{in} > 1.6$  GHz have to be undersampled, signals below that threshold are within the operating range of the first Nyquist zone and are sampled at 4 GHz. For undersampling, the sampling frequency is calculated according to Fig. 4.23 in order to maximize the OSR and to fulfill Eq. (4.48) according to Eq. (4.45)-(4.46) [22].

As both the DVB-T and LTE signal have a low carrier frequency, it is possible to operate within the first Nyquist zone [22]. For an optimized performance

Table 4.2 Selected wireless services for evaluation based on simulation. The carrier frequencies and bandwidths are chosen according to their respective standards. The second part states the parameters and some results of the evaluated  $\Sigma\Delta$ -modulator, © 2015 IEEE.

Standard	DVB-T	LTE	GSM	ITS-G5
Band	60	20	DCS 1800	G5SC1
$f_{in}/\text{MHz}$	786	820	1879.8	5880
$f_B/\text{MHz}$	7.61	20	0.2	10
$N_{Nyq}$	1	1	4	4
$f_s/\text{GHz}$	4	4	1	3.5
OSR	263	100	2500	175
$f_n/f_s$	0.20	0.21	0.12	0.32
$SQNR_{max}/\text{dB}$	74.93	66.03	58.48	52.62

regarding the SQNR, the sampling frequency is set to the maximum value of 4 GHz and causes the 20 MHz wide LTE signal to be oversampled by factor 100. As the signals of GSM and ITS-G5 are higher than the upper limit of the operating range within the first Nyquist zone, undersampling has to be used. To fulfill the boundary conditions (maximize OSR, Eq. (4.45)-(4.46) [22] and Fig. 4.23), the sampling frequencies are set to 1 GHz and 3.5 GHz respectively. Despite the low sampling rate of the GSM signal, still a high OSR can be achieved, as the signal's bandwidth is comparatively low (0.2 MHz). Fig. 4.24 shows SQNR values for each wireless system varying input amplitude between  $-60$  dBFS and  $0$  dBFS. For the evaluated systems, maximum SQNR values between  $52.62$  dB and  $74.93$  dB are calculated. Furthermore, it can be recognized from Fig. 4.24 that for signals with a higher input frequency the SQNR is getting better. For example the GSM signal at  $1.8$  GHz with an  $OSR = 2500$  has an around  $5 - 10$  dB better SQNR performance compared to the ITS-G5 signal with an  $OSR = 175$  although it is placed  $4$  GHz above the GSM-signal. This is because the  $\Sigma\Delta$ -modulator has a performance dependency of the input-frequency  $f_{in}$  if the  $\Sigma\Delta$ -modulator operates in undersampling mode. The lowest Nyquist zone is  $N_{Nyq} = 4$  for the  $\Sigma\Delta$ -modulator-architecture synthesized in Section 4.2.3. Therefore, for a higher located signal like ITS-G5 compared to GSM or DVB-T, a higher sampling frequency can be used. This results in a better SQNR. It



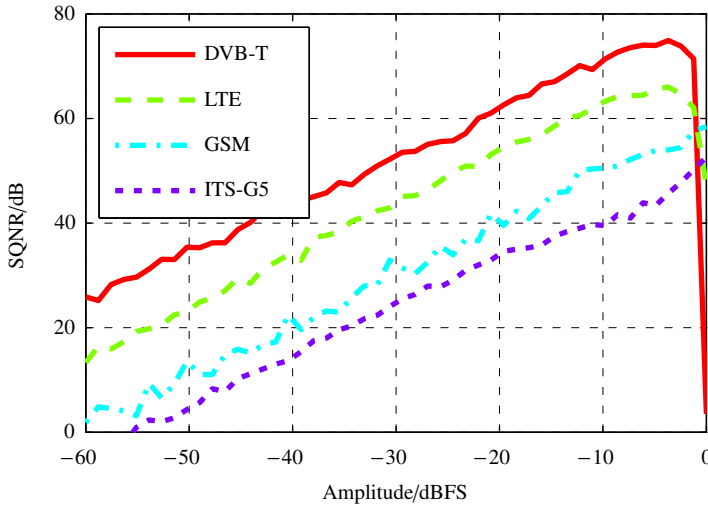


Figure 4.24 SQNR in dependency of input amplitude for different radio systems according to Table 4.2. Both the noise aggregating behavior for undersampling with regards to the maximum signal frequency as well as the positive impact of the oversampling with regards to the signal's bandwidth can be seen.

becomes clear if the OSR is based on a constant signal bandwidth. A signal with a bandwidth of 10 MHz has a constant OSR within the first Nyquist zone. For the fourth Nyquist zone, the sampling frequency according to the signal's input frequency has to be adapted in order to always place it optimally within the fourth Nyquist zone.

These findings lead to the following observations regarding the required flexibility and reconfigurability by frequency-agility as well as multistandard capability:

**Observation 4.6.** *The presented ADC based on a novel approach on reconfigurable continuous-time bandpass  $\Sigma\Delta$ -modulators allows noise shaping and thus noise reduction at the position of the notch within the noise floor. By appropriate selection of feedback coefficients within the FIR-DAC of the modulator, frequency agility can be achieved. The notch frequency can be changed by adjusting the feedback coefficients. An extension of the frequency range is possible by employing undersampling techniques and thus sampling signals in*

higher Nyquist zones. Digitization of signals from radio services at different positions within the overall operating range is possible at sufficient SQNR, both for signals within the first Nyquist zone and for signals in higher order Nyquist zones when undersampling is used [22].

**Observation 4.7.** *Multiple parallel cascaded  $\Sigma\Delta$ -modulators with a dedicated frequency synthesis for the sampling frequency enable simultaneous processing of multiple broadband signals. The number of required modulators depends on the number of wireless systems to be processed in parallel. Usually, one radio system requires one  $\Sigma\Delta$ -modulator.*

#### 4.4.2 System-Level Assessment based on OFDM Simulation

So far, the ADC design from Section 4.2 has been evaluated with special focus on multiservice compatibility due to reconfigurable and flexible properties regarding the operating frequencies. For these assessments, performance indicators related to either signal or noise power have been taken into account. Following a black-box testing approach, the proposed ADC is now evaluated based on a system-level approach which allows evaluation of the performance on the bitstream layer by analyzing the symbol error rate and error vector magnitude for a given signal.

##### 4.4.2.1 Methodology: System-Level Black-Box Testing with OFDM Test Signals

Following the concept of black-box testing, the ADC from this chapter shall be evaluated on the bitstream layer. This Section provides a brief description of the approach, the methodology as well as the ADC-related results have been published. For further information refer to [5].

For dynamic evaluation, a system-level approach is used to evaluate hardware on the bitstream layer. According to Table 2.1, many of the wireless services with relevance for automotive use employ Orthogonal Frequency Division Multiplex (OFDM) with some kind of Quadrature Amplitude Modulation (QAM). The integration into an ideal mixed-mode multidomain OFDM transceiver and receiver enables black-box testing of the hardware under test and allows for an evaluation based on symbol error rate (SER) and error vector magnitude (EVM) for most relevant wireless services. For evaluation of the ADC and signal canceling hardware, the respective components are either substituted (ADC) or additionally inserted (signal canceling). The concept of black-box testing refers

Table 4.3 Numerical values for selected OFDM parameters.

Parameter	2k-mode			
Elementary period $T/\mu\text{s}$	$\frac{7}{64}$			
Number of carriers $K$	1705			
$K_{\min}$	0			
$K_{\max}$	1704			
Duration $T_U/\mu\text{s}$	224			
Carrier spacing $1/T_U/\text{Hz}$	4467			
$N$ (IDFT points)	$2^{11}$			
Central frequency $f_c/\text{GHz}$	1.59			
Guard interval $G$	$\frac{1}{4}$	$\frac{1}{8}$	$\frac{1}{16}$	$\frac{1}{32}$
Guard interval duration $\Delta/\mu\text{s}$	56	28	14	7
Symbol duration $T_S/\mu\text{s}$	280	252	238	231

to the concept of system theory, where a given system is characterized based on comparison of an input signal the the respective output signal.

For this evaluation a DVB-T signal is selected due to its simplicity [32]. An ideal transmitter and receiver is setup in Matlab [105] according to [5, 127, 128]. In the transceiver an OFDM symbol with  $N$  subcarriers and can be written in simplified form as

$$s(t) = \frac{1}{N} \sum_{k=0}^{N-1} s_k(t), \text{ with sub-carrier } s_k(t) = \text{Re}\{c_k(t)e^{j2\pi(f_c+k\Delta f)t}\}, \quad (4.49)$$

complex symbol  $c_k(t)$ , carrier frequency  $f_c$ , symbol rate  $\Delta f$  and index  $k = 0, 1, 2, \dots, N-1$ . A DVB-T signal in 2k-mode according to [32] consists of frames, each of which is built-up out of 68 symbols. Depending on the transmission mode, each symbol has  $K$  subcarriers. For the 2k-mode,  $K = 1705$  carriers. All parameters for signal generation and analysis are presented in Table 4.3. Now,

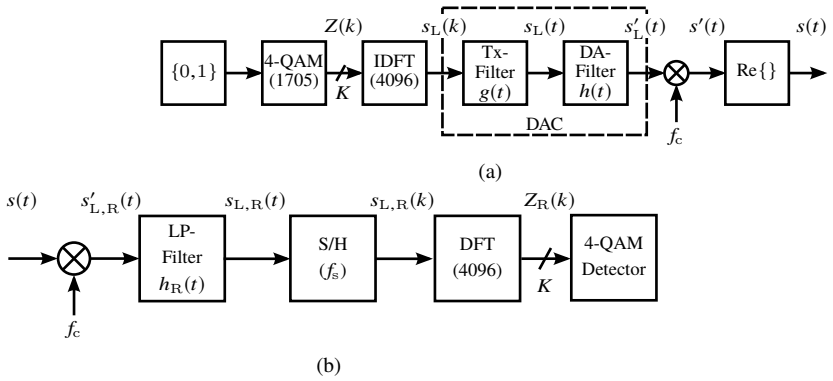


Figure 4.25 (a) Transmit and (b) receive chain of the OFDM system used for component evaluation, adapted from [5], © 2015 IEEE

the OFDM signal of a single symbol is represented by

$$s(t) = \text{Re} \left\{ e^{j2\pi f_c t} \sum_{k=K_{\min}}^{K_{\max}} c_{0,0,k} e^{j2\pi \frac{(k-K_{\max}+K_{\min})(t-\Delta)}{2T_U}} \right\} \quad (4.50)$$

for  $t \in [0; T_S]$ . This signal is generated and transmitted over an ideal channel to a receiver. A possible realization that implements the transmit chain is given in Fig. 4.25a. By mapping 3410 random numbers with a 4-QAM mapping scheme to complex symbols  $\{1 + j, 1 - j, -1 + j, -1 - j\}$ , finally 1705 symbols exist related to symbol  $c_{0,0,k}$  and are passed on in parallel form to the IDFT block. In each of the  $K$  branches, a symbol is conveyed. Furthermore, to avoid aliasing oversampling is introduced by applying zero padding [127]. This is achieved by doubling the IDFT operation to  $2N$ . To get a continuous-time signal, the signal is delivered to a DAC in the next step. The filter function  $g(t)$  corresponds to a holding function of the signal  $s_L(k)$  [5, 98]. The second filter  $h(t)$  applies lowpass filtering to remove signal replica generated by  $g(t)$  whereby the signal is smoothed in time domain. Finally, the baseband signal  $s'_L(t)$  with a bandwidth of 7.61 MHz is shifted to the carrier frequency  $f_c$  and the real part is extracted to finally result in the transmission signal  $s(t)$  according to Eq. (4.50). The receiver is based on an inversed structure as shown in Fig. 4.25b [5].

As only ideal components are used, the approach is suitable for evaluation of different, then non-ideal components along the previously described chain

as long as all other components except the device under test are kept ideal. By analysis of the output signal and comparison to the known predetermined input signal, calculation of SER and EVM is possible to characterize the system under test.

#### 4.4.2.2 Scenario and Implementation

Ongoing from the previously introduced methodology, the  $\Sigma\Delta$ -modulator-ADC from Section 4.2 shall be evaluated and serves as the ADC under test. It is plugged into the ideal receive chain from Fig. 4.25b. As it is capable of direct RF sampling at various frequencies within the necessary operating range, the ADC under test replaces the first three components in the receive chain, particularly the mixer for downconversion (direct RF sampling is possible, downconversion and separation of real and imaginary parts are done in digital domain), the anti aliasing lowpass filter (in undersampling, intentional aliasing is used for an extension of operating range) and the sample-and-hold element (the  $\Sigma\Delta$ -modulator-ADC contains its own S/H-device). Thus, now the generated OFDM-signal according the parameters of Table 4.3 for the selected 2k-mode  $s(t)$  is fed directly to the  $\Sigma\Delta$ -modulator [5]. For this application, the ADC is operated at  $f_s = 4$  GHz, the DVB-T signal is positioned close to the upper end of the first Nyquist zone<sup>56</sup> at  $f_c = 1.59$  GHz.

Now, the influence of the  $\Sigma\Delta$ -modulator has to be mapped onto the input signal  $s(t)$ . Firstly, only the noise spectrum of the  $\Sigma\Delta$ -modulator is calculated by letting the input power equal zero. Subsequently the spectrum of  $s(t)$  and the modulator's noise spectrum  $N_{\Sigma\Delta M}$  are superimposed to

$$S_{\Sigma\Delta M}(f) = \mathcal{F} \{s(t)\} + N_{\Sigma\Delta M}(f). \quad (4.51)$$

Fig. 4.26 shows the spectrum of the superimposed signal  $S_{\Sigma\Delta M}(f)$ . The overall spectrum contains a notch in the quantization noise due to the noise shaping ability of the  $\Sigma\Delta$ -modulator [5, 22]. This leads to an improved SQNR at the notch position  $f_n$ . The superposition like shown in Eq. (4.51) is possible due to linearity of the Fourier transform [98] and comprises the influence of both the ADC under test and the OFDM signal chain. As the latter only uses ideal components, the analysis of the resulting signal gives an insight on the performance of the ADC [5].

<sup>56</sup>Due to the diverging behavior of the FIR-DAC coefficients, the operating range within the first Nyquist zone is restricted to 0.1 to 0.4 (relative notch positions  $f_n/f_s$ ), see Section 4.2.3.

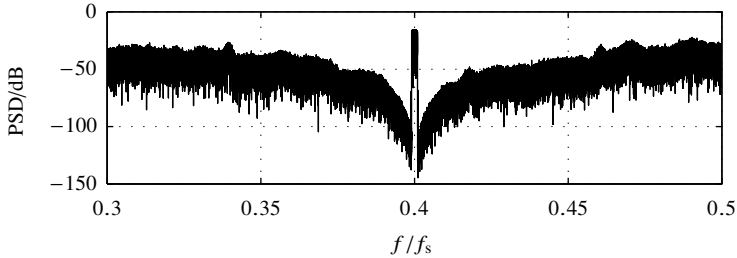


Figure 4.26 Section of the power spectral density of the superimposed signal  $S_{\Sigma\Delta M}(f)$  which includes the effects of the ADC under test: the notch within the ADC's noise floor due to noise shaping is clearly visible at the relative frequency  $f/f_s = 0.4$ .

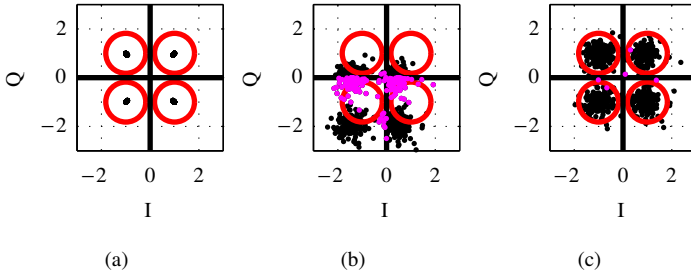


Figure 4.27 Constellation diagram for the received signals in (a) without offset compensation at 0 dBFS, in (b) without offset compensation at  $-80$  dBFS and in (c) with offset compensation at  $-80$  dBFS. Magenta dots represent erroneous symbols.

#### 4.4.2.3 Evaluation

After digitization within the ADC under test, the signal is processed by a DSP with ideal components like shown in Fig. 4.25b. After filtering to separate the OFDM signal, downconversion and separation of the signal into its subcarriers by applying a DFT, the processed signal is projected onto an IQ diagram for qualitative analysis as well as determination of the EVM and SER. Fig. 4.27 displays the respective constellation diagrams for different input amplitudes. It shows the signal as a scatter plot in the complex plane, where magenta scatter dots represent erroneous symbols. For small input amplitudes, an offset can be detected like depicted in Fig. 4.27b in comparison to Fig. 4.27a, where

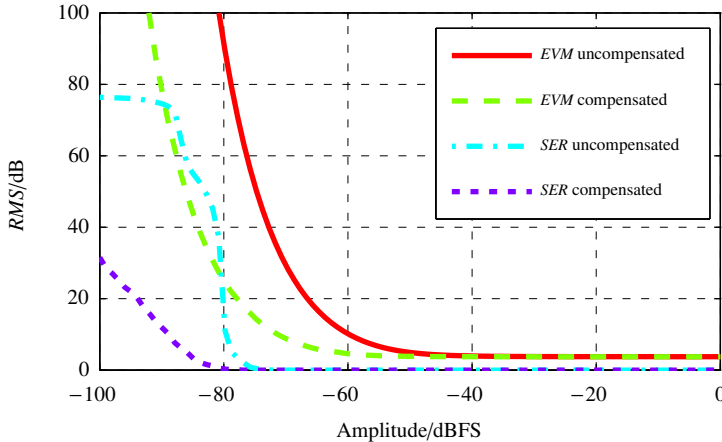


Figure 4.28 Qualitative analysis of the compensated and uncompensated SER and EVM for different amplitudes of the input signal.

the maximum amplitude has been used. This effect occurs due to a slightly malpositioned notch at 1.59 GHz. The effect can be resolved by either doing a highly accurate frequency correction or by applying an offset correction which appears to be more realistic and less complex for future realization. For the results in Fig. 4.27c the latter approach is used based on a linear regression between transmitted and receives signals. This procedure reduces the number of erroneous symbol and is comparable to the evaluation of pilot signals which are known to the receiver for channel estimation, see e. g. [129]. The offset compensation allows for significant improvement of SER and EVM [5]. Fig. 4.28 presents a quantitative analysis. An acceptable value of  $EVM = 8\%$  is reached at  $-57$  dBFS without offset compensation and already at  $-68$  dBFS when offset compensation is applied. The first symbol error without offset compensation occurs at  $-72.7$  dBFS whereas with offset compensation it appears only at  $-77.8$  dBFS. Depending on the input amplitude, limits for both SER and EVM can be defined to subsequently derive requirements for signal processing stages especially before the ADC [5].

In addition to Observations 4.6 and 4.7 regarding the requirements with regards to reconfigurability by frequency agility as well as multistandard capabilities in the previous section, the results from this evaluation on a system-level lead to

**Observation 4.8.** *The designed  $\Sigma\Delta$ -modulator shows proper performance with regards to error vector magnitude and symbol error rate without further signal conditioning before or after the ADC under test. The proposed methodology isolated the ADC's performance as only ideal components besides the ADC under test are used. Based on this black-box testing approach, requirements for the analog signal conditioning in front of the ADC can be derived.*

Chapter 5 deals with systems for signal preconditioning and coexistence and interference management. These systems are also evaluated within this chapter. Wireless services like LTE [30] define detailed specifications regarding the overall system's performance regarding SNR on power level or EVM on bitstream level [129].



# RF Signal Processing with Frequency Agile Components in the Analog Domain

All wireless communications systems rely on available frequency resources to transmit or receive information with a certain bandwidth and transmission power. As more and more radio communications systems are deployed both on micro- and macroscopic level and techniques like carrier aggregation are implemented to augment data rates<sup>57</sup>, it can be concluded that available frequency resources are a scarce good. The regulative situation is evaluated in detail in Section 2.2.1 and [5, 24] within the scope of this work<sup>58</sup>.

*Interference* is one of the major performance-limiting factors for wireless communication systems [85]. Interference can occur due to non interference-free frequency assignments (e. g. within ISM-bands), guard bands between two systems which are laid out too narrow or any other reason which causes RF energy to leak into the victim-system's frequency band of operation. The interference setup can become more severe especially in environments, where the RF noise level in general is elevated (like urban environments) as well as in areas with many arbitrary RF nodes being active simultaneously - both on a macroscopic level like in an urban environment with presence of many base stations and user equipment as well as on a microscopic level like a vehicle, where multiple wireless systems can be active both transmitting and receiving in parallel, see Section 2.2.2.

**Observation 5.1.** *To ensure proper function of any wireless system it is necessary, that a given system does not influence itself and is not influenced by another system in any negative way. This leads to the previously already used term of coexistence which describes the peaceful parallel operation of different communications systems of the same or different technologies.*

All technologies discussed in Section 2.1 and Table 2.1 have a system-inherent design to deal with or mitigate interference, mostly on the macroscopic layer.

---

<sup>57</sup>Both the channel capacity of SISO- and MIMO-systems is proportional to the bandwidth  $B$ , see Section 3.3.2

<sup>58</sup>Further information can also be found in [28–32, 38–40], as well as secondary sources like [34–36].

The ecosystem of vehicular connectivity requires multiple systems based on the same as well as different standards to be integrated and operated in coexistence within a vehicle. At first, this chapter focuses on interference between different sub-systems on the microscopic layer, thus on vehicular level. Section 5.1 gives a brief overview of the interference environment and focuses on typical exemplary scenarios. As a second step, the implications on RF front-end design for frequency-agile multistandard transceivers with focus on Tx-leakage are analyzed in Section 5.2. These two insights lay out the necessity of *signal conditioning* to make the received signals ADC compatible (prevent it from blocking or clipping), cf. Fig. 2.7 and Sec. 2.3.1 in general). Subsequently, Sec. 5.3 proposes and analyses an active architecture to mitigate interference due to other intra-vehicle sub-systems (inter-sub-system interference) as well as Tx-leakage (intra-sub-system interference).

## 5.1 Coexistence Management and Interference Mitigation for Vehicular Connectivity

Chapter 2 intensively discusses the ecosystem of vehicular connectivity. Especially Observation 2.4 and Fig. 2.4 clearly state the OEM's role as system integrator who has to ensure the peaceful coexistence of multiple both complementary and coherent sub-systems to each other. Based on the partitioning of the complete RF system into sub-systems, all interference problems occurring in the automotive domain can be classified into *inter-sub-system interference*<sup>59</sup>, where an  $i$ -th sub-system is interfering into a  $j$ -th sub-system as well as *intra-sub-system interference*, where interference occurs within one and the same sub-system. The latter is of special importance in the context of RF front-end design without frequency-fixed components to realize completely frequency-agile and multistandard transceivers. This topic is covered in Sec. 5.2.

---

<sup>59</sup>Literature like [130, 131] also uses the term *in-device coexistence (IDC) interference*, which seems not to be applicable here, as the relevant transceivers are positioned within the same device or ECU (in the automotive context). However, in the context of multistandard-capable transceivers, IDC interference appears to be reasonable, even though the author's distinction still remains valid.

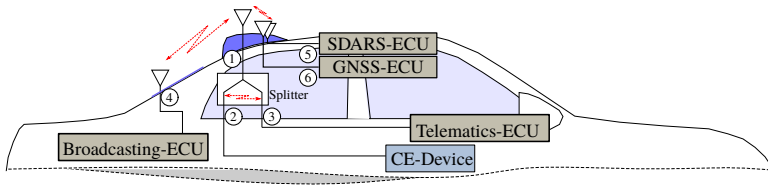


Figure 5.2 Partitioning of different subsystems to realize vehicular connectivity for ADAS applications, a connection of the passengers' CE-devices to the vehicle's outside antenna system as well as reception of various broadcasting services. Note, that for the sake of simplicity of the visualization, antennas for MIMO operation and diversity are omitted here.

A general interference situation is shown in Fig. 5.1 where a desired signal being received at a certain power level is predominated by another signal at a higher level which would cause the respective receiver stages and ADC to be blocked due to the high signal power. The above classification differentiates the source of the interfering signal as either originating from another transmitter not belonging to the blocked receiver or as coming from the corresponding transmitter.

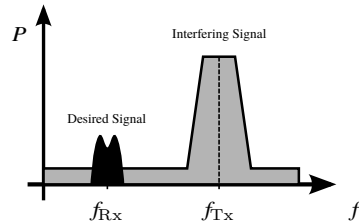


Figure 5.1 Representation of a general interference situation in the frequency domain.

Figure 5.2 exemplifies typical coexistence situation in the automotive domain. It is mostly defined by the following sub-systems: (3) the vehicular telematics module to enable cellular connectivity for ADAS applications (this architecture is the focus of Chapters 2, 3 and 4), (2) a physical connection of passengers' cellular devices to the vehicles antenna (1) in order to circumvent the shielding of the car body and metalized windows [44] via a single or multiple active or passive coupling devices and (4) multiple receivers of broadcasting services like digital terrestrial broadcasting for audio (DAB) or video (DVB-T) as well as (5) satellite radio (SDARS) and (6) a positioning system via GNSS.

Section 2.2.2 about the ecosystem of vehicular connectivity with its multitude of different radio systems has already introduced major examples of interference issues based on the components from above enumeration, which are investigated in detail in the following paragraphs.

**Observation 5.2.** *Based on the need for ubiquitous connectivity, especially in*

*the vehicular domain, either multiple radio systems or a communication system with multistandard capabilities are operated concurrently in an environment of limited spectrum availability and thus with little frequency separation. Due to this simultaneous and close (both w.r.t. frequency and physical separation) operation, undesirable emission like out-of-band or spurious emissions, harmonics and intermodulation products can occur and radiate as interference into the receive branch. This leads to a raised noise and interference level and subsequently to a low SINR as well as a reduced receiver sensitivity (e. g. due to the limited resolution of the ADC) or even blocking, if filters of the victim are unable to remove<sup>60</sup> or sufficiently suppress the unwanted signals.*

A detailed visualization of frequency allocations is given in Fig. 5.3. In the lower part of the plot, frequency allocations including their potentially small separation or overlapping is depicted. The upper part of the plot depicts maximum transmit powers and typical receiver sensitivities of the radio systems with respect to possible frequency ranges. This figure represents a more detailed version of Fig. 2.2 and uses the same sources<sup>61</sup>. Typical scenarios from automotive domain are (list is not exhaustive):

1. parallel operation of multiple cellular transceivers within the vehicle, e. g. the telematics ECU concurrently to a passenger's CE device.
2. Operation of multiple different radio technologies with little frequency separation: impairment of DVB-T reception occurs during an active transmission of the vehicle's LTE transceiver on frequencies close to the DVB-T; challenges regarding coexistence between LTE in band 30 and SDARS as well as cellular bands neighboring bands for industrial, scientific and medical (ISM) use (e. g. LTE bands 40 TDD, 7 in uplink and band 38 TDD)<sup>62</sup>.
3. Intermodulation products or harmonics originating at the interfering transmitter: the second harmonics of cellular frequencies in bands 13 and 14 fall into the GNSS L1 band<sup>63</sup>.

<sup>60</sup>Total removal is usually not possible, see Sec. 5.3.2

<sup>61</sup>Primarily [28–32, 38–40], as well as secondary sources like [34–36].

<sup>62</sup>LTE band 40 TDD: 2300–2400 MHz, ISM band: 2400–2483.5 MHz, LTE band 7 uplink: 2500–2570 MHz, LTE band 38 TDD: 2570–2620 MHz [30].

<sup>63</sup>LTE band 13 uplink: 777–787 MHz, LTE band 14 uplink: 788–798 MHz, GNSS L1: 1559–1610 MHz [30].

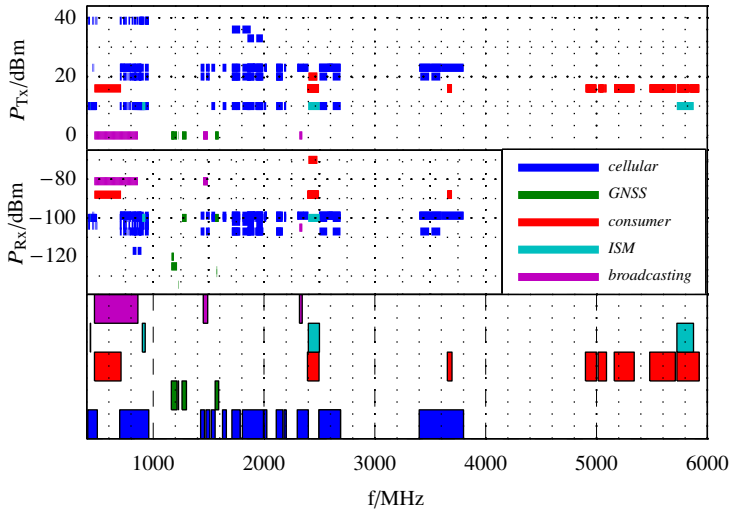


Figure 5.3 Detailed visualization of frequency allocations for relevant wireless communication systems in the automotive domain. Here, SDARS is treated as a broadcasting service.

For scenario 1, multiple transceivers for cellular communications are connected via a power splitter/coupler to the same antenna<sup>64</sup>. For the receive case, the device acts as a splitter, for the transmit case as a coupler. Now, the performance of the overall system is limited by the coupling device, which interconnects both sub-systems to the antenna, but at the same time has to isolate the sub-systems from each other. This effectiveness of this isolation is determined by the

<sup>64</sup>Of course, deployment and utilization of dedicated antennas for this purpose would be possible, but according to Section 3.1 integration spaces for antenna systems are scarce in the vehicular domain. Besides, integration volumes other than the roof usually yield an unavoidable performance degradation due to a directive influence of the vehicle's body itself. As the roof-top antenna is always reserved for the vehicles telematics ECU, the CE-device's connection would be subject to unpredictable performance degradation, especially at cell edges. If this concept of multiple antennas is still implemented, the isolation within the coupler is replaced by the decoupling between the different antennas.

attenuation  $S_{3,2}$  between ports 2 and 3 and vice versa (see Fig. 5.2 for port numbering).

Of course, the severity of this coexistence situation is dependent on the utilized frequencies for each device. The worst case situation for Germany occurs in band 20 between two MNOs, where the DL of one MNO and the UL of the second MNO (each 10 MHz wide) are directly adjacent to each other with only 11 MHz band-to-band separation, as depicted in Fig. 5.4. Due to the limited isolation of the coupler

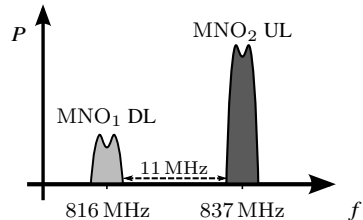


Figure 5.4 Close positioning of UL and DL frequencies with a band-to-band separation of 11 MHz in LTE band 20.

(usually in the magnitude of 15 – 25 dB, the transmitted signal leaks into the receiving system and causes interference as the receive SINR is severely reduced. Common transceivers usually do not have to work in such an environment, thus the receiver's band and channel selection is not as selective as required in this scenario. Based on the LTE standard's [30] classification of different interference scenarios, this *out-of-band* interference setup requires an SINR of at least  $-44$  dB. Note, that the signal power of the interferer exceeds the power of the desired signal (cf. Fig. 5.4), thus the SINR is negative. This requirement allows the interfering signal to be at most 44 dB larger, than the desired signal. Thus, within this worst case channel allocation and with a maximum transmit power of 23 dB and a receiver sensitivity of  $-94$  dB, an attenuation of at least 73 dB would be required. Besides, [30] calls for a maximum receiver input power of  $-25$  dB. These specifications cannot be achieved with typical RF splitting/coupling devices. However, of course these conditions are only violated if both devices are transmitting and receiving at the same time (which can be unlikely when time diversity mechanisms are used in two non-synchronized systems) and the appropriate frequencies are used by both devices. The SINR requirement is relaxed for larger separations frequency wise between the desired signal and the interferer. Nevertheless, these situation can occur and have to be resolved by applying suitable measures.

A similar situation occurs when cellular systems are operated in parallel to broadcasting services. This scenario is now exemplarily investigated for the coexistent operation of LTE and DVB-T. It can be easily transferred to the coexistence of LTE and SDARS by applying the same principles and referring

to the respective standardization documents<sup>65</sup> [30].

After the second digital dividend (spectrum refarming in favor of the mobile network operators, see Sec. 2.2.1), digital broadcasting services are operated in the frequency range from 470 MHz to 790 MHz and is subject to interference from the adjacent LTE deployment in band 20 from 790 MHz to 862 MHz. Due to the close assignment of frequencies, the positioning of the cellular uplink and downlink frequencies have already been swapped to achieve a larger guard band between both services. Usually, FDD channels are assigned pairwise with the UE's uplink range being lower than the downlink, as lower frequencies are subject to less free space path loss, cf. Sec. 3.3.1 about losses or [63, 85, 87]. Nevertheless, due to the low distances between cellular antennas mounted e. g. in a roof-top antenna and broadcasting antennas in the rear view window and fixed side windows, interference as depicted in Fig. 5.2 can still occur [24, 43, 47]. Again, the limited isolation between the cellular antenna (port 1) and the broadcasting antenna (port 4), cf. Fig. 5.2, causes power to leak into the receive path and subsequently blocking of the ADC or any other part of the receiver stages. The most important requirement is the least necessary attenuation of a transmitted signal which has coupled into the reception path. This means, the interferer has to be attenuated that it can be sampled by the ADC without driving it into saturation and at sufficient resolution. This would allow further filtering in the digital domain. Figure 5.5 from [24] serves as an example for the given setup and leads to a minimum attenuation of 61 dB. The noise power is calculated based on the thermal noise level for a 10 MHz wide signal according to  $N = k \cdot \Delta f \cdot T$  with  $k = 1.38 \cdot 10^{-23}$  Ws/K being the Boltzmann constant,  $\Delta f$  being the bandwidth and  $T$  being the temperature in Kelvin [85]. For the exemplary frequency-agile transceiver AD9361 [132], an additional noise figure of 2 dB is added for frequencies around 800 MHz and a temperature of 25 °C. Thus, the noise floor is at least around -102 dB.

The receiver within the AD9361 transceiver has a 12 bit resolution which leads to a dynamic range of 74 dB (see Sec. 4.1.2). This sets the maximum possible scannable input power to -28 dB. Together with a maximum transmit power of 23 dBm at 800 MHz and an addition of 10 dB for the peak to average ratio (PAPR) due to the OFDM multiplexing [133] leads to the minimum attenuation of 61 dB as visualized in Fig. 5.5. This power level plan is valid for in-band interference but can also be applied to out-of-band interference by additionally

---

<sup>65</sup> *SiriusXM* operates a satellite radio system, the respective technical documents are not publicly available but have been partially accessible during this work due to the author's work position.

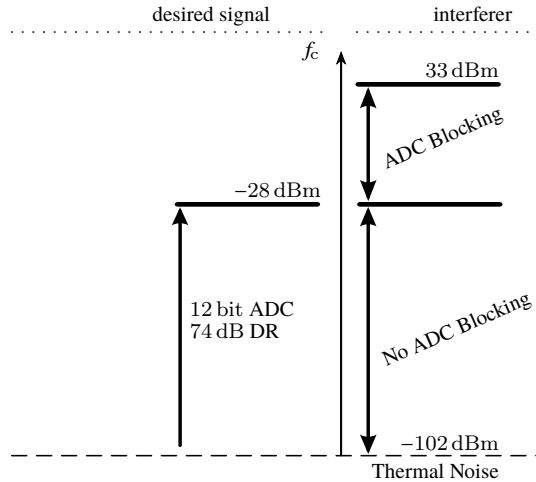


Figure 5.5 Minimum requirements regarding attenuation for successful suppression of the interfering signal together with the ADC [24], © 2015 IEEE.

considering a minimum required SNR. The concept of in-band interference mitigation is used for example for full duplex architecture, where transmitting and receiving can occur simultaneously on the same frequency [133, 134]. This work however focuses on the concept of frequency-agile transceivers with multistandard capabilities. This requires the omission of frequency fixed components.

## 5.2 Waiving of Frequency Fixed Components

The previously described scenarios can be allocated in the previously defined category of inter-sub-system interference, as *different* sub-systems are affected. Interference in the nature of common Tx-leakage can also occur within one and the same sub-system, which leads to the classification of inter-sub-system interference. Transceivers usually consist of a dedicated transmit and receive branch with a shared antenna. The branches are commonly connected via a frequency-selective duplexer. This devices, as well as other band and channel selecting filter components exhibit frequency-fixed components and prevent Tx-leakage either from the own transmitter or a foreign transmitter into the receiver. Today, interference is usually mitigated by using integrated tunable



filters with varying number of paths or special receiver designs [135]. Besides these system-inherent measures, other approaches to decrease coupling can already be applied at the antenna: examples thereof are physical separation, polarization diversity or use of directive antennas (directional separation).

**Observation 5.3.** *Common approaches introduce frequency-fixed components into the system as even tunable filters are only adjustable to a certain (predefined) extent and are not fully frequency-agile as discussed and required in Sec. 2.3.1. In order to ensure full reconfigurability, frequency-fixed filters for band and channel selection as well as duplexers cannot be used [24].*

Besides these passive suppression methods also active concepts are possible. Note, that all interference-causing signals within the context of automotive connectivity are known. They are referred to as *self-made interference*. This leads to

**Proposition 5.1.** *The knowledge of the interfering signals enables the use of cancellation-based approaches, where a part of the interfering signal is coupled into the receive path with an inverted phase to cancel out the interfering signal by being superposed with an inverted copy of itself and thus being eliminated [24].*

## 5.3 Design of a Signal-Canceling-Architecture

To prevent receiver blocking or a performance-degrading reduction of the available SNR within multistandard transceivers, a signal-canceling architecture is introduced. In the following subsections, the operation principle of the cancellation system is described in a general manner and subsequently detailed based on the derivation of a mathematical model to theoretically describe the system behavior.

### 5.3.1 Operation Principle and Theoretical Investigation

According to the previous findings, the transceiver shall be able to process multiple radio access systems simultaneously. This can be achieved by employing for example an SDR-like architecture as shown in Fig. 2.6. Now, to ensure coexistence management by interference mitigation as defined previously within this chapter, an additional cancellation path is added to the generic transceiver setup like in [24, 136] as shown in Fig. 5.6.

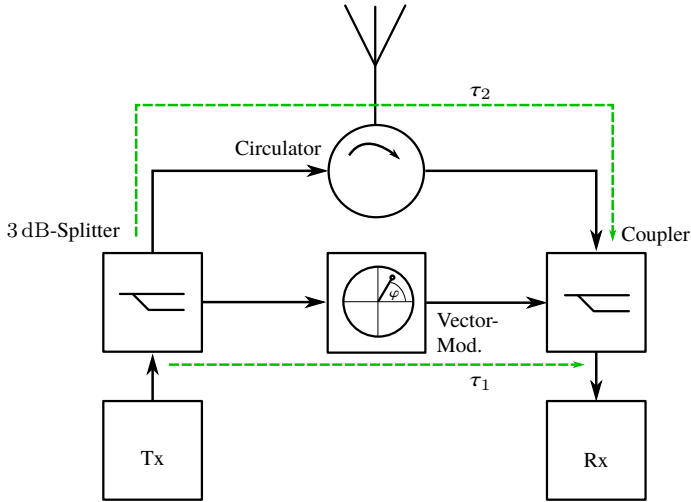


Figure 5.6 Block diagram of the signal canceling setup under investigation [24], © 2015 IEEE.

To characterize the influence of the signal canceling architecture on the Tx-leakage from the transmitter of one radio system into the receiver of another radio system, again the setup from Fig. 5.6 is examined. The attenuation of the interfering signal in dependency of the frequency is required, thus the transfer function  $H(j\omega)$  has to be determined.

Besides the matched amplitude of the signals in both paths also timing and phase information are of major importance, which is why the system model is first created in the time domain and then transferred into the frequency domain by a Fourier transform. This approach is loosely following the concept in [137], which was originally used to suppress Tx leakage in passive backscattering RFID devices. Here, the context of vehicular connectivity introduced above is applied.

Now, the overall impulse response  $h(t)$  consists of the superposition of the two signals at the coupler in the receiver's branch. Both signals are delayed by a value  $\tau_1$  and  $\tau_2$  and changed (weighted) in amplitude by  $A_1$  and  $A_2$ . Furthermore, the concatenated impulse response of the vector modulator  $p(t)$  has to be considered:

$$h(t) = \underbrace{A_2 \cdot \delta(t - \tau_2)}_{\text{circulator path}} - \underbrace{A_1 \cdot \delta(t - \tau_1) * p(t)}_{\text{VM path}}. \quad (5.1)$$

Total cancellation is achieved, if both summands are equal<sup>66</sup>, thus  $\Delta\tau = \tau_2 - \tau_1 = 0$ ,  $A_1 = A_2 = 1$  and  $|p(t)| = 1$ . As only  $\Delta\tau$  is relevant, set  $\tau_2 = 0$  without loss of generality. With these simplifications, Eq. (5.1) can be simplified to

$$h(t) = \delta(t) - \delta(t - \Delta\tau) * p(t). \quad (5.2)$$

In general, the vector modulator manipulates amplitude and phase of an incoming signal. For this derivation, the vector modulator is initially considered as a variable phase shifter, which alters the phase of an input signal by  $\varphi$ . This corresponds to a multiplication of the input signal with  $e^{j\varphi}$ . The weighting influence of the vector modulator is considered by the factor  $A_1$  as shown in Eq. (5.1). Thus,  $p(t)$  can be written as

$$p(t) = \delta(t) \cdot e^{j\varphi} \quad (5.3)$$

$$= (\cos(\varphi) + j \sin(\varphi)) \cdot \delta(t). \quad (5.4)$$

Here, the quadrature component can be expressed by introducing the Hilbert transform  $\mathcal{H}(\cdot)$  according to [138] with  $\mathcal{H}(x(t)) = x(t) * 1/(\pi t)$ . This modification yields

$$p(t) = \cos(\varphi)\delta(t) + \sin(\varphi) \cdot \frac{1}{\pi t}, \quad (5.5)$$

as  $\mathcal{H}(\delta(t)) = 1/(\pi t)$ . Now, by inserting  $p(t)$  into Eq. (5.2), the impulse response can be rewritten and subsequently simplified due to the sifting property<sup>67</sup> of  $\delta(t)$  as follows:

$$h(t) = \delta(t) - \delta(t - \Delta\tau) * \left( \cos(\varphi) \cdot \delta(t) + \sin(\varphi) \cdot \frac{1}{\pi t} \right) \quad (5.6)$$

$$= \delta(t) - \left( \cos(\varphi) \cdot \delta(t - \Delta\tau) + \sin(\varphi) \cdot \delta(t - \Delta\tau) * \frac{1}{\pi t} \right). \quad (5.7)$$

Next, the transfer function  $H(j\omega)$  is calculated by applying a Fourier Transform on the above equation of  $h(t)$ :

$$H(j\omega) = \mathcal{F} \{h(t)\} \quad (5.8)$$

$$= 1 - \left[ \cos(\varphi) \cdot e^{-j\omega\Delta\tau} + \sin(\varphi) \cdot e^{-j\omega\Delta\tau} \cdot (-j \operatorname{sgn}(\omega)) \right], \quad (5.9)$$

<sup>66</sup>To ensure equality of the signals' amplitudes ( $A_1 = A_2 = 1$ ), both signals have to be aligned to each other (w.r.t. amplitude) either by attenuation or by amplification within the cancellation path.

<sup>67</sup>When convolving (denoted by  $*$ ) a function  $f(t)$  with a delayed delta function  $\delta(t - t_0)$ , the convolution extracts the value of the original function at the point of the delay, cf. [90]:  $\int f(t) \cdot \delta(t - t_0) dt = f(t_0)$ .

where the correspondences for delayed and non-delayed Dirac functions are used according to [90]. A convolution with the Hilbert transformer  $1/(\pi t)$  in the time domain corresponds to a multiplication with  $-j \operatorname{sgn}(\omega)$  in frequency domain [90, 138].

In this application, the attenuation of the signal canceling device is most important, thus the amplitude or absolute value  $|H(j\omega)|$  is relevant. By expanding the term from above, sorting for real and imaginary summands and subsequently calculating the absolute value for non-negative frequencies, the frequency characteristic of the architecture like shown in Fig. 5.6 behaves according to

$$|H(j\omega)| = \sqrt{2(1 - \cos(\varphi + \omega\Delta\tau))}. \quad (5.10)$$

### 5.3.2 System Behavior and Sensitivity

The absolute value of the transfer function  $|H(j\omega)|$  from Eq. (5.10) above behaves periodically in  $\omega$ . Furthermore, its periodicity and length of the period is influenced by  $\Delta\tau$ : for small values with  $\Delta\tau \rightarrow 0$ , the period tends to infinity which yields an infinite bandwidth of attenuation. Increasing values of  $\Delta\tau$  however decrease the length of the period of Eq. (5.10) which results in a smaller attenuation bandwidth. The behavior of  $|H(j\omega)|$  is visualized in Fig. 5.7 for different values of  $\Delta\tau$  to highlight its influence on periodicity and thus the realized attenuation bandwidth. Note, that  $|H_i(j\omega)|$  reaches local maxima at 6 dB for certain values of  $\omega$ . For this overall parameter configuration, constructive interference occurs which doubles the signal level. The minima, one of them being at 800 MHz, are caused by destructive interference, where the original signal is annihilated successfully. Both the maxima and minima occur based on the periodicity of  $|H(j\omega)|$ .

**Observation 5.4.** *Full annihilation at a target frequency  $f_0$  is achieved, if the cos-term within Eq. (5.10) equals one and causes  $|H(j\omega)|$  to go towards (linear) zero. This is the case if its argument equals integral multiples of  $2\pi$ , thus  $\varphi + \omega\Delta\tau = 2\pi n$ ,  $n \in \mathbb{Z}$  at  $\omega = \omega_0 = 2\pi f_0$ .*

Besides the influence of the delay mismatch on the cancellation bandwidth, a variation of  $\Delta\tau$  obviously also changes the argument of the cosine term and thus directly the magnitude of  $|H(j\omega)|$ . Nevertheless, this influence of the magnitude of the system's transfer function can be compensated by updating the phase  $\varphi$  in Eq. (5.10). Besides changes in cancellation bandwidth, this retuning allows to minimize  $|H(j\omega)|$  for any value of  $\Delta\tau$  at any frequency  $f$ . Due to the

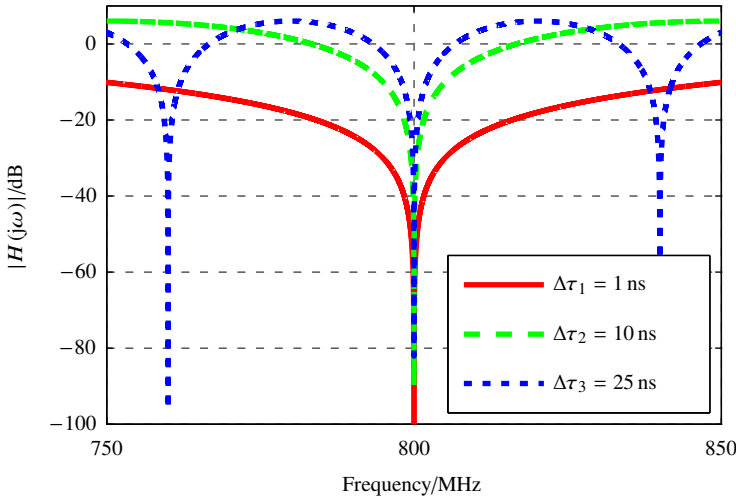


Figure 5.7 Plot of the transfer functions  $|H_i(j\omega)|$  for different values of  $\Delta\tau$ . The system has been tuned to the appropriate value of  $\varphi$  for each example to ensure maximum attenuation at 800 MHz.

band-limited behavior of  $|H(j\omega)|$ , this correction by phase adaption only works at a given frequency, but repeats itself each period.

With appropriate tuning of the parameters amplitude  $A_i$  and phase  $\varphi$  for the respective time difference  $\Delta\tau$ , a minimum attenuation  $L$  can be achieved within the bandwidth  $\Delta f = f_u - f_l$ , whereas the maximum attenuation is reached at  $f_0$ . For facilitated interpretation and to account for a practical realization, the delay offset  $\Delta\tau$  can also be expressed as an offset of the electrical length  $\Delta l = \Delta\tau \cdot c_0$  of the RF lines, as depicted in Fig. 5.8 for different cancellation bandwidths<sup>68</sup>. The evaluation of above figures leads to

**Observation 5.5.** Any offset, either in electrical length  $l$  or delay  $\tau$  causing  $\Delta l$  or  $\Delta\tau$  to be different from zero, leads to a degradation in isolation between the interferer and the victim due to a misadjusted signal canceling stage.

This theoretical system behavior based on considering ideal assumptions for the derivation of the system model is subject to external influence which has

<sup>68</sup>The bandwidths used in Fig. 5.8 are typical bandwidths used within LTE deployments around 800 MHz [30].

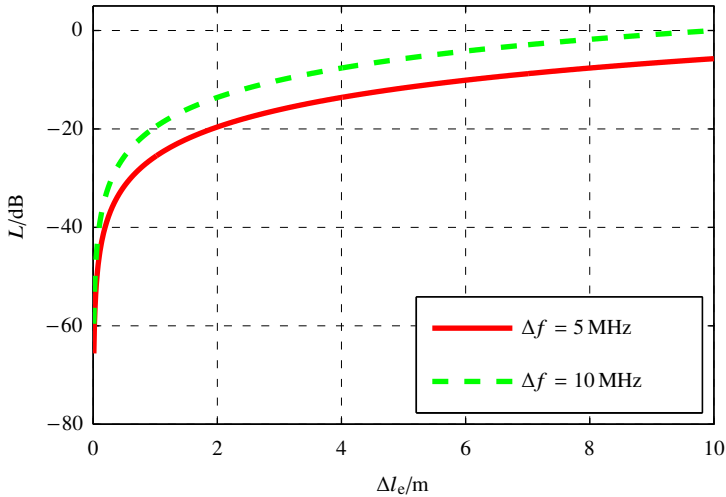


Figure 5.8 Achievable attenuation  $L$  plotted over the electrical length difference  $\Delta l_e$  between the transceiver path and cancellation path for different cancellation bandwidths  $\Delta f$ .

been neglected so far. This additional impact on the system and its performance can be classified as follows:

*Linear effects* can be traced back to any (additional) attenuation or amplification as well as any further delays which can occur both inside and outside of the the system. The latter could e.g. occur due to multipath reflections within the communication channel which couple over the antenna into the system or even a mismatched antenna which causes signals to be reflected back into the system. Additional *non-linear effects* e.g. due to utilization of semiconducting materials can cause intermodulation and thus evoke signal distortion (cf. signal to noise and distortion ratio in Section 4.1.2 which subsequently degrades the performance of the communications system. Furthermore, the increase of analog components by adding the cancellation path also raises the general noise level of the overall system.

Besides the external introduction of multiple delayed signals, they can also be caused internally. Both real (non-ideal) splitters and couplers yield a limited isolation. The isolation of a component quantifies the unwanted transmission between two ports of a multiport network. For a splitter, the isolation describes

the coupling between its output ports; for a coupler, the isolation corresponds to the coupling between its input ports. As shown in Fig. 5.9, signals originating from the cancellation path couple into the receive path due to the finite and limited isolation of the coupler and propagate through the receive path, the forward path of the circulator into the transmit path and eventually back into the cancellation path. Due to the loop-like propagation path within the system, these signals are referred to as *loop signals*.

Both internally as well as externally originated signals cause a multi-tap behavior of the impulse response  $h(t)$  of the overall system (circulator path as well as cancellation path) due to replica of an identical signal arriving at different times and amplitudes. If only one cancellation path is used, the adjustment of the phase  $\varphi$  can only compensate one delay tap which would leave components of the signal to be canceled in the output signal and thus cause a performance degradation of the signal canceling architecture.

Besides these typical linear and non-linear effects, (*phase*) *noise* additionally deteriorates the performance of the cancellation system. Besides the limited resolution and noise figure of the either amplifying (amplifier in cancellation path) or attenuating and phase adjusting components (vector modulator in cancellation path) as well as phase resolution, [139] identifies the phase noise of oscillators as a fundamental limit.

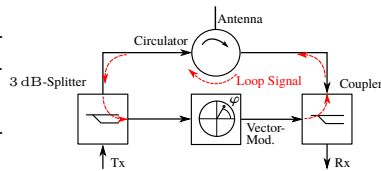


Figure 5.9 Simplified representation of loop signals due to limited isolation of real splitter and coupler components.

Now, to ensure proper performance of the interference suppression, the cancellation path has to reproduce all effects from within the transmitter path as good as possible. The superposition of all linear effects (based on attenuation, amplification and delay) can be reproduced by an infinite number of cancellation paths with the correct electrical length to match the required delay. Each of the cancellation paths is equipped with a vector modulator to adjust the signal's amplitude and phase. Of course, by raising the number of cancellation paths, the overall system complexity and the effort for coordination and tuning is also increased. Multipath signal canceling system are investigated in more detail e.g. in [140].

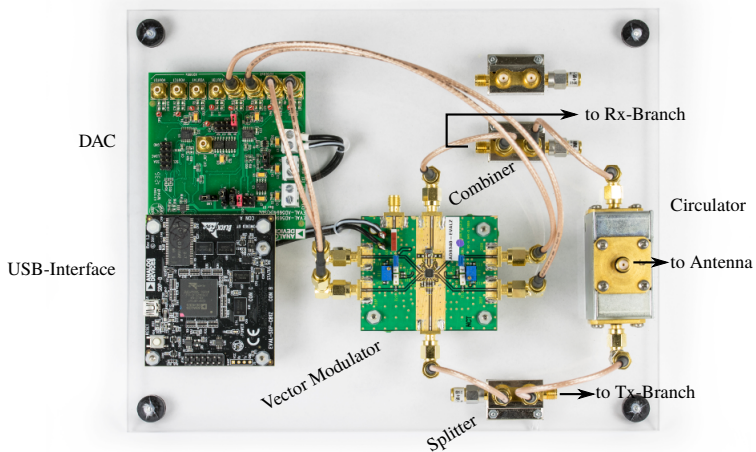


Figure 5.10 Prototype of the signal canceling architecture based on connectorized components and evaluation boards. The realized setup follows the block diagram from Fig. 5.6.

## 5.4 Prototyping and Realization

In the previous section the concept of active signal canceling for interference mitigation has been introduced and was subsequently analyzed analytically by derivation of a model to calculate the system's transfer function  $|H_i(j\omega)|$  as well as simulation based on the model of a first order signal canceling architecture. To prove the operating principle as well as performance and sensitivity to manipulation of the characteristic values (see previous section) measurements shall be carried out. This section briefly introduces the system setup and the components used for prototyping.

Fig. 5.10 shows the overall setup of the prototypic realization, where all components are mounted on a common acrylic glass board. The prototype shall represent the system with one cancellation path as discussed in the previous section and as depicted in Fig. 5.6. This reduces complexity but maintains the basic operating principle. Furthermore, amplifying components within the cancellation path are waived. To allow equality of both signals as required for derivation of Eq. (5.2), a 3 dB splitter and coupler are used to separate the



branches for tuning of the delays  $\tau_i$ , amplitudes  $A_i$  (here both with  $i = \{1, 2\}$ , as only one cancellation path is used) and phase  $\varphi$ . For the transmit path, this yields a loss of half the available transmit power and is thus only suitable for a prototype with reduced system complexity [24]. Furthermore, the absence of a non-linear amplifier (including its additional noise) allows for easier isolation of setup and operating principle specific effects.

To split and merge the signals two connectorized power splitters / combiners ZX10Q-2-13+ from Mini-Circuits [141] are used, each with an insertion loss<sup>69</sup> of around 0.4 dB for frequencies below 1 GHz. It yields an isolation of around 20 dB which is sufficient for the limitation of propagation of loop signals [140] as well as a phase shift of  $90^\circ$  at port 1 which finds its way into the overall phase  $\varphi$ . As the coupler is not based on transmission line technology, the introduced additional time delay can be neglected.

The circulator is custom made and yields a port to port insertion loss in the forward path of 0.2 dB and an isolation of at least  $-20$  dB in the frequency range of 750-1070 MHz. Further details can be taken from Fig. 5.11. For tuning of

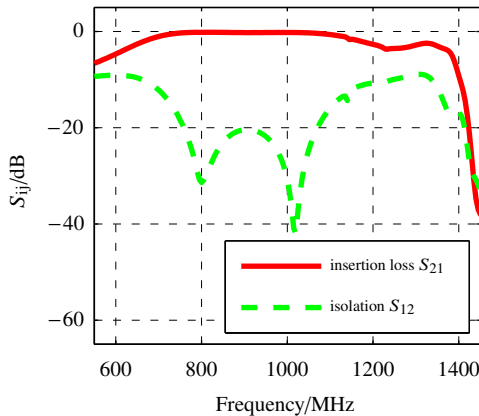


Figure 5.11 Plot of the measured insertion loss  $S_{21}$  and isolation (trap attenuation)  $S_{12}$  of the custom made circulator between ports 1 and 2 exemplarily. Other port combinations behave accordingly.

<sup>69</sup>The insertion loss neglects the splitter loss of 3 dB. The total loss can be calculated as the sum of both insertion loss and splitter loss.

amplitude and phase within the cancellation circuit an RF vector modulator AD8340 from Analog Devices [142] which performs manipulation of the phase  $\varphi$  of an input signal from  $\{0 \dots 2\pi\}$  and an attenuation of the amplitude in a range from  $-2$  dB to  $-32$  dB. The device works as a linear RF vector modulator with Cartesian controls: amplitude and phase of the RF output signal are adapted by individually tuning the relative amounts of in-phase and quadrature RF signal components by adjusting the voltages at the Cartesian control interface<sup>70</sup>. The manipulated in-phase and quadrature RF signal components are then summed at the RF output of the vector modulator.

The four inputs of the control interface are driven by a 16 bit quad DAC (AD5686R [143]) which itself is controlled via an SPI bus<sup>71</sup> by either a Matlab [105] script or a dedicated C# application.

It is setup and works as follows: The SPI module offers a connection to the DAC as well as a common USB interface to allow controlling and timing via the tuning software. In this prototype stage, the C# application offers open-loop control of the hardware, while the Matlab application is enabled to read data from a spectrum analyzer at a set frequency to measure the power of the interfering signal within the receive branch. This allows the setup to automatically tune the input parameters to optimum values for best cancellation. Here however, the focus was set on the working principle of the setup as well as its application for coexistence management in a multi-service RF environment.

---

<sup>70</sup>The Cartesian control for both the in-phase and quadrature components of the RF signal require four differential baseband inputs.

<sup>71</sup>A Serial Peripheral Interface (SPI) bus is a communication interface for synchronous serial data transfer between two ICs.

This chapter summarizes and concludes the major findings and novelties of this thesis by re-evaluating the observations which were deduced within this work. Subsequently, an outlook on the open issues or further topics as well as implications that result from the findings within this work is given.

Already today, vehicular connectivity is one of the major enabler technologies of forward-looking and trend-setting applications to provide and improve customer function in the domains of increased comfort, infotainment and safety. In the future, highly and fully automated driving use cases will be added. Here, connectivity of the vehicle serves as an enabler of the function itself (e. g. by back-end controlled route clearings which are time-critically transmitted into the vehicle to enable the automated driving mode) as well as applications for the enjoyable use of the time, when the vehicle is driving on its own.

This thesis focused on the analysis of the physical layer to provide these means of vehicular communications - both with focus on the special requirements from the automotive domain as well as the implications from a fast moving, customer electronics driven communications industry. To approach this broad field, the problem at hand has been divided into smaller parts, in particular

1. the characteristics and requirements of **vehicular connectivity**, subsumption to the ecosystem of wireless connectivity in general, including standardization and regulation [10, 12, 22],
2. derivation of a future-proof vehicular **connectivity architecture** which takes the high innovation pace of the communications industry as well as the product life cycle of the automotive industry into account [22],
3. partitioning, integration and evaluation of **vehicular multi-element antenna systems** to provide high data rates and reliability [6, 7, 9, 13–16, 18–21, 27],
4. synthesis and implementation of **reconfigurable, frequency-agile and multi-standard radio frequency front ends** to cover the multitude of different radio systems to be covered as well as the worldwide fragmentation of frequency resources [5, 8, 22, 23] and

5. provisioning of a **frequency-agile interference and coexistence management** to allow parallel operation of multiple wireless services simultaneously [24–26].

To ensure future compatibility, interoperability and facilitated implementation and integration within the highly flexible ecosystem of vehicular connectivity, a centralized, SDR-like connectivity architecture with reconfigurable characteristics was proposed. The antenna system serves as the air interface of the vehicle to connect to different services and is considered as the bottleneck of the overall system. Values on impedance and radiation level alone are not sufficient to determine the overall performance of a multi-element antenna system, especially in the automotive domain, where challenges with regards to integration and requirements with regards to guaranteed performance like data rate, reliability and availability arise. Thus, further key performance indicators like eigenvalue distribution, ergodic channel capacity as well as the zero-outage capacity which all allow an evaluation on system level were derived to take into account the antenna system's performance on full-vehicle system level but also including any effects on impedance and radiation layers on component and integration level.

In addition to a simulative characterization of the performance indicators, two extreme scenarios have been evaluated by measurement: a co-located antenna system with both antenna elements being positioned within the sharkfin antenna was compared to a distributed antenna setup for which the external rear view mirrors were each equipped with one antenna. Both system were characterized by measurement on a 9 km long urban and sub-urban test track within a LTE network at 800 MHz and subsequent post-processing and evaluation of the MIMO channel matrix by calculating the above mentioned performance indicators.

Digitization of received signals close to the feeding point of the antenna appears to be a promising solution and requires suitable ADCs for sampling and quantization. An individual reconfigurable and tunable continuous-time bandpass  $\Sigma\Delta$ -modulator was synthesized for direct sampling of RF signals over a very broad frequency range. Its combined use of over- and undersampling techniques allows noise shaping and thus noise reduction at the position of the notch within the noise floor with extended frequency range. By appropriate selection of feedback coefficients within the FIR-DAC of the modulator, frequency agility could be achieved. An extension of the frequency range was possible by employing undersampling techniques and thus sampling signals in

higher Nyquist zones. Digitization of signals from radio services at different positions within the overall operating range is possible at sufficient SQNR, both for signals within the first Nyquist zone as well as for signals in higher order Nyquist zones when undersampling is used, as proved by evaluation on power and bitstream level.

Finally, a reconfigurable setup for coexistence and interference management was introduced to ensure proper function of any the reconfigurable ADC by reducing intra-system interference within a multistandard connectivity platform based on signal canceling. To make signals ADC-compatible (due to the limited dynamic range of an ADC), a cancellation-based approach was proposed as well as evaluated analytically and by measurement, where a part of the interfering signal is coupled into the receive path with an inverted phase to cancel out the interfering signal by being superposed with an inverted copy of itself and thus being eliminated.



## Bibliography

- [1] McKinsey & Company, “Competing for the connected customer – perspectives on the opportunities created by car connectivity and automation,” Tech. Rep., 2015.
- [2] GSMA, “2025 every car connected: Forecasting the growth and opportunity,” GSM Association, Tech. Rep., 2012.
- [3] N. Heuvel dop, “Ericsson mobility report,” Ericsson, Tech. Rep., 2017.
- [4] ISO, “Information technology - open systems interconnection - basic reference model,” International Organization for Standardization, Geneva, ISO ISO/IEC 7498-1:1994, 1994.
- [5] A. Posselt, D. Berges, O. Klemp, and B. Geck, “Evaluation of a frequency agile direct RF ADC based on mixed-signal OFDM simulation,” in *European Conference on Personal Indoor and Mobile Radio Communications (PIMRC)*, September 2015.
- [6] A. Posselt, L. Ekiz, O. Klemp, B. Geck, and C. Mecklenbrauker, “System level evaluation for vehicular MIMO antennas in simulated and measured channels,” in *Antennas and Propagation (EuCAP), 2014 8th European Conference on*, April 2014, pp. 3051–3054.
- [7] C. Arendt, A. Posselt, P. Fertl, H. Boche, and J. Nötzel, “Evaluation of vehicular antenna concepts under delay-limited capacity as performance measure for safety critical message transfer,” in *2017 IEEE 28th Annual International Symposium on Personal, Indoor, and Mobile Radio Communications (PIMRC)*, Oct 2017.
- [8] A. Posselt, D. Berges, and O. Klemp, “Radio receiver for a motor vehicle, motor vehicle, method and computer program for a radio receiver,” Jan. 28 2016, Bayerische Motoren Werke AG, Patent Applications DE102014214555A1, WO002016012153A1.
- [9] A. Posselt, A. Friedrich, L. Ekiz, O. Klemp, and B. Geck, “System-level assessment of volumetric 3D vehicular MIMO antenna based on

- measurement,” in *2014 International Conference on Connected Vehicles and Expo (ICCVE)*, Nov 2014, pp. 222–226.
- [10] L. Ekiz, A. Posselt, O. Klemp, and C. Mecklenbrauker, “System level assessment of vehicular MIMO antennas in 4G LTE live networks,” in *Vehicular Technology Conference (VTC Fall), 2014 IEEE 80th*, Sept 2014, pp. 1–5.
- [11] A. Friedrich, B. Geck, O. Klemp, and H. Kellermann, “On the design of a 3D LTE antenna for automotive applications based on MID technology,” in *Microwave Conference (EuMC), 2013 European*, Oct 2013, pp. 640–643.
- [12] O. Klemp, A. Friedrich, B. Geck, and A. Posselt, “3D-Antennensysteme Anforderungen an die Fahrzeugintegration,” *ATZ-Automobiltechnische Zeitschrift*, vol. 116, no. 12, pp. 60–65, 2014.
- [13] A. Posselt, O. Klemp, L.-Y. Ekiz, and C. Lottermann, “Method and device for selecting transmission channels in a network radio connection,” Sept. 25 2015, Bayerische Motoren Werke AG, Patent Applications DE102013215855A1, WO002014154576A1, KR102015135254A, CN000105247797A, US020160014793A1, EP000002979371A1.
- [14] A. Posselt, C. Arendt, and P. Fertl, “Transceiver, Vehicle, Method, and Computer Program for a Transceiver,” Dec. 22 2016, Bayerische Motoren Werke AG, Patent Applications DE102015211336A1, WO002016202496A1, EP000003311498A1, US020180123632A1.
- [15] A. Posselt, D. Gozalvez Serrano, and S. Zimmermann, “Application-controlled geo-beamforming,” Aug. 04 2016, Bayerische Motoren Werke AG, Patent Applications DE102015201641A1, US020170330462A1, WO002016120236A1.
- [16] A. Posselt, A. Friedrich, and O. Klemp, “Antennenelement, Empfänger, Sender, Sendeempfänger, Fahrzeug und Verfahren zum Herstellen eines Antennenelements,” Mar. 02 2017, Bayerische Motoren Werke AG, Patent Application DE102015216147A1.
- [17] A. Posselt, C. Arendt, D. Gozalvez Serrano, M. Kaindl, and M. Steingruebner, “Antennenanordnung für ein Fahrzeug und Fahrzeug,” Apr. 05 2018, Bayerische Motoren Werke AG, Patent Application DE102016219163A1.



- [18] A. Posselt and C. Arendt, "Antennenanordnung für ein Fahrzeug und Fahrzeug," Apr. 05 2018, Bayerische Motoren Werke AG, Patent Application DE102016219164A1.
- [19] —, "Fahrzeugscheibe und Fahrzeug mit einer Fahrzeugscheibe," Apr. 05 2018, Bayerische Motoren Werke AG, Patent Application DE102016219167A1.
- [20] A. Posselt, M. Kaindl, M. Steingruebner, and M. Rottelberger, "Antennenanordnung, Karosserieteil und Fahrzeug," Apr. 19 2018, Bayerische Motoren Werke AG, Patent Application DE102016220238A1.
- [21] A. Posselt, C. Arendt, P. Fertl, and D. Gozálvez Serrano, "Kommunikationssteuergerät für ein Fahrzeug," Apr. 24 2018, Bayerische Motoren Werke AG, Patent Application DE102016222983A1.
- [22] A. Posselt, D. Berges, O. Klemp, and B. Geck, "Design and evaluation of frequency-agile multi-standard direct RF digitizing receivers for automotive use," in *Vehicular Technology Conference (VTC Spring), 2015 IEEE 81st*, May 2015.
- [23] A. Posselt, D. Gozálvez Serrano, M. Kaindl, and M. Steingruebner, "Vorrichtung für ein Fahrzeug zur drahtlosen Kommunikation und Verfahren zur Einrichtung drahtloser Kommunikation gemäß einem zweiten Kommunikationsstandard ebendieser," Mar. 29 2018, Bayerische Motoren Werke AG, Patent Application DE102016218580A1.
- [24] A. Posselt, M. Welpot, C. Bohm, O. Klemp, and B. Geck, "Evaluation and optimization of active signal canceling for coexistence management in vehicular multistandard transceivers," in *Microwave Conference (GeMiC), 2015 German*, March 2015, pp. 331–334.
- [25] A. Posselt and C. Böhm, "A Filter and a Method for Isolating Terminals in a Transceiver Front End," Aug. 09 2017, Bayerische Motoren Werke AG, Patent Application EP000003203641A1.
- [26] —, "A Filter and a Method for Filtering an Analog Radio-Frequency Input Signal," Aug. 09 2017, Bayerische Motoren Werke AG, Patent Application EP000003203640A1.

- [27] A. Friedrich, B. Geck, O. Klemp, A. Posselt, and I. Kriebitzsch, “3D-antennensysteme - Design und Validierung,” *ATZelektronik*, vol. 9, no. 6, pp. 44–51, 2014.
- [28] ETSI, “Digital cellular telecommunications system (phase 2+); GSM release 1999 specifications,” European Telecommunications Standards Institute, Sophia Antipolis, France, ETSI TS 101 805, 1999.
- [29] 3GPP, “Requirements for the UMTS terrestrial radio access (UTRA) system,” 3rd Generation Partnership Project, Sophia Antipolis, France, 3GPP TS 21.01U, 1997.
- [30] —, “Evolved universal terrestrial radio access (E-UTRA); user equipment (UE) radio transmission and reception,” 3rd Generation Partnership Project, Sophia Antipolis, France, 3GPP TS 36.101, 2015.
- [31] IEEE, “Wireless LAN Standard Family,” Institute of Electrical and Electronics Engineers, New York, USA, IEEE 802.11, 2012.
- [32] ETSI, “Digital video broadcasting (DVB); framing structure, channel coding and modulation for digital terrestrial television (ETSI EN 300 744 v1.6.1),” European Telecommunications Standards Institute, Sophia-Antipolis, Standard, Jan. 2009.
- [33] A. Osseiran, F. Boccardi, V. Braun, K. Kusume, P. Marsch, M. Maternia, O. Queseth, M. Schellmann, H. Schotten, H. Taoka, H. Tullberg, M. Uusitalo, B. Timus, and M. Fallgren, “Scenarios for 5G mobile and wireless communications: the vision of the METIS project,” *Communications Magazine, IEEE*, vol. 52, no. 5, pp. 26–35, May 2014.
- [34] M. Sauter, *Communication Systems for the Mobile Information Society*. Wiley, 2006.
- [35] Y. Zaki, *Future Mobile Communications: LTE Optimization and Mobile Network Virtualization*, ser. Advanced Studies Mobile Research Center Bremen. Springer Fachmedien Wiesbaden, 2012.
- [36] H. Abut, J. Hansen, and K. Takeda, *Advances for In-Vehicle and Mobile Systems: Challenges for International Standards*. Springer Science & Business Media, 2010.

- [37] ETSI, “Intelligent transport systems (ITS); european profile standard for the physical and medium access control layer of intelligent transport systems operating in the 5 ghz frequency band,” European Telecommunications Standards Institute, Sophia Antipolis, France, ETSI ES 202 663, 2009.
- [38] J. S. Marcus, L. Nett, M. Scanlan, U. Stumpf, M. Cave, and G. Pogorel, “Flexibilisierung der Frequenzregulierung,” WIK-Consult, Bad Honnef, Germany, Studie für die Bundesnetzagentur, 2005.
- [39] Bundesnetzagentur, “Strategische Aspekte zur Verfügbarkeit von Frequenzen für den Breitbandausbau in Deutschland,” Tech. Rep., July 2013.
- [40] P. Lamy, “Results of the work of the high level group on the future use of the UHF band (470-790 MHz),” European Commission, Brussel, Report to the European Commission, Aug. 2014.
- [41] CONVERGE, “Project Deliverable D3 - Functional Requirements and Architecture Options,” CONVERGE - COmmunication Network VEHICLE Road Global Extension, Germany, Tech. Rep. D3, 2014.
- [42] J. Franz, *EMV: Störungssicherer Aufbau elektronischer Schaltungen*, ser. Vieweg Studium. Vieweg+Teubner Verlag, 2011.
- [43] G. Baruffa, M. Femminella, F. Mariani, and G. Reali, “Protection ratio and antenna separation for DVB-T/LTE coexistence issues,” *Communications Letters, IEEE*, vol. 17, no. 8, pp. 1588–1591, August 2013.
- [44] A. Ott, U. Siart, T. Eibert, O. Klemp, and R. Steffen, “Enhanced investigations of 433 MHz - 10 GHz time invariant wireless in-car communication channels,” in *German Microwave Conference*, 2011, pp. 1–4.
- [45] METIS, “Project Deliverable D 1.1 - Scenarios, requirements and KPIs for 5G mobile and wireless system,” METIS - Mobile and wireless communications Enablers for Twenty-twenty (2020) Information Society, Tech. Rep. D 1.1, 2013.
- [46] J. Rodriguez, *Fundamentals of 5G Mobile Networks*. Wiley, 2015.

- [47] Electronic Communications Committee (ECC), “Measurements on the performance of DVB-T receivers in the presence of interference from the mobile service,” Electronic Communications Committee within CEPT, Marseille, Report of the European Conference of Postal and Telecommunications Administrations (CEPT), June 2010.
- [48] J. Mitola, “The software radio architecture,” *IEEE Communications Magazine*, vol. 33, no. 5, pp. 26–38, May 1995.
- [49] A. Abidi, “The path to the software-defined radio receiver,” *Solid-State Circuits, IEEE Journal of*, vol. 42, no. 5, pp. 954–966, May 2007.
- [50] F. K. Jondral, “Software-defined radio - basics and evolution to cognitive radio,” *EURASIP Journal on Wireless Communication and Networking*, 2005.
- [51] H. Arslan, *Cognitive Radio, Software Defined Radio, and Adaptive Wireless Systems*, ser. Signals and Communication Technology. Springer, 2007.
- [52] V. Giannini, J. Craninckx, and A. Baschirotto, *Baseband Analog Circuits for Software Defined Radio*, ser. Analog Circuits and Signal Processing. Springer, 2008.
- [53] M. Ihmig and A. Herkersdorf, “Flexible multi-standard multi-channel system architecture for software defined radio receiver,” in *2009 9th International Conference on Intelligent Transport Systems Telecommunications (ITST)*, Oct 2009, pp. 598–603.
- [54] L. Stolz, M. Ihmig, and W. Stechele, “An evaluation on using gpu coprocessing for software radios on a low-cost platform,” in *Proceedings of the 2012 Conference on Design and Architectures for Signal and Image Processing*, Oct 2012, pp. 1–8.
- [55] L. Stolz, K. Weckemann, H. Lim, and W. Stechele, “A prototypical in-car entertainment setup using software defined radio and ethernet/ip-based in-vehicle communication,” in *The First International Conference on Advances in Vehicular Systems, Technologies and Applications (VEHICULAR)*, Venice, Italy, Jun 2012.

- [56] R. Bagheri, A. Mirzaei, M. Heidari, S. Chehrazi, M. Lee, M. Mikhemar, W. Tang, and A. Abidi, "Software-defined radio receiver: dream to reality," *IEEE Communications Magazine*, vol. 44, no. 8, pp. 111–118, Aug. 2006.
- [57] H. Nyquist, "Certain topics in telegraph transmission theory," *American Institute of Electrical Engineers, Transactions of the*, vol. 47, no. 2, pp. 617–644, April 1928.
- [58] G. J. Foschini and M. J. Gans, "On limits of wireless communications in a fading environment when using multiple antennas," *Wireless Personal Communications*, vol. 6, pp. 311–335, 1998.
- [59] IEEE, Institute of Electrical and Electronics Engineers, "IEEE standard test procedures for antennas," ANSI/IEEE Std 149-1979, New York, USA, Tech. Rep., 1979.
- [60] C. Balanis, *Antenna Theory: Analysis and Design*. Wiley, 2012.
- [61] ———, *Modern Antenna Handbook*. Wiley, 2011.
- [62] T. Milligan, *Modern Antenna Design*. Wiley, 2005.
- [63] D. Tse and P. Viswanath, *Fundamentals of Wireless Communication*, ser. Wiley series in telecommunications. Cambridge University Press, 2005.
- [64] H. Levin and P. McEwan, *Cost-Effectiveness Analysis: Methods and Applications*. SAGE Publications, 2001.
- [65] V. Rabinovich, N. Alexandrov, and B. Alkhateeb, *Automotive Antenna Design and Applications*. CRC Press, 2010.
- [66] D. Manteuffel and M. Arnold, "Considerations on configurable multi-standard antennas for mobile terminals realized in LTCC technology," in *Antennas and Propagation, 2009. EuCAP 2009. 3rd European Conference on*, March 2009, pp. 2541–2545.
- [67] E. Gschwendtner and W. Wiesbeck, "Ultra-broadband car antennas for communications and navigation applications," *Antennas and Propagation, IEEE Transactions on*, vol. 51, no. 8, pp. 2020–2027, Aug 2003.

- [68] O. Klemp and H. Eul, "Diversity efficiency of multimode antennas impacted by finite pattern correlation and branch power imbalances," in *Wireless Communication Systems, 2007. ISWCS 2007. 4th International Symposium on*, Oct 2007, pp. 322–326.
- [69] R. Martens, E. Safin, and D. Manteuffel, "On the relation between the element correlation of antennas on small terminals and the characteristic modes of the chassis," in *Antennas and Propagation Conference (LAPC), 2010 Loughborough*, Nov 2010, pp. 457–460.
- [70] —, "Inductive and capacitive excitation of the characteristic modes of small terminals," in *Antennas and Propagation Conference (LAPC), 2011 Loughborough*, Nov 2011, pp. 1–4.
- [71] —, "Selective excitation of characteristic modes on small terminals," in *Antennas and Propagation (EUCAP), Proceedings of the 5th European Conference on*, April 2011, pp. 2492–2496.
- [72] T. Hansen and F. Hofmann, "Automotive multi- and broadband monopole antenna for GSM, WLAN and UWB applications," in *Ultra-Wideband, 2008. ICUWB 2008. IEEE International Conference on*, vol. 2, Sept 2008, pp. 219–222.
- [73] A. Saitou, K. Aoki, K. Honjo, and K. Watanabe, "Design considerations on the minimum size of broadband antennas for UWB applications," *Microwave Theory and Techniques, IEEE Transactions on*, vol. 56, no. 1, pp. 15–21, Jan 2008.
- [74] Z. Chen, "Broadband planar monopole antenna," *Microwaves, Antennas and Propagation, IEE Proceedings*, vol. 147, no. 6, pp. 526–528, Dec 2000.
- [75] B. Heydari and A. Islamdoost, "A new broadband trapezoidal flat monopole antenna," in *Antennas and Propagation in Wireless Communications (APWC), 2012 IEEE-APS Topical Conference on*, Sept 2012, pp. 1246–1249.
- [76] D. Manteuffel, M. Grimm, and R. Martens, "Optimization of ultrawideband bow-tie antennas for cable based operation," in *Antennas and Propagation Conference (LAPC), 2010 Loughborough*, Nov 2010, pp. 585–588.

- [77] M. Cerretelli and G. Gentili, "Progress in compact multifunction automotive antennas," in *Electromagnetics in Advanced Applications, 2007. ICEAA 2007. International Conference on*, Sept 2007, pp. 93–96.
- [78] H. El-Sallabi, "Polarization consideration in characterizing radio wave propagation in urban microcellular channels," in *Personal, Indoor and Mobile Radio Communications, 2000. PIMRC 2000. The 11th IEEE International Symposium on*, vol. 1, 2000, pp. 411–415 vol.1.
- [79] D. Valderas, *Ultrawideband Antennas: Design and Applications*. Imperial College Press, 2011.
- [80] D. Pozar, *Microwave Engineering, 4th Edition*. Wiley, 2011.
- [81] W. Weichselberger, "Spatial structure of multiple antenna radio channels," Ph.D. dissertation, Technische Universität Wien, Institut für Nachrichtentechnik und Hochfrequenztechnik, 2008.
- [82] A. A. Abouda, H. M. El-Sallabi, L. Voukko, and S. G. Häggman, "Performance of stochastic kronecker MIMO radio channel model in urban microcells," in *IEEE 17th International Symposium on Personal, Indoor and Mobile Radio Communications*, 2006, pp. 1–5.
- [83] K. Yu and B. Ottersten, "Models for MIMO propagation channels," *Wiley Journal on Wireless Communications and Mobile Computing, Special Issue on Adaptive Antennas and MIMO Systems*, 2002.
- [84] J. P. Kermaol, L. Schumacher, K. I. Pedersen, and P. E. Mogensen, "A stochastic MIMO radio channel model with experimental validation," *IEEE Journal on selected Areas in Communications*, vol. 20, pp. 1211–1225, 2002.
- [85] T. Rappaport, *Wireless Communications*. Prentice Hill, 2002.
- [86] J. Gibson, *Mobile Communications Handbook, Third Edition*, ser. Electrical Engineering Handbook. Taylor & Francis, 2012.
- [87] A. Goldsmith, *Wireless Communications*. Cambridge University Press, 2005.
- [88] B. Hassibi and B. Hochwald, "How much training is needed in multiple-antenna wireless links?" *Information Theory, IEEE Transactions on*, vol. 49, no. 4, pp. 951–963, April 2003.

- [89] J. H. Kotecha and A. Sayeed, "Transmit signal design for optimal estimation of correlated mimo channels," *Signal Processing, IEEE Transactions on*, vol. 52, no. 2, pp. 546–557, Feb 2004.
- [90] I. Bronshtein, K. Semendyayev, G. Musiol, and H. Mühlig, *Handbook of Mathematics*. Springer Berlin Heidelberg, 2015.
- [91] E. A. Jorswieck and H. Boche, "Delay-limited capacity of parallel fading channels," in *Signal Processing Advances in Wireless Communications, 2005 IEEE 6th Workshop on*, June 2005, pp. 495–499.
- [92] B. Sklar, "Rayleigh fading channels in mobile digital communication systems - part i," *IEEE Communications Magazine*, vol. 35, no. 7, pp. 90–100, 1997.
- [93] J. Salo, P. Suvikunnas, H. M. El-Sallabi, and P. Vainikainen, "Ellipticity statistic as measure of MIMO multipath richness," *Electronics Letters*, vol. 42, no. 3, pp. 160–162, Feb 2006.
- [94] A. Papoulis and S. Pillai, *Probability, random variables, and stochastic processes*, ser. McGraw-Hill electrical and electronic engineering series. McGraw-Hill, 2002.
- [95] E. Ohlmer, G. Fettweis, and D. Plettemeier, "MIMO system design and field tests for terminals with confined space - impact on automotive communication," in *Proceedings of the 5th European Conference on Antennas and Propagation (EUCAP)*, April 2011, pp. 2886–2890.
- [96] T. K. Sarkar and A. Taaghool, "Near-field to near/far-field transformation for arbitrary near-field geometry utilizing an equivalent electric current and mom," *Antennas and Propagation, IEEE Transactions on*, vol. 47, no. 3, pp. 566–573, 1999.
- [97] S. M. Mikki and Y. M. M. Antar, "On cross correlation in antenna arrays with applications to spatial diversity and mimo systems," *IEEE Transactions on Antennas and Propagation*, vol. 63, no. 4, pp. 1798–1810, April 2015.
- [98] J. G. Proakis, *Digital signal processing*, 3rd ed., ser. Prentice Hall international editions. Upper Saddle River, NJ: Prentice Hall, 1996.



- [99] K. Ogata, *Discrete-time control systems*. Englewood Cliffs, NJ: Prentice-Hall, 1987.
- [100] D. Johns, *Analog integrated circuit design*. New York: John Wiley & Sons, 1997.
- [101] I. Ahmed, *Pipelined ADC Design and Enhancement Techniques*. Dordrecht: Springer, 2010.
- [102] C. Shannon, "Communication in the presence of noise," *Proceedings of the IEEE*, vol. 86, no. 2, pp. 447–457, Feb 1998.
- [103] S. Henzler, *Time-to-digital converters*. London: Springer, 2010.
- [104] J. M. Pinto de la Rosa, *CMOS sigma-delta converters*. Chichester: Wiley, 2013.
- [105] MATLAB, *version 7.11.1.866 (R2010b)*. Natick, Massachusetts: The MathWorks Inc., 2010.
- [106] R. G. Lyons, *Understanding digital signal processing*, 3rd ed. London: Prentice Hall ; Pearson Education International, 2011.
- [107] R. Walden, "Analog-to-digital converter survey and analysis," *IEEE Journal on Selected Areas in Communications*, vol. 17, no. 4, pp. 539–550, Apr. 1999.
- [108] R. Schreier, *Understanding delta-sigma data converters*. Piscataway, NJ : Hoboken, N.J. ; Chichester: IEEE Press ; Wiley, 2005.
- [109] J. de la Rosa, "An empirical and statistical comparison of state-of-the-art sigma-delta modulators," in *2013 IEEE International Symposium on Circuits and Systems (ISCAS)*, May 2013, pp. 825–828.
- [110] S. Gupta, D. Gangopadhyay, H. Lakdawala, J. Rudell, and D. Allstot, "A 0.8-2 GHz fully-integrated QPLL-timed direct-RF-sampling bandpass ADC in 0.13 m CMOS," *IEEE Journal of Solid-State Circuits*, vol. 47, no. 5, pp. 1141–1153, May 2012.
- [111] J. Candy, "A use of double integration in sigma delta modulation," *IEEE Transactions on Communications*, vol. 33, no. 3, pp. 249–258, Mar. 1985.

- [112] J. de la Rosa and R. Río, *CMOS Sigma-Delta Converters: Practical Design Guide*, ser. Wiley - IEEE. Wiley, 2013.
- [113] S. Asghar, R. del Rio, and J. de la Rosa, “Undersampling RF-to-digital CT sigma-delta modulator with tunable notch frequency and simplified raised-cosine FIR feedback DAC,” in *2013 IEEE International Symposium on Circuits and Systems (ISCAS)*, May 2013, pp. 1994–1997.
- [114] N. Beilleau, H. Aboushady, and M.-M. Louerat, “Using finite impulse response feedback DACs to design sigma; delta; modulators based on LC filters,” in *48th Midwest Symposium on Circuits and Systems, 2005*, Aug. 2005, pp. 696–699 Vol. 1.
- [115] G. Molina-Salgado, G. Jovanovic-Dolecek, and J. de la Rosa, “Band-pass continuous-time sigma-delta modulators with widely tunable notch frequency for efficient RF-to-digital conversion,” in *2013 IEEE 56th International Midwest Symposium on Circuits and Systems (MWSCAS)*, Aug. 2013, pp. 566–569.
- [116] G. Molina-Salgado, A. Morgado, G. Jovanovic Dolecek, and J. de la Rosa, “LC-based bandpass continuous-time sigma-delta modulators with widely tunable notch frequency,” *IEEE Transactions on Circuits and Systems I: Regular Papers*, vol. 61, no. 5, pp. 1442–1455, May 2014.
- [117] J. M. Pinto de la Rosa, *Systematic design of CMOS switched-current band-pass sigma-delta modulators for digital communication chips*. Boston: Kluwer Academic, 2002.
- [118] Z. Gao, Y. Xu, P. Sun, E. Yao, and Y. Hu, “A programmable high-speed pulse swallow divide-by-n frequency divider for PLL frequency synthesizer,” in *2010 International Conference on Computer Application and System Modeling (ICCA SM)*, vol. 6, Oct. 2010, pp. 315–318.
- [119] D. Gupta, T. Filippov, A. Kirichenko, D. Kirichenko, I. Vernik, A. Sahu, S. Sarwana, P. Shevchenko, A. Talalaevskii, and O. Mukhanov, “Digital channelizing radio frequency receiver,” *IEEE Transactions on Applied Superconductivity*, vol. 17, no. 2, pp. 430–437, June 2007.
- [120] M. Snelgrove, “ADC architectures and technology,” in *IEEE Compound Semiconductor Integrated Circuit Symposium, 2004*, Oct. 2004, pp. 27–30.

- [121] L. Smaini, *RF analog impairments modeling for communication systems simulation application to OFDM-based transceivers*. Chichester, West Sussex; Hoboken, N.J.: Wiley, 2012.
- [122] A. Naderi, M. Sawan, and Y. Savaria, "On the design of undersampling continuous-time bandpass delta-sigma modulators for gigahertz frequency a/d conversion," *IEEE Transactions on Circuits and Systems I: Regular Papers*, vol. 55, no. 11, pp. 3488–3499, Dec. 2008.
- [123] D. Akos, M. Stockmaster, J. B. Y. Tsui, and J. Caschera, "Direct bandpass sampling of multiple distinct RF signals," *IEEE Transactions on Communications*, vol. 47, no. 7, pp. 983–988, July 1999.
- [124] R. Vaughan, N. Scott, and D. White, "The theory of bandpass sampling," *IEEE Transactions on Signal Processing*, vol. 39, no. 9, pp. 1973–1984, Sept. 1991.
- [125] P. Aziz, H. Sorensen, and J. Van der Spiegel, "Performance of complex noise transfer functions in bandpass and multi band sigma delta systems," in *1995 IEEE International Symposium on Circuits and Systems, 1995. ISCAS '95*, vol. 1, Apr. 1995, pp. 641–644 vol.1.
- [126] D.-K. Pham, P. Desgreys, P. Loumeau, and T. Ridgers, "Optimized new ADC architecture using SD modulators for nonlinearly distorted signals," in *New Circuits and Systems Conference (NEWCAS), 2012 IEEE 10th International*, June 2012, pp. 245–248.
- [127] R. v. Nee, *OFDM wireless multimedia communications*, ser. Artech House universal personal communications library. Boston: Artech House, 2000.
- [128] G. Acosta and M. A. Ingram, "OFDM simulation using matlab," Georgia Tech - School of Electrical and Computer Engineering, Atlanta, Tech. Rep., Aug. 2000.
- [129] H. Holma and A. Toskala, Eds., *LTE for UMTS: OFDMA and SC-FDMA based radio access*. Chichester, U.K: Wiley, 2009.
- [130] Z. Hu, R. Susitaival, Z. Chen, I. K. Fu, P. Dayal, and S. K. Baghel, "Interference avoidance for in-device coexistence in 3GPP LTE-Advanced: challenges and solutions," *IEEE Communications Magazine*, vol. 50, no. 11, pp. 60–67, November 2012.

- [131] S. K. Baghel, M. A. Ingale, and G. Goyal, "Coexistence possibilities of LTE with ISM technologies and GNSS," in *Communications (NCC), 2011 National Conference on*, Jan 2011, pp. 1–5.
- [132] Analog Devices, "AD9361: RF agile transceiver, datasheet," 2014.
- [133] D. Bharadia, E. McMillin, and S. Katti, "Full duplex radios," *SIGCOMM Comput. Commun. Rev.*, vol. 43, no. 4, pp. 375–386, Aug. 2013.
- [134] S. S. Hong, J. Mehlman, and S. Katti, "Picasso: Flexible RF and spectrum slicing," in *Proceedings of the ACM SIGCOMM 2012 Conference on Applications, Technologies, Architectures, and Protocols for Computer Communication*, ser. SIGCOMM '12. New York, NY, USA: ACM, 2012, pp. 37–48.
- [135] J. Zhou, A. Chakrabarti, P. R. Kinget, and H. Krishnaswamy, "Low-noise active cancellation of transmitter leakage and transmitter noise in broadband wireless receivers for FDD/co-existence," *IEEE Journal of Solid-State Circuits*, vol. 49, no. 12, pp. 3046–3062, Dec 2014.
- [136] S. Kannangara and M. Faulkner, "Adaptive duplexer for multiband transceiver," in *Radio and Wireless Conference, 2003. RAWCON '03. Proceedings*, Aug 2003, pp. 381–384.
- [137] G. Lasser, R. Langwieser, and A. L. Scholtz, "Broadband suppression properties of active leaking carrier cancellers," in *2009 IEEE International Conference on RFID*, April 2009, pp. 208–212.
- [138] A. Poularikas, *Handbook of Formulas and Tables for Signal Processing*, ser. Electrical Engineering Handbook. CRC Press, 1998.
- [139] A. Sahai, G. Patel, C. Dick, and A. Sabharwal, "On the impact of phase noise on active cancellation in wireless full-duplex," *IEEE Transactions on Vehicular Technology*, vol. 62, no. 9, pp. 4494–4510, Nov 2013.
- [140] S. Kannangara and M. Faulkner, "Analysis of an adaptive wideband duplexer with double-loop cancellation," *Vehicular Technology, IEEE Transactions on*, vol. 56, no. 4, pp. 1971–1982, July 2007.
- [141] Mini-Circuits, "Power Splitter/Combiner ZX10Q-2-13+, Datasheet," 2015.

- 
- [142] Analog Devices, “AD8340: 700 MHz to 1000 MHz RF vector modulator,” 2014.
- [143] —, “AD5686R: Quad 16 bit nanoDAC, datasheet,” 2014.
- [144] T. Taga, “Analysis for mean effective gain of mobile antennas in land mobile radio environments,” *IEEE Transactions on Vehicular Technology*, vol. 39, no. 2, pp. 117–131, May 1990.



# Curriculum Vitae

## Personal Data

Name	Adrian Posselt
Date of Birth	6th of February, 1988
Nationality	German

## Education

2007	<i>Abitur</i> at St. Ursula-Schule Hannover, Germany
2007–2012	Electrical engineering studies at Leibniz Universität Hannover, Germany graduating as <i>Dipl.-Ing.</i>
2012–2019	Ph. D. student at Institute of Microwave and Wireless Systems, Leibniz Universität Hannover, Germany

## Work Experience

2012–2015	Researcher at BMW Group Research and Technology
since 2015	Various project management and engineering specialist positions at BMW Group development